THESIS

COMPARISON OF DIGITAL TERRAIN AND FIELD-BASED CHANNEL DERIVATION METHODS IN A SUBALPINE CATCHMENT, FRONT RANGE, COLORADO

Submitted by

Blaine Hastings

Department of Ecosystem Science and Sustainability

In partial fulfillment of the requirements

For the Degree of Master of Science

Colorado State University

Fort Collins, Colorado

Summer 2012

Master's Committee:

Advisor: Stephanie Kampf

Melinda Laituri
Jeffrey Niemann

ABSTRACT

COMPARISON OF DIGITAL TERRAIN AND FIELD-BASED CHANNEL DERIVATION METHODS IN A SUBALPINE CATCHMENT, FRONT RANGE, COLORADO

Understanding the reliability of digitally derived channel networks for mountainous headwater catchments is important to many water resource and land-use management applications. Digital elevation models (DEMs) have become an essential tool for an increasing array of mountain runoff analyses. The purpose of this study is to investigate the influence of digitally-derived topographic variables on channel network formation for a high-elevation glaciated watershed. To accomplish this, our objectives were to (1) test how differences in gridded DEM resolution affect spatially distributed topographic parameters of local slope (tan β), specific contributing area (α_s), and topographic wetness index (TWI) derived from both eight and infinite directional flow algorithms, (2) map the actual stream channel network at Loch Vale and examine the influence of surface variables on channel initiation, and (3) evaluate the performance of common methods for deriving channel networks from gridded topographic data by comparing to the observed network.

We found that coarser DEM resolution leads to a loss of detail in spatial patterns of topographic parameters and an increase in the calculated mean values of $\ln(\alpha_s)$ and TWI. Grid cell sizes above 1m result in a substantial shift in the overall cumulative frequency distributions of $\ln(\alpha_s)$ and TWI towards higher values. A field survey at Loch Vale revealed a complex and disjointed channel network, with 242 channelized points and 30 channel heads. We found no predictable relationships between channel head locations and geomorphic process domains.

Analysis of variance (ANOVA) showed no statistically significant difference in mean $\ln(\alpha_s)$ and TWI for channel head locations grouped by elevation, aspect, slope, formation process or upslope land cover type. For most DEM resolutions and flow partitioning algorithms, deriving channel networks with spatially constant flow accumulation and TWI thresholds provides poor network representation. The publicly available National Hydrography Dataset (NHD) layer oversimplifies the channel network by neglecting almost all first and second order channels. Many of the DEM-derived channel networks that use spatially constant flow accumulation and TWI thresholds also do not reproduce the locations of low order channels in the observed channel network well. Assumptions of topographic control on channel initiation are not shown to be valid at Loch Vale, likely due to their inability to capture subsurface processes and geologic features important to channel formation.

However, if using these topographically dependent threshold methods to delineate channel networks, we suggest the use of field-based survey data to identify appropriate thresholds. With appropriate thresholds, both 1m and 10m DEMs can produce channel networks with similar drainage densities to the observed network, even if locations of low order channels are not predicted accurately. Performance degrades for 30m DEMs, so we suggest that DEMs with resolutions coarser than 10m should be avoided for channel network delineation.

ACKNOWLEDGEMENTS

I would like express my gratitude to my advisor Stephanie Kampf for all of her guidance and feedback throughout this study, as well as my graduate committee members Melinda Laituri and Jeffrey Niemann. I would also like to acknowledge Rocky Coleman for generously allowing us access to high-accuracy GPS units, Care Moore for her help in the field, the Colorado State University Statistical Laboratory for assisting with statistical analyses, and the U.S. Geological Survey and the Natural Resource Ecology Laboratory for providing GIS data. Finally, special thanks to Lindsay Hastings for her unwavering support, both in the field and on the home front.

TABLE OF CONTENTS

LIST OF TABLES

LIST OF FIGURES

1. Introduction

Topography plays an important role in the spatial patterns of runoff and stream channel networks in steep, high elevation watersheds (Anderson and Kneale, 1982). While other factors such as bedrock topography and spatial variability of physical soil properties contribute to channel network development, methods for deriving networks based on topographic characteristics have proven useful for a range of environments. With the increased availability of geographic information systems (GIS) and digital elevation data has come a growing reliance on using digital elevation models (DEMs) to map the location of stream channels. GIS-based methods derive channel networks by analyzing topography through gridded calculation of slope, contributing area (Hancock, and Evans, 2006; Tarboton et al., 1991; Wolock and McCabe, 2000; Zhang and Montgomery, 1994) and various forms of topographic wetness indices (Dietrich et al., 1993). Yet, prior research has shown that the locations and shapes of DEM derived networks vary both with the methods of calculation (O'Callaghan and Mark, 1984; Montgomery and Foufoula-Georgiou, 1993) and the spatial resolution of the DEM used (Deng et al., 2007; Wolock and McCabe, 2000; McMaster, 2002). When discussing a DEM representation of the landscape we use the term resolution to mean the grid cell size, which corresponds to the smallest area or topographic feature on the ground that can be represented by the DEM. We distinguish this from "scale", which is applied to mean the extent of the real-world hydrologic or geomorphic unit whose response and/or form is being characterized. For example, units of interest can range from microscale rock outcrops to more mesoscale hillslopes, to the macroscale catchment.

Accurate demarcation of channel locations and extents is important to many hydrological and environmental applications. For modeling purposes, neglecting lower order channels can

result in variations of hillslope flow length, channel head location, and drainage density, features that all control how water is routed through the landscape and ultimately the nature of simulated hydrographs (Zhang and Montgomery, 1994). This becomes particularly significant with the many topographically-driven hydrologic models in use today, where the difference between representation of channelized and hillslope processes can have large effects on both simulated discharge and spatial patterns of groundwater and soil moisture. Improved channel network representation can also inform many environmental issues, including water distribution and availability for ecological analysis (Iverson et al., 1997), point and non-point source pollution management plans (Jaeger et al., 2007), timber harvesting in streamside management zones and wildfire remediation (Vides-Solorio, 2003; Garcia-Corona et al., 2004).

1.1 Research Objectives

The objectives of this study are to (1) examine how differences in gridded DEM resolution for Loch Vale, a glaciated Rocky Mountain headwater catchment, affect spatially distributed topographic parameters of local slope (tan β), specific contributing area (α_s), and topographic wetness index (TWI) derived from both eight and infinite directional flow algorithms, (2) map the actual stream channel network at Loch Vale and examine the influence of surface variables on channel initiation, and (3) evaluate the performance of common methods for deriving channel networks from gridded topographic data by comparing to the observed network. Several studies have examined these issues in lower elevation undulating terrain (Hancock and Evans, 2006; McMaster, 2002; Zhang and Montgomery, 1994), but few have addressed channel network delineation in exceptionally steep, high elevation basins whose runoff

is dominated by melting of a seasonal snowpack. The study location, Loch Vale, represents just such a basin, and because of its extreme topography and ongoing history of hydrologic research it is an ideal site for this investigation. Study methods include three related phases: (1) DEM analysis, (2) Observed channel network analysis, and (3) GIS derivation of channel networks.

For the Loch Vale watershed, we hypothesize that DEM resolution will have a significant effect on terrain representation and the accuracy of the modeled channel network. Channel network derivation methods are expected to perform well for downslope channel locations having high contributing areas, but will be less accurate for first and second order channels where analysis of surface topography cannot characterize important subsurface influences like bedrock topography, macropores, bedrock fractures, and piping.

1.2 Background

Digital elevation models and LiDAR

Topography can be digitally represented in a number of ways through digital elevation models (DEM). One type of DEM is the triangulated irregular network (TIN), which implicitly represents stream channels with a network of triangular planes to characterize valleys, ridgetops and hillslopes with elevations stored at their corners. TINs offer some advantages because they can capture curved features and easily incorporate variable spatial resolution (O'Callaghan and Mark, 1984); however because gridded representation of elevation with rasters has become the most commonly used form of DEM, these will be the only type addressed here.

As remote sensing technologies continue to improve, the resolution of gridded DEMs has also improved. Landscapes represented by 90, 30, and 10m grid cells that cover entire continents

are widely available through outlets like the U.S. Geological Survey's (USGS) National Elevation Dataset (NED). These DEMs are often derived from traditionally developed contour maps or optical sensors like the Advanced Spaceborne Thermal Emission and Reflection Radiometer. More recently, the use of Light Detection and Ranging (LiDAR) technology has allowed for the development of custom elevation datasets with resolutions as fine as $1m^2$. Airborne LiDAR uses active remote sensing systems to send downward pulses of light to measure the distance between the sensor and terrestrial surfaces. Distance is calculated by relating the known elevation of the sensor, speed of light and measured return times of the reflected light, resulting in a high density collection of elevation points. Various processing algorithms are applied to filter the millions of discrete data points within a sampling footprint and identify returns from specific surface classes, including vegetation canopy, buildings, and the ground surface. The filtered bare ground elevations are then interpolated to construct a fine resolution DEM (Evans et al., 2006). Development of environmental applications for LiDAR data remains a promising and active area of research.

Contributing area thresholds for channel initiation

Distributed channel network models often simulate transitions from hillslope to channelized flow based on a contributing area threshold ($T\alpha$) calculated from a DEM. Algorithms for calculating contributing area typically determine the change in elevation between a given grid cell and neighboring cells and then route flow to adjacent cells based on these directional derivatives. The D8, or steepest descent algorithm, routes flow to the single downslope cell with the greatest drop in elevation. An alternate algorithm uses planar triangular facets to route flow towards as many as two cells based on calculation of flow angle, allowing

for an effectively infinite number of possible directions (D∞; Tarboton, 1997). D∞ is able to represent divergent flow, which can result in more realistic flow networks. Applications of these flow direction algorithms have shown mixed results, but some evidence suggests that allowing for multi-directional flow can affect the distribution of contributing area and TWI, as well as modeled flow pathways (Quinn et al., 1991; Tarboton, 1997; Wolock and McCabe, 1995). However, it has also been shown that both algorithms can perform equally well in deriving stream networks for steep terrain (McMaster, 2002).

Using flow direction information, it becomes possible to estimate the area of land contributing flow to a given cell of a DEM as the sum of the areas of all upslope contributing cells. GIS-based channel delineation methods often use a contributing area threshold to estimate the headward extent of channelization. By assuming a threshold contributing area for channel initiation, one can then derive a gridded estimation of the channel network. This method is rooted in theory first developed by Gilbert [1877] relating slope, distance, and volume of erosion and was later refined by Horton [1945], who characterized channel head location by minimum overland flow length required to initiate fluvial erosion. O'Callaghan and Mark [1984] applied this method using a DEM by setting a contributing area threshold for stream channel initiation. The threshold value can be estimated from prior knowledge of the region, DEM analysis of slope-area relationships, or from other information such as blue line vector features in the USGS National Hydrography Dataset (NHD). All of these methods present challenges, as field information may not be available or would involve arduous field surveys. Existing channel network maps are often interpreted from aerial imagery and may neglect low order channels concealed by canopy cover.

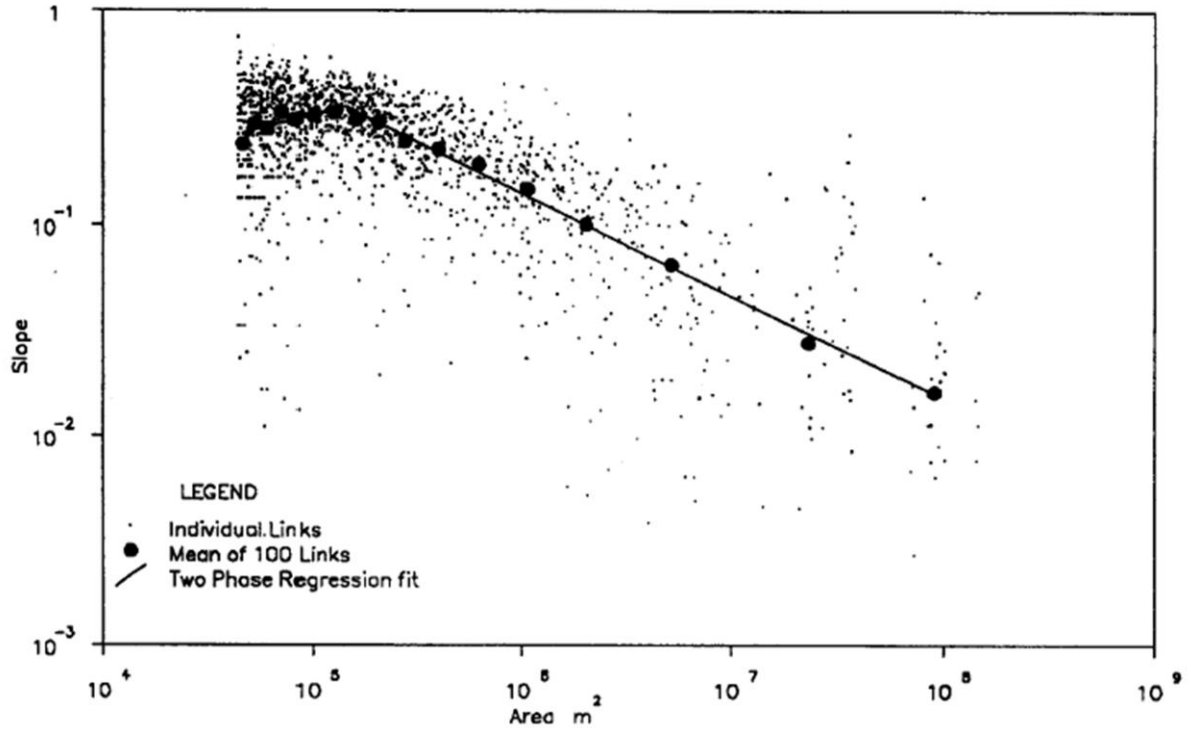

Figure 1: Link slope-source area plot for Big Creek basin, Idaho (Tarboton et al., 1991).

Tarboton et al. [1991] proposed defining contributing area thresholds for channel initiation through analysis of slope-area relationships (Figure 1). In their approach, selection of a threshold involves derivation of many channel networks for a range of assumed threshold contributing areas and plotting the resulting slopes of channel segments against their contributing areas. After regression analysis of averaged values, the location of a point of inflection between positive and negative slopes of the regression line represents the contributing area that can be used as a threshold.

Montgomery and Foufoula-Georgiou [1993] pointed out that selection of valid thresholds in this manner has shortcomings, in that it is constrained by the previously and arbitrarily defined networks used as inputs to derive a final network. They also showed that these methods often predict erroneously large slope lengths in steep terrain. Instead, they propose estimating

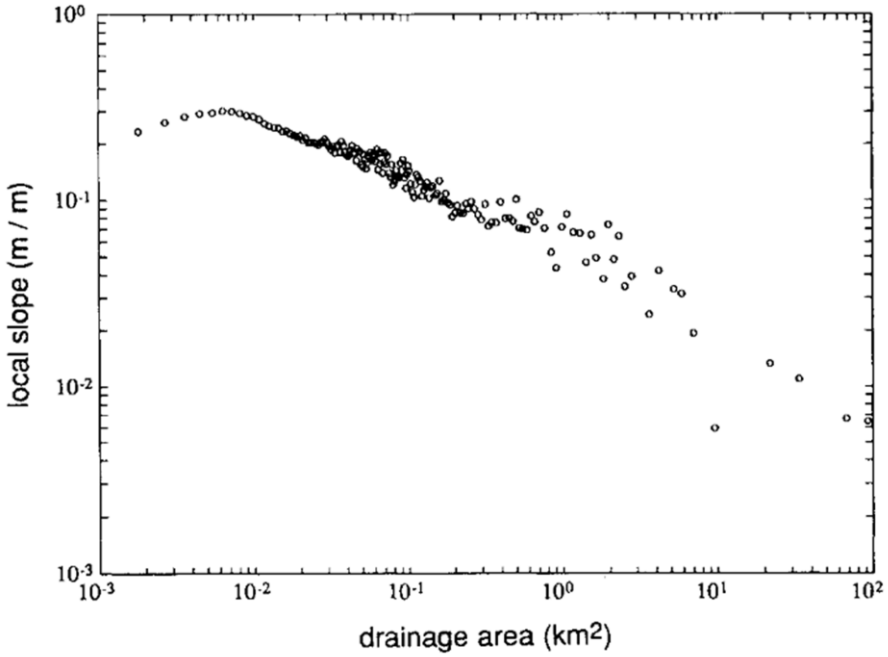

Figure 2: Averaged local slope versus contributing area plot for Schoharie Creek, New York (Montgomery and Foufoula-Georgiou, 1993).

appropriate contributing areas through scatterplot analysis of a DEM. For two separate mountainous basins, they show that plotting local slope against contributing area for each grid cell reveals discrete trends in the relationship that signify physical changes in persistent sediment transport process domains. First, there is a break from positive to negative slope of the relationship at low contributing areas (Figure 2). This is correlated to a change in sediment transport processes at the transition from hillslope to valley landforms, and the breakpoint contributing area they identified coincides with reasonable hillslope lengths for the study landscape. A break from less negative to more negative gradient is found at larger contributing areas, attributed to where alluvial channel processes begin to persist. In lower elevation soil-mantled landscapes, this positioning of channel heads will tend to vary over short timescales relative to bedrock dominated areas. The authors conclude that for their study basins in coastal

Oregon, coastal Northern California, and the Catskill Mountains of New York, DEM analysis cannot accurately locate current channel head locations and more involved methods are thus needed. Ijjasz-Vasquez and Bras [1995] analyzed the slope-area relationship on a pixel-by-pixel basis for an Alabama catchment and observed four regions of the scatterplot that were distinct in nature. When averaged using bins of at least 500 data points each and plotted on a log-log axis, they too found a reversal in the relationship from positive to negative gradient for hillslope to valley transitions at small contributing areas and an inflection between unchanneled valleys and alluvial channels at larger contributing areas. However, the authors also observed a domain between these two regions with a slope-area relationship of very little slope; they assumed that slopes below this region are in a fluvial channel domain, as in Willgoose [1989]. This flat portion is a result of the averaging procedure, where both channelized and unchannelized pixels of similar contributing area are found. This characteristic allowed them to identify a threshold for channel initiation by taking the diagonal of a quadrilateral formed by separate linear regression lines for each bounding region. The intersection of the diagonal and the data represents a useful flow accumulation threshold value (Figure 3). Henkle [2011] applied slope-area analysis to an extensive channel survey of the Colorado Front Range, finding that channel heads do generally coincide with the predicted regions.

Well-defined channel initiation thresholds may not be evident in regions where bedrock characteristics have greater influence on channel location. As such, other researchers have reproduced slope-area analyses for a variety of landscapes with mixed outcomes. Jaeger et al. [2007] studied locations of channel heads in two Washington state landscapes with basalt and sandstone lithologies and saw no significant slope-area relationship for channel initiation. They hypothesized that this was due to unknown subsurface characteristics and/or small sample sizes.

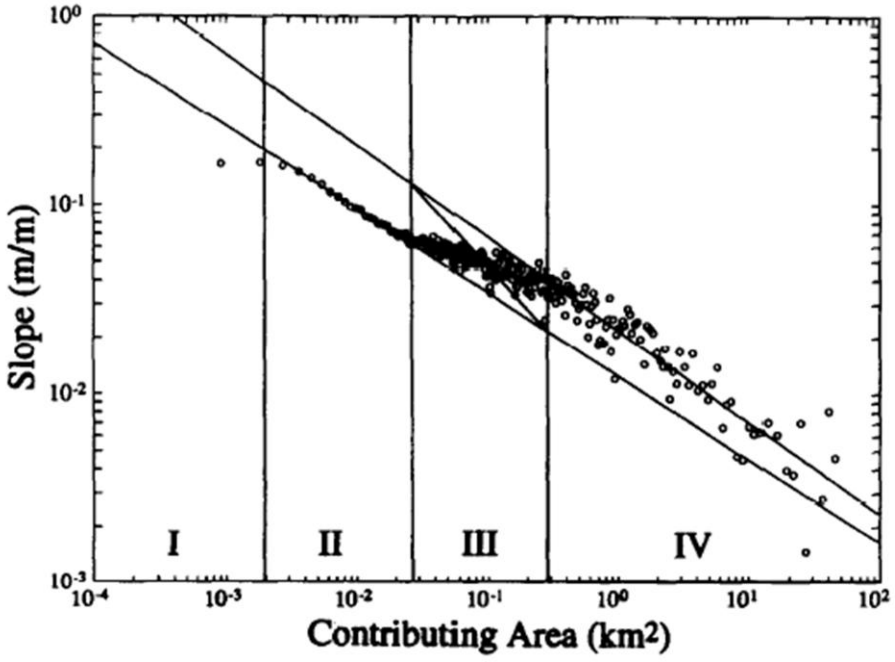

Figure 3: Log-log plot of averaged local slope versus contributing area showing process domains and region III threshold diagonal for Raccoon Creek basin, Pennsylvania (Ijjasz-Vasquez and Bras, 1995).

Heavily glaciated basins have a complex structure that is not solely controlled by fluvial erosion processes, as shown by Brardinoni and Hassan [2006], who examined channel networks in the coastal mountains of British Columbia that inherited their landscapes through glacial sculpting. Slope-area process domains of previous theory were found to hold on a fine scale in this area but were more segmented according to glacial landforms.

Several more intensive methods for estimating channel initiation have been developed, including a shear stress threshold method presented in Dietrich et al. [1993]. This model derived erosional thresholds which physically are a function of soil properties, precipitation, and topography but are estimated based on a ratio of soil transmissivity and runoff rate. Soil transmissivity was estimated with field data, and runoff rates were derived from characterizations of landscape curvature and associated assumptions for likelihood of saturation.

The authors then apply this ratio with a roughness coefficient to estimate a critical shear stress threshold for channel initiation. Spatially distributed boundary shear stress is calculated as a function of critical shear stress, precipitation, roughness, and slope. The authors conclude that a useful shear stress threshold can only be calibrated with a map of the complete observed drainage network. They do however propose a topographic threshold taking into account $\alpha_s * S^2$, where S = local slope. This approach has been applied with some success elsewhere (Orlandini et al., 2011). While these and other proposed channel initiation models (Passalacqua et al., 2010) are promising, we have chosen not to include them in this investigation.

Despite its common use for deriving channel networks, appropriate values for the contributing area threshold method have been found to vary widely for different basins. Channel heads may form from convergent overland flow, convergent subsurface flow, or landsliding, each of which may be controlled by upslope topography yet exhibit varying contributing areas sufficient for channel initiation (Montgomery and Dietrich, 1994). In all three cases, thresholds for channel initiation can be treated as a function of flow accumulation necessary to produce some critical pressure sufficient to mobilize sediment. Depending on local factors and the mechanisms of channel initiation such as physical soil characteristics or vegetative cover, appropriate values for a contributing area threshold may vary from basin to basin (Kampf and Mirus, in press), and often within a single basin (Passalacqua et al., 2010). In areas heavily influenced by geologic and subsurface piping, surface contributing area thresholds may provide little utility (Jaeger et al., 2007; Orlandini et al., 2011). This suggests significant limitations in applying a single threshold value for a given region or catchment, yet application of this approach is widespread because practical limitations often inhibit detailed field-based mapping of channel networks. In the setting closest to the study area for this thesis, Henkle et al. [2010]

recently characterized channel head initiation over a wide area of the Colorado Front Range and found an average contributing area threshold of 108,258m^2, although results display a wide variance in observed values. For channel heads mapped at elevation ranges similar to those of Loch Vale, an average contributing area of 129,372m^2 was observed. However, they note that the relationship between contributing area and channel initiation tended to break down in basins with steep hillslopes (>19%).

Topographic wetness indices

Topographic analyses have also been used to predict the spatial distribution of runoff generation. The topographic wetness index (TWI) was developed to predict areas of soil saturation and likely locations of overland flow for use in the runoff model TOPMODEL (Beven and Kirby, 1979). TWI is a function of contributing area and local slope, based on the assumption that locations with larger surface area contributing flow and shallower slopes are more likely to saturate and accumulate surface water. The index is generally expressed as

$$TWI = ln\left(\frac{\alpha_s}{\tan\beta}\right) \quad (1)$$

where α_s = specific contributing area, and tan β = local slope (Frankenberger et al., 1999; Sorenson et al., 2005). Also referred to as specific catchment area, specific contributing area is defined as the total upslope area contributing flow to a given location, divided by the specific contour length (Chirico et al., 2005; Galant and Hutchinson, 2011). The DEM cell edge length has been applied as the value for specific contour length in several terrain analyses (Zhang and Montgomery, 1994; Wolock and McCabe, 1995). TWI is commonly tested as a gridded predictor

of saturation excess overland flow (Western, 1999; Lyon et al., 2004; Lin, 2006), where higher index values represent areas more likely to saturate and produce overland flow from a uniform precipitation input event. We propose that areas of mountain headwater catchments regularly producing runoff via this process may be more likely to channelize, and thus there is the potential for using a characteristic TWI threshold for channel initiation in network derivation. A related concept has been applied for use in predicting stream channel locations based on research that found channel initiation to be closely correlated to areas producing saturation excess overland flow in humid landscapes (Dietrich et al., 1992; Dietrich et al., 1993; Montgomery and Dietrich, 1994). In many environments, the steepest portions of mountain headwater catchments have shallow soils, more sparse vegetation, and more mass wasting events which all serve to reduce the required contributing area threshold for initiation. Grayson and Western [2001] note that catchments where TWI can perform well as a predictor of runoff are rare. In short, TWI requires lateral flow, and they argue that there are a limited number of environments meeting the assumptions that allow for this. Environments with suitable characteristics are limited to a particular range of precipitation to evapotranspiration ratios, areas with relatively impermeable layers in the subsurface that promote lateral flow, and specific soil and vegetation characteristics. Similarly, Woods and Sivapalan [1997] conclude that TWI-based runoff models are most appropriate for "well-organized" networks of large area and whose form is a result of catchment-scale processes. Thus, TWI may not be a viable channel prediction method in more arid, rugged landscapes with a thin soil mantle.

Existing linear feature datasets

Channel networks can also be derived by digitizing channel locations from aerial imagery. A commonly available resource of vector hydrography is the NHD, for which water features were taken from aerial imagery and existing USGS topographic maps. This method contains inherent subjectivity in the representation of lower order channels based on map scale or visual interpretation, especially when channels are shielded from above by vegetative cover. Another widely available source with global hydrographic coverage is the World Wildlife Fund/USGS HydroSHEDS dataset. While covering an impressive global extent, HydroSHEDS layers were generated from a DEM with a resolution of 3 arcseconds (~90m) and a uniformly set flow accumulation threshold of 1000 cells, or about 8km^2 at the equator (Lehner et al., 2006). This methodology results in networks that include only high order channels and are not suitable for use in more detailed network mapping. Because of this, researchers have long cautioned against the use of such pre-existing line features for drainage analysis (Coffman et al., 1972; Scheidegger, 1966).

Effects of DEM spatial resolution

Variations in the reliability of topographic algorithms for channel network delineation are confounded by the effects of DEM spatial resolution. Wolock and McCabe [2000] examined the effects of 100m versus 1000m DEMs for 50 different locations throughout the United States, pointing out a loss of information and smoothing effect on terrain from 100m to 1000m. In a semi-arid Colorado basin, they found that the 1000m DEM had an increase in the ratio of cells exceeding the contributing area threshold, a decreased minimum slope, and an overall increase in TWI values. They also concluded that smoothing effects are more pronounced in steep terrain,

which is a dominant characteristic of our study area in the Colorado Front Range. Other studies have presented varying conclusions on the resolution of DEM that is most appropriate for channel network derivation. Montgomery and Foufoula-Georgiou [1993] concluded that a DEM with a resolution finer than 30m is needed to represent topographic characteristics essential to stream channel initiation in steep terrain. McMaster [2002] found deterioration in channel network derivation performance in DEMs larger than 180m for the Adirondack Mountains of New York state. Deng et al. [2007] found large variation in TWI values depending on DEM resolution, concluding that a resolution finer than 10m should be used for a rugged mountain landscape in Southern California. Zhang and Montgomery [1994] also found that a 10m resolution was necessary to represent steep terrain, adding that grid cell size should be at least as small as the typical hillslope length required for topographically driven process modeling. Orlandini et al. [2011] investigated the effects of DEM resolution on contributing area thresholds extracted to observed channel heads, and using 1, 3, 5, 10, 20, and 30m DEMs and found a predictable increase in threshold contributing area with grid cell size. Orlandini and Moretti [2009] suggest an appropriate grid cell size for flow path delineation of

$$h \leq 0.15A^{0.4} \tag{2}$$

where h is grid cell size and A is basin area in square meters.

The selection of appropriate DEM resolution is intimately linked to the issue of scale in hydrologic and landscape analysis. While investigating the processes most important to a given hydrologic response, the best DEM resolution will depend on both the scale at which these dominate processes operate as well as the nature of the problem being addressed. For example, coarse resolution data may be able to effectively capture important processes that are a function of glacial macroforms or catchment-scale controls dictating landscape structure. Fine resolution

data may instead be required to represent hillslope or microtopographic characteristics that might have substantial influence on the channel network development in rugged landscapes. When considering the scale associated with the problem of interest, forest hydrologists aiming to study the relationship between headwater channel development and upland forest structure may require a fine resolution DEM to parse out important variables in a small 1 km^2 headwater catchment, whereas urban water resource managers may only need a coarse 30m DEM to accurately model discharge from a larger 5,000 km^2 basin at downstream outlets far removed from remote headwater catchments.

2. Study Site

Loch Vale is a 7.3 km^2 watershed in northern Colorado's Front Range within Rocky Mountain National Park. The watershed ranges in elevation from 3110m at the outlet to 4192m at its highest point along the Continental Divide. Loch Vale's geology is characterized by heavily glaciated terrain, which has formed U-shaped valleys bounded almost entirely by steep cliffs with extremely porous talus and thin soils covering the lower side slopes and valley floors (Figure 4). Because the topography at Loch Vale is inherited from a glaciated past, at the catchment scale current geomorphic processes shaping the landscape persist as secondary influences within pre-existing glacial troughs. Basins of this nature tend to exhibit altered geomorphic domains, often related to the existence of hanging glacial valleys, that are in apparent disequilibrium with general theories of colluvial and fluvial systems (Brardinoni and Hassan, 2006; Weekes, 2009). Eastwardly flowing Andrews Creek and Icy Brook are the main stream channels, and both streams are partially fed by glacier remnants. Andrew's Creek converges with Icy Brook, which then feeds a 0.053 km^2 lake that drains to the basin outlet. Vegetation is primarily made of up of subalpine fir (*Picea engelmanii*) and Englemann spruce (*Abies lasiocarpa*) forest in the lower valleys. Higher elevations consist of alpine vegetation or exposed bedrock (Clow et al., 2003). The annual hydrograph at Loch Vale is snowmelt dominated. On average, the watershed receives 105cm of annual precipitation, with about 62% falling between October and April. The winter preceding our channel network survey was unusually wet, with 104.7cm of precipitation measured from October through April alone (NADP, 2012).

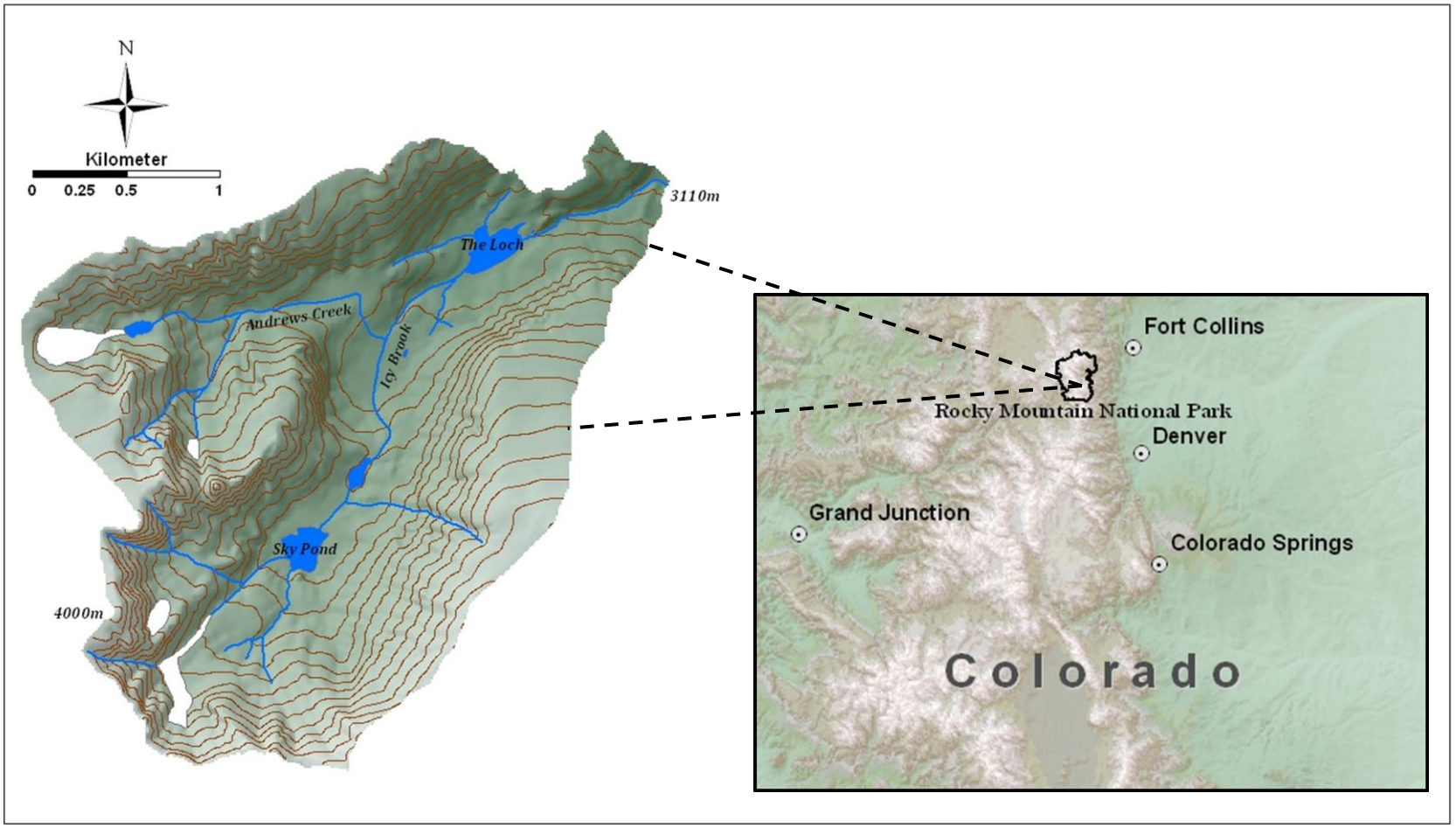

Figure 4: Loch Vale study site, Front Range Colorado, USA.

3. DEM Analysis

3.1. Methods

For the DEM analysis we calculate and compare slope, contributing area, and TWI for 1, 10, and 30m DEMs with both flow algorithms. We then plot contributing area and local slope for the 1m DEM to look for any systematic relationships that can be used to identify potential topographic thresholds for channel initiation.

Elevation data source

Three DEMs with grid cell sizes of 1x1, 10x10, and 30x30m are used for analysis. We reference each DEM by its cell edge length, e.g. "the 10m DEM". The 1m DEM was collected via an airborne LiDAR sensor flight commissioned by the USGS. Data were collected during August 2010 for Grand County, Colorado and some portions of nearby Larimer and Park counties, including Loch Vale. Elevation data were collected and delivered in the Universal Transverse Mercator (UTM) projected coordinate system for zone 13, using the 1983 North American Datum (NAD). Vertical accuracy is reported to meet a 15cm standard. At 95% confidence level, horizontal accuracy is estimated to be at or below 1.04cm in both easting and northing coordinates for quality control checks against ten separate base stations. This dataset is publicly available through the USGS Center for LiDAR Coordination and Knowledge. Both 10 and 30m DEMs are also available for Loch Vale from a variety of public sources, including the NED. However, in order to isolate the influence of grid cell size from those associated with the vertical and/or horizontal accuracy of original elevation data collection methods, the 10 and 30m DEMs were created in ArcGIS by resampling the 1m DEM with the commonly used nearest neighbor technique, which assigns an elevation value to the pixel based on that of the nearest

input value, thereby maintaining real elevation values of the original dataset. Bilinear interpolation and cubic convolution are other common resampling methods, but have been shown to result in a greater degree of terrain smoothing due to averaging of neighborhood elevation values (Le Coz et al., 2009; Wu et al., 2008).

Data processing

To investigate the effects of DEM resolution on overall terrain characteristics, each of the three DEMs were processed in the following series steps. First, we preprocessed them to remove sinks, which represent areas of isolated depression that prevent the flow algorithms from moving accumulated overland flow down slope. In terrain analysis for hydrological applications sinks are often treated as spurious artifacts of DEM production, although it is important to note that DEM data may include sinks that are in fact natural features, especially in glacial terrain and with the use of a fine resolution DEM (Temme et al., 2005). The existence of natural sinks is likely to increase in steep basins that experience "damming" as a result of landslides and debris flow. Ultimately, the utilization of depressionless DEMs may result in less attenuated simulated hydrographs and decreased sedimentation in transient soil distribution models (Temme et al., 2005). The removal of sinks is required for the flow routing methods tested in this study to resolve flow directions and produce a valid flow accumulation grid, and thus we include this step here while acknowledging the aforementioned considerations. Next, we calculated each of the input variables for TWI (Equation 1). Local slope ($\tan \beta$) of each cell is calculated within ArcMap as percent rise by taking the vertical and horizontal directional derivative to find direction of and maximum difference in elevation between neighboring cells divided by the

distance between the cell centers. It is converted to percent rise by multiplying the value by 100. Conceptually, this can be expressed as

$$\tan\beta = \left(\frac{\Delta z}{\Delta L}\right) \times 100 \tag{3}$$

where

$$\Delta z = \sqrt{\left(\frac{dz}{dx}\right)^2 + \left(\frac{dz}{dy}\right)^2} \tag{4}$$

and ΔL is the horizontal distance between cell centers. Percentages can range from 0.00 for flat areas, 100.00 for 45° slopes, and approach infinity when vertical. By determining the direction of steepest descent, this step inherently determines flow direction. To allow for calculation of a TWI, we changed flat cells with slopes of zero to a small arbitrary slope ($5x10^{-7}$). This approach has been used in similar studies (Wolock and McCabe, 1995; Wolock and McCabe, 2000) and is based on the assumption that even water flowing to flat cells eventually reaches the basin outlet. D∞ slope was calculated in the RiverTools DEM software package as rise/run, as described in Tarboton et al. [1997], and imported into ArcMap. Slope values were then multiplied by 100 to convert to percent rise.

To calculate specific contributing area (α_s), we computed flow direction with the D8 algorithm in ArcMap's ArcHydro toolset as well as the D∞ algorithm within RiverTools. These two flow direction algorithms are applied for each DEM. The resulting flow direction rasters were then used to calculate a total of six contributing area rasters created by summing the number of cells contributing flow to the target cell and adding a value of 1 to include the target cell's area and ensure valid TWI calculations. Finally, α_s was calculated as the number of

contributing cells (Fac) multiplied by the area of each cell (L^2), and divided by the length of the cells (L) within the DEM (Equation 5).

$$\alpha_s = \frac{Fac * L^2}{L} \quad (5)$$

Analysis

To compare topographic variables between DEMs, we calculated summary statistics and cumulative frequency distributions of tan β, ln(α_s),, and TWI for the 1, 10, and 30m rasters using both D8 and D∞ flow direction algorithms.

Additionally, following the methodologies outlined in Montgomery and Foufoula-Georgiou [1993] and Ijjasz-Vasquez and Bras [1995], upslope contributing area was plotted against local slope for each grid cell to identify distinct process domains evident in the nature of the relationship between the two variables. For this analysis, actual contributing area is used in lieu of specific contributing area, as this is the default input parameter for defining channelized pixels within most GIS toolsets. Keeping with convention, slope was analyzed in the form m m^{-1}. Data for this plot were extracted from the 1m DEM because it provides the resolution necessary to capture the fine-scale topographic complexity at Loch Vale. McMaster [2002] found that slope and contributing area grids derived using D∞ flow partitioning more accurately represented slope-area relationships, and thus this flow partitioning algorithm was applied here. When plotting over 7.3 million data points from the 1m DEM, tremendous scatter in the data results. In order to observe overall trends in the relationship both variables were log transformed, first adding a value of 1 to each slope to avoid values of 0 becoming infinity after transformation. Data points were then averaged by taking the mean corresponding slope for 0.1m^2 bins of contributing area values. This reduced the number of data points to 159. After transformation,

two-phase linear regression analysis was performed to identify a breakpoint in the slope-area gradient that represents a threshold between unchanneled and channelized pixels. This was found by searching for the equations of two regression lines, applied separately to some division of our data, that meet to form a breakpoint and minimize the sum of squared residuals (SSR) between the data points and regressions (similar to regression lines found in Figure 1). This was followed by a bootstrapping procedure to test the null hypothesis that the change in the slope of the regressions at the breakpoint is not significant, based on a significance level of 0.05. If the resulting p-value is < 0.05, we reject the null hypothesis and accept the break as statistically significant. The corresponding flow accumulation value at the breakpoint can then be used as a threshold value ($T\alpha$) to define channelized pixels later in the analysis. We also applied the method outlined above from Ijjasz-Vasquez and Bras [1995] that identifies a threshold value in terrain that has a more complex slope-area relationship. Here we visually identified regions with trends of distinctive gradient. A transition point was extracted from the diagonal of a quadrilateral formed when linear regressions for regions II and IV are connected. The intersection of this diagonal with the data signifies a flow accumulation threshold for channelization.

3.2. Results

DEM resolution and flow partitioning algorithm

Because DEMs use a single elevation value to represent the entire area of a grid cell, terrain smoothing occurs as cell area increases, resulting in an inherent loss of topographic information. This effect is demonstrated in Figure 5, which shows the elevation profile extracted

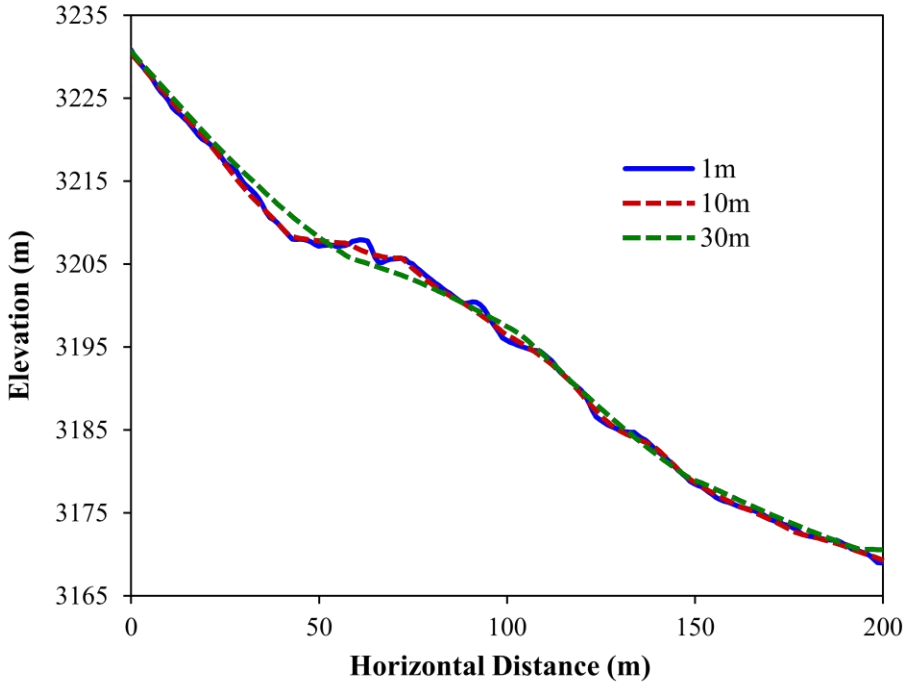

Figure 5: Elevation profile of a Loch Vale hillslope with horizontal distance of 200m. Y-axis is displayed with a 2.5:1 vertical stretch.

in ArcMap from a Loch Vale hillslope transect with a horizontal distance of 200m. The loss in topographic detail can be seen as variations at a 1m resolution are smoothed out with coarser DEM resolution.

Spatial resolution has the same effect on other topographic parameters derived from the original DEM. Upon visual inspection, the influence on the spatial distribution of topographic parameters is striking (Figures 6a-c). Changing resolution from 1 to 10m results in a significant loss of detail in spatial patterns of slope, specific contributing area, and TWI. For the 30m DEM these patterns become essentially unrecognizable. Potentially important hydrologic processes occurring at sub-cell length scales cannot be captured. Over very large areas with more moderate slope, this may not be an issue, and computer processing limitations could outweigh the need for fine discretization. However, as previously indicated fine resolution topographic data may prove

essential for deriving accurate runoff networks in basins as steep and rugged as Loch Vale. At first glance, both contributing area and TWI seem to represent realistic flow patterns (Figures 6b-c). This intuitively reinforces the current reliance on easily derived topographic parameters for creating stream networks. The D∞ flow partitioning algorithm offers a visual improvement over the idealized network derived from D8, as evident in the more natural spatial patterns of contributing area and TWI. By allowing runoff to flow into more than one adjacent cell, D∞ better represents the braided and often divergent nature of observed flow networks.

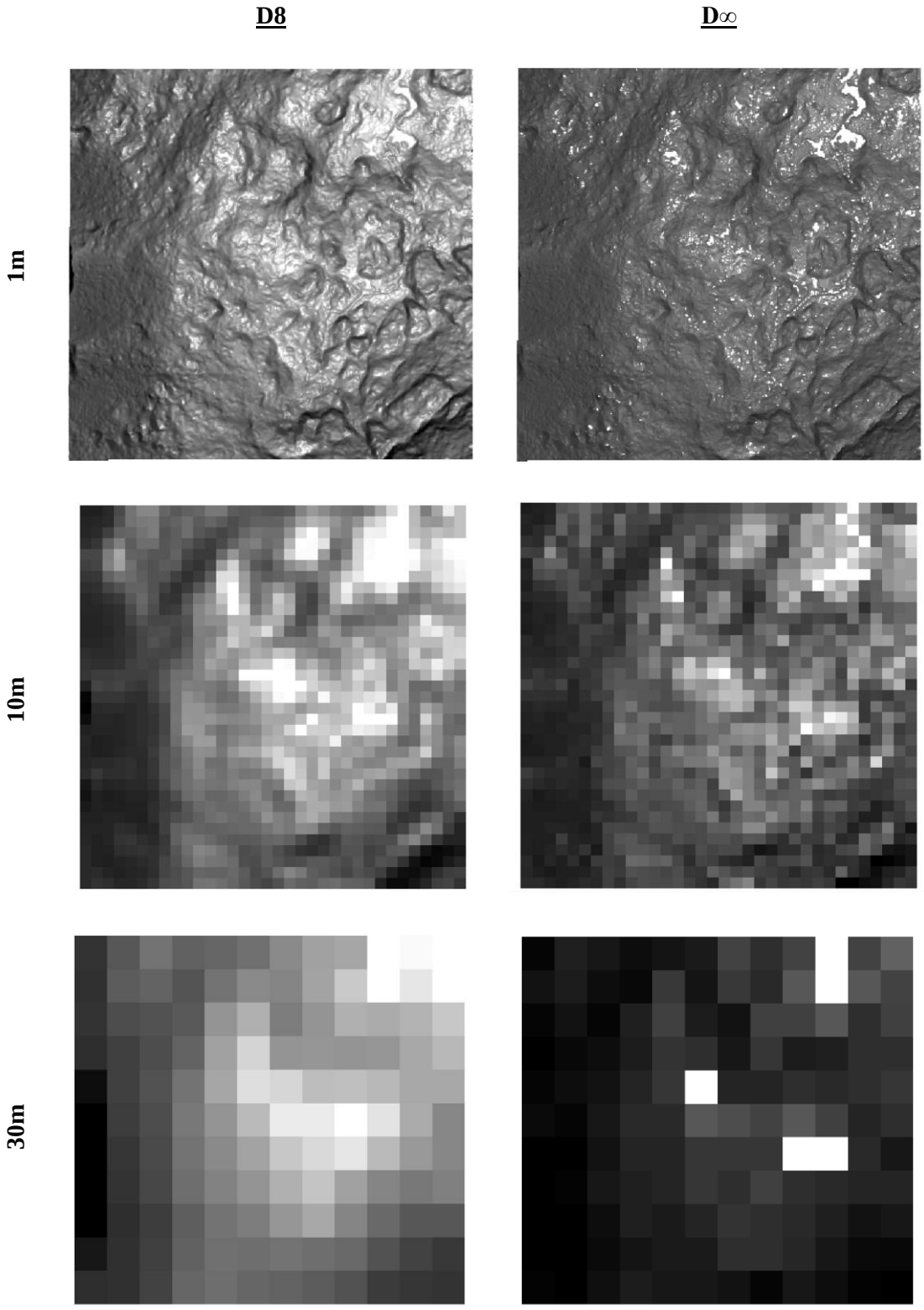

Figure 6a: Images of ln(tan β) for a 0.12km^2 portion of Loch Vale. Darker pixels represent higher values.

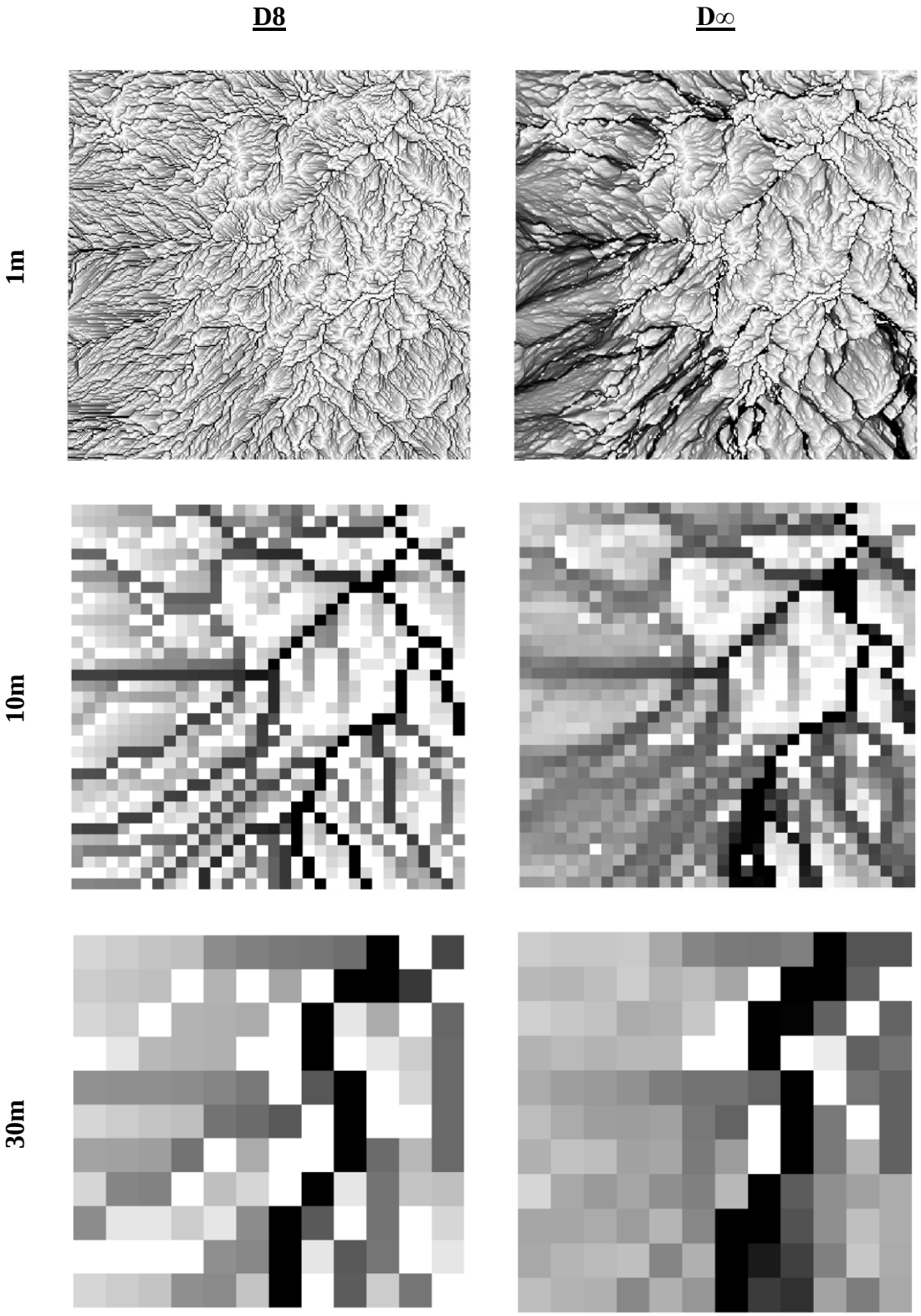

Figure 6b: Images of $\ln(\alpha_s)$ for a 0.12km^2 portion of Loch Vale. Darker pixels represent higher values

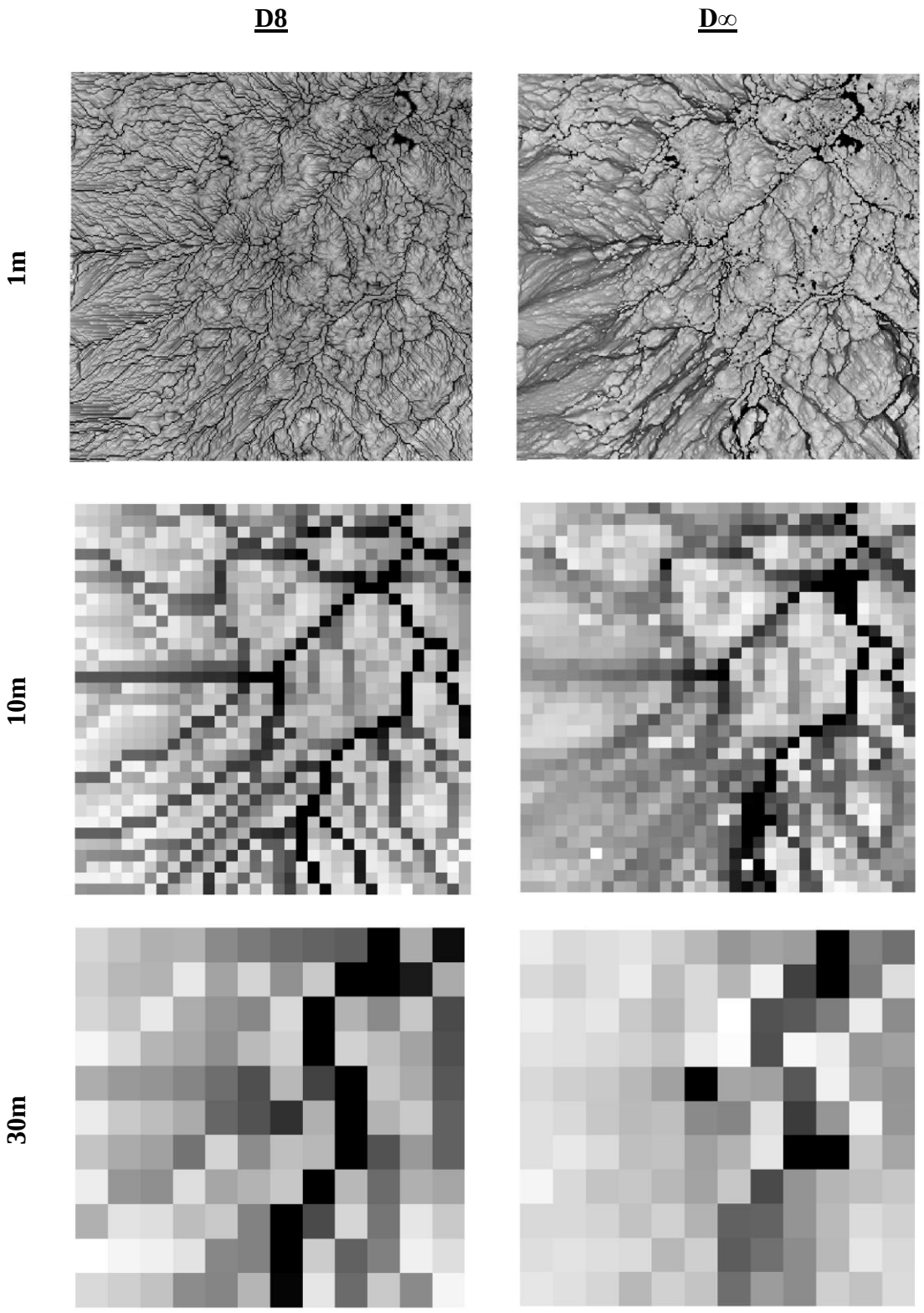

Figure 6c: Images of TWI for a 0.12km^2 portion of Loch Vale. Darker pixels represent higher values.

Table 1: Summary statistics of topographic parameters for 1, 10, and 30m DEMs using D8 and D∞ flow partitioning. $T\alpha_4$ symbolizes the NHD averaged contributing area threshold of 40,485m^2, and $T\alpha_5$ the averaged contributing area threshold of 129,372m^2 from Henkle et al. [2010], with values indicating percentage of basin area exceeding the threshold.

		ln(tan β)			**ln(α_s)**					**TWI**		
		Mean	Max.	Min.	Mean	Max.	Min.	% $\geq T\alpha_4$	% $\geq T\alpha_5$	Mean	Max.	Min.
D8	**1m**	3.80	8.61	-14.51	2.11	15.81	0.00	0.31	0.13	-1.69	30.32	-8.52
	10m	3.88	6.67	-14.51	4.09	13.50	2.30	3.00	1.27	0.21	27.89	-4.37
	30m	3.92	5.85	-14.51	4.95	12.41	3.40	9.56	3.89	1.03	26.79	-2.45
D∞	**1m**	3.71	9.26	-14.51	3.25	15.81	0.00	0.32	0.15	-0.46	30.32	-9.21
	10m	3.76	7.32	-14.51	4.61	13.50	2.30	2.91	1.45	0.21	27.89	-4.37
	30m	3.62	6.29	-14.51	5.25	12.41	3.40	9.00	3.99	1.63	26.91	-2.81

The statistical effects of DEM resolution and flow partitioning algorithm on topographic parameters are presented in Table 1. Summary statistics of TWI and log-transformed tan β and α_s for the 1, 10, and 30m DEMs were calculated using both the D8 and D∞ flow partitioning algorithms. For D8, as DEM cell size increases mean slope increases. While the effect is slight, it is notable in contrast to findings of prior studies (Wolock and McCabe, 2000; Zhang and Montgomery, 1994). The positive relationship at Loch Vale could be due to a greater degree of ruggedness where isolated areas of little to no slope are averaged into larger cells, as opposed to rolling terrain with continuous slopes. Maximum slope generally decreases with greater cell size for both D8 and D∞ as a result of smoothing. Minimum ln(tan β) is a function of the derivation methodology applied, with minimum possible slope specified as $5x10^{-7}$. Although the mean and maximum values of ln(tan β) change with DEM resolution, the cumulative frequency distributions for slope are nearly the same for all resolutions (Figure 7).

DEM resolution has the largest effect on $\ln(\alpha_s)$, a finding that is consistent with prior studies (Montgomery and Foufoula-Georgiou, 1993; Zhang and Montgomery, 1994; Wolock and McCabe, 2000). Mean $\ln(\alpha_s)$ nearly doubles from 1m to the other DEMs, while its cumulative frequency distribution shifts substantially out towards higher values with coarser resolution. There is a small shift in $\ln(\alpha_s)$ between 10 and 30m, but is not as large as the shift between the 1 and 10m DEMs. This is also exhibited by an order of magnitude increase from the 1 to 10m DEM in the percentage of basin area exceeding both the NHD averaged $T\alpha_4$ of 40,485 m^2 and the Henkle et al. [2010] observed average $T\alpha_5$ of 129,372 m^2. Because TWI is a function of both $\tan \beta$ and α_s, these effects translate to an overall increase in TWI values. Mean TWI and its cumulative distribution both increase with cell size, with the largest shift from 1 to 10m resolution with D8.

When comparing flow algorithms, D∞ results in lower mean $\ln(\tan \beta)$ and higher mean $\ln(\alpha_s)$ for all DEMs. D∞ also produces generally higher mean TWI, with the exception of the 10m DEM which showed no change. Effects from flow algorithm are less apparent for cumulative frequency distributions, and there is only a slight increase in the percentage of area exceeding the contributing area thresholds.

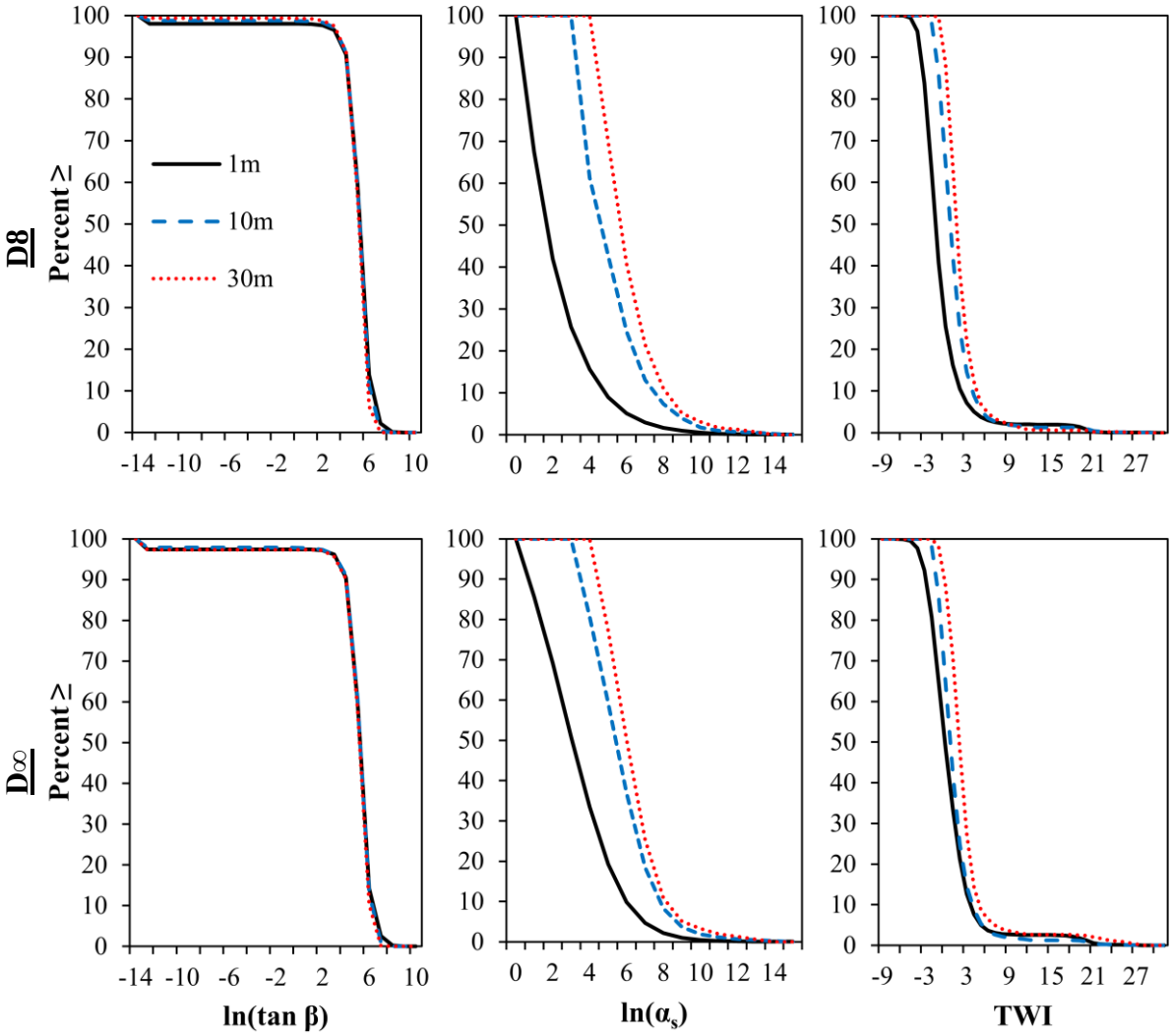

Figure 7: Cumulative frequency distributions of topographic parameters for Loch Vale DEMs of 1, 10, and 30m resolution.

Slope-area relationship

Our plot of averaged slope vs. contributing area for the 1m DEM of Loch Vale shows that local slope generally varies inversely with contributing area (Figure 8a), as found in other studies. Analysis of breakpoints in this plot demonstrates a more complex relationship, with gradient varying systematically over four distinct regions of the plot (Figure 8b). Such regions are indicative of different sediment transport process domains. Region I is characterized by a

positive slope at low values of contributing area with an inflection at approximately 1.55m^2 on the x-axis. This positive to negative inflection has been said to represent a transition from convex to concave slope profiles, or hillslopes to valleys. Here, this corresponds to a contributing area of only 4.7m^2, or hillslope lengths of 4.7 m, which is more representative of microscale topographic features rather than a hillslope length scale. After this inflection, Region II exhibits a moderately negative gradient that could be representative of unchanneled valleys. At high contributing areas, Region IV is characterized by a break to more negative gradient. This difference in behavior between regions II and IV has been attributed in prior studies to the difference between unchanneled and channelized domains (Tarboton, 1989; Montgomery and Foufoula-Georgiou, 1993; Ijjasz-Vasquez and Bras, 1995). A transitional region III with low negative gradient is likely a product of our averaging procedure, which contains slope values averaged from both channeled and unchanneled pixels. Within this region likely lies some threshold value above which there is sufficient contributing area to initiate channelization (Ijjasz-Vasquez and Bras, 1995). The results of a two-phase regression analysis identify a breakpoint representing a potential contributing area threshold to be within region III at $\ln(\alpha) = 7.3m^2$, translating to a total contributing area threshold of 1480.3m^2 (Figure 8b). Bootstrapping analysis confirmed this to be significant at a 0.05 level, with a calculated p-value = 0.0461 (Table 2). Note that this procedure is rooted in analysis that suggests a single breakpoint in the data exists that can be interpreted as the threshold between unchanneled and channeled valleys (Tarboton, 1989; Montgomery and Foufoula-Georgiou, 1993). Thus, the calculated breakpoint of 1480.3m^2 does not visually coincide with the multiple breakpoints seen in the binned data plot, although it does fall within the transitional region III suggested by Ijjasz-Vasquez and Bras, [1995] to represent a transition from unchanneled to channelized grid cells. Linear regression lines calculated separately for

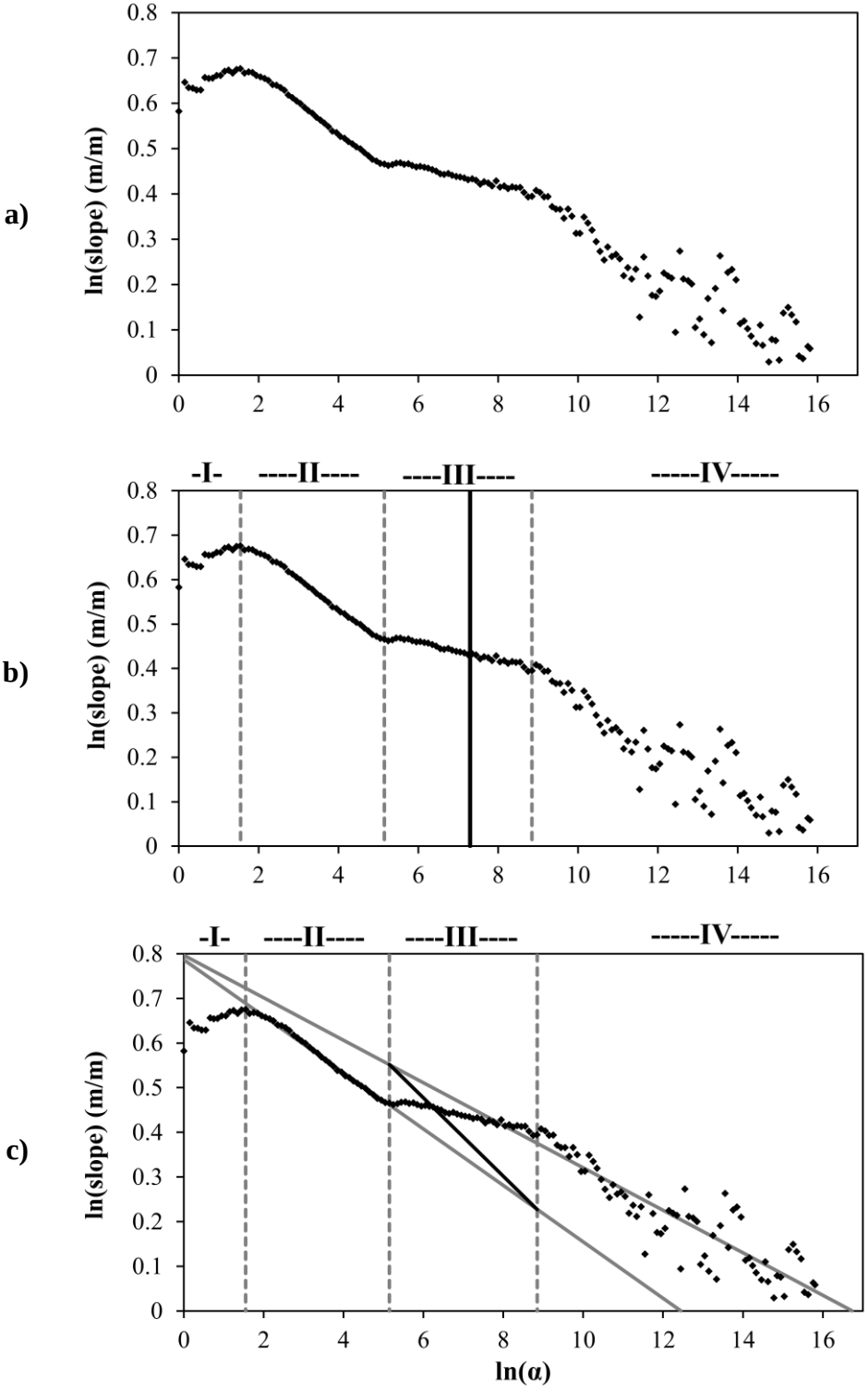

Figure 8: Slope-area plot with averaged data points derived from 1m DEM using D∞. Process domain regions separated by vertical dashed lines are included in b) and c). The solid line in b) is the breakpoint calculated with two-phase linear regression. For c), the breakpoint is found at the intersection of the diagonal with the data in region III.

Table 2: Results of two-phase linear regression on slope-area plot derived from 1m DEM using D∞.

n	Calculated Breakpoint	SSR	Significance Level	Calculated p-value
159	$7.3m^2$	0.211	0.05	0.0461

regions II and IV form a quadrilateral with the vertical lines separating the regions (Figure 8c). The diagonal through region III would represent the statistical divide between the unchanneled and channelized areas following the method of Ijjasz-Vasquez and Bras [1995]. This divide corresponds to a contributing area threshold of $468.5m^2$.

3.3 Discussion

DEM resolution and flow partitioning algorithm

Using the NHD and the Henkle et al. [2010] *T*α values as examples in Table 1, we see that if a singular contributing area threshold is applied to an entire basin, a coarser DEM will generally result in a large increase in the percentage of cells defined as channels. Also, increasing TWI values with cell size suggests that using a coarser DEM will result in more area being likely to saturate. Hydrologically, this means that when modeling saturation excess overland flow using TWI, the water table will intersect the land surface over a larger percentage of the basin during a given precipitation event. The same is observed for using D∞ when compared with D8. Routing an order of magnitude more water as channelized flow rather than diffuse overland or subsurface flow will result in shorter lag-to-peak and higher overall peaks in modeled hydrographs. With sufficient discharge data, it may be possible to analyze many

different DEMs for predictable effects of grid cell size on hydrograph response in a given basin, permitting the development a calibration equation to improve performance when finer resolution data are unavailable or infeasible.

Because applying singular topographic thresholds is so common when deriving channel networks, it is important to consider the nature of the landscape when determining appropriate DEM resolution. In steep rugged landscapes, microscale topographic features may be important controls on hydrologic processes. We have shown that increasing precision of landscape discretization at Loch Vale improves the ability to represent recognizable spatial patterns and also results in shifts of parameter distributions that are not found between the 10 and 30m DEMs. Considering this as well as the typical hillslope lengths and scale of hydrologic processes at Loch Vale, for the three DEMs examined we suggest that a 1m resolution is most appropriate when deriving hydrologically important parameters from topography.

The visual improvement of D∞ over D8 flow partitioning is marked, with evidence of increased cumulative parameter distributions. The eventual influence of flow algorithm on positional accuracy of networks will be addressed later in this investigation. For runoff modeling purposes, one could hypothesize that the relative importance of flow partitioning is less for steep slopes that tend to have more unidirectional flow, as found by McMaster [2002]. Again, further research into the effects of flow partitioning algorithm on hydrograph response may identify predictable relationships. Quantification of hydrologic response is not explicitly addressed in this study but does represent an area for future investigation.

Slope-area relationship

When examining the relationship between averaged contributing area and local slope, the data at Loch Vale exhibit the systematic relationship identified in studies of other landscapes. We identified three distinct process domains defined by the slope-area plot, similar to the process domains previous researchers have attributed to hillslopes, unchannelized valleys, and channelized alluvial domains; however, the hillslope length identified in this analysis is quite small and likely not a good indicator of most hillslope lengths in Loch Vale. Two-phase linear regression and visual analysis of the plots give us predicted contributing area thresholds for channel initiation of 1480.3 and 468.5m^2, respectively. These values are also considerably smaller than potential thresholds encountered elsewhere, and as a consequence suggest either that channel networks are much denser than predicted in prior studies or that the plot-derived thresholds do not accurately capture the transition to channelization in Loch Vale. As applied to our D∞ cumulative frequency distribution for $\ln(\alpha_s)$, these thresholds predict that 8.84% or 3.71% of the basin grid cells will be represented as channelized in the 1m DEM. This is likely to have a significant effect on hydrographs when routing flow in a runoff model.

The smaller predicted contributing area thresholds in our analysis may be the result of several factors. First, the topographic signatures identified here might persist in reality but the location of channel heads may be more significantly controlled by subsurface processes. These subsurface controls would not be represented in the slope-area relationship. Also, prior analyses of the slope-area relationship used DEM resolutions generally only as fine as 30m (Tarboton et al., 1991; Montgomery and Foufoula-Georgiou, 1993; Ijjasz-Vasquez and Bras, 1995; McMaster, 2002; Brardinoni and Hassan, 2006). By using a 1m DEM it is possible the signatures we see here are from microtopographic landscape features whose form exists below the scale of

processes controlling landscape and channelization structure. Finally, it is possible that the glaciated terrain of Loch Vale is fundamentally different than those environments where a slope-area relationship was found to accurately depict channel initiation thresholds. In glaciated terrain of Loch Vale, the distribution of slope-area regions may not be a straightforward translation to corollary landforms on a map, as most prior research on identifying thresholds from slope-area plots did not consider the role of glacial landforms. Current geomporphic processes are operating secondarily to pre-existing glacial macroforms which shifts the traditional structure of geomorphic process domains typically seen with increasing contributing area. One study of glaciated landscapes in British Columbia found that hillslope and valley landforms have a different geomorphological relationship than more "idealized" rolling topography (Brardinoni and Hassan, 2006). In fact, a slope-area relationship may only be predictive of channelization thresholds in terrain that is naturally smooth, or where terrain features have been forcefully smoothed due to coarse DEM representation of the landscape.

Nonetheless, because the shape of the slope-area relationship is similar to those identified in previously validated methods, the thresholds we have identified may be of significance. We test these thresholds for Loch Vale and how the predicted values translate to the accuracy of derived channel networks in Chapter 5.

4. Observed Channel Network Analysis

4.1 Methods

Locations of the actual channel network at Loch Vale were collected to examine the influence of topographic variables on real world channel heads within the basin and test the effects of DEM resolution and derivation methods on the accuracy of derived networks. During the summer of 2011 (July – October) a field survey was conducted to map the location and extent of channels within the lower portion of the Loch Vale watershed. This area stretches from the Loch outlet to the top of Andrews Meadow towards the northwest, below Timberline Falls along Icy Brook towards the southwest, and the eastern end of The Loch. Because of time and safety considerations, our targeted area could only cover a sub-set of the watershed. For our study, a channel was considered any fluvially eroded area that has visible indications of current or past concentrated flow within steepened banks (Montgomery and Dietrich, 1989). Reaches of channels that transitioned into unchannelized but consolidated overland flow were also included as points in the survey. This is necessary due to the large amount of exposed bedrock throughout Loch Vale. Many continuous flow paths proceed downslope with spatially discontinuous sections flowing over bedrock where channelization is hindered. An inability to access the highest portions of the catchment and those made up of extremely steep trough walls represents likely sampling bias in our field data collection. We recognize this, but saw it as unavoidable under the scope of this investigation. As a result, most of the surveyed channel data was confined to valley bottoms which potentially neglect colluvial and bedrock channels. This limits an analysis of channel heads as applied to a catchment-wide slope-area plot and the subsequent relation to geomorphic process domains. Given our applied definition of a channel and the

practical implications of this study for various hydrologic applications, our field survey can still inform a better understanding of high-elevation headwaters and the specific objectives addressed here.

To obtain a digital map of the reference network, we collected NAD 1983 projected UTM coordinates with a Trimble GeoExplorer handheld GPS unit at the furthest downslope point along a flow path and approximately every 5 to 10 meters along the length of each feature, up to and including the point of channel initiation or overland flow (whichever was observed to be furthest upslope). Each GPS location was averaged over 10-50 readings to achieve a sub-meter horizontal accuracy after differential post-processing correction. GPS points were also taken periodically along the main reaches of Icy Brook.

The rugged forest terrain at Loch Vale presents issues with accessibility and maintaining GPS satellite coverage. Collection of continuous reference line features was not feasible, so a robust sample of points was obtained instead. Linear and point features were generated from these data to use as reference features for analyzing spatial accuracy of predicted channel networks.

Additional observable characteristics were recorded at each channel head, including photographs of channel initiation points, upslope land cover type (rock or soil/vegetated), presence or absence of flow, and formation process – convergent overland flow (cof), convergent subsurface flow (csf), or landsliding (L). Evidence of convergent overland flow includes vegetation directed downslope and/or debris deposited immediately above the channel head, while landsliding can be interpreted from obvious signs of mass wasting. Convergent subsurface flow is characterized by a lack of either of the previous signs and/or the presence of seepage (Jaeger et al., 2007).

After digitizing and overlaying GPS points onto our 1m D∞ rasters, we extracted variables of tan β, α_s, TWI, aspect and elevation for each point. Here we use D∞, as this was shown in McMaster [2002] to be superior when calculating upslope contributing areas in a high relief mountainous study area. While it is possible to estimate contributing area and slope from field observations, in many instances the only practical method is to extract these from a DEM in a GIS. Channel formation process and dominant upslope land cover type attributes were also added to each channel head. We divided points into categories according to these attributes and calculated the corresponding mean contributing area and TWI for each category. Analysis of variance (ANOVA) was used to test for a meaningful difference between categories in mean contributing area and TWI, and a Scheffe test was conducted to identify which specific groups varied significantly from one another. We also plotted channel heads on our slope-area figures to see how they relate to predicted geomorphic process domains. Lastly, we compared contributing area and TWI summary statistics as extracted from our 1, 10, and 30m rasters.

4.2 Results

Field survey

A field survey produced 242 individual GPS points of observed channels within the targeted area at Loch Vale. These points were digitized into vector line features representing 41 individual flow paths. Of the surveyed points, 30 are identified as channel heads (Table 3), many of which begin as flow emerges at the base of talus fields. Figures 9 and 10 display maps of survey results. A complete list of surveyed points is included in Appendix A. The alphanumeric Point ID convention was developed to assign unique identifiers to each reach and GPS point, but

it is not based on any stream ordering methodology. The first letter indicates whether the channel is a tributary to Icy Brook (A) or Andrew's Creek (B). Subsequent letters increase for tributaries (and their tributaries) as we moved upstream during GPS point collection. Numbers indicate the GPS point with 01 being the furthest downslope point (often at a confluence).

We observed the channel network at Loch Vale to be quite complex, with disjointed stream segments and many localized areas of ground saturation. The geologic and glacial influences at Loch Vale have resulted in the development of many subsurface cavities through loose talus. Eleven channel heads were observed at points of exfiltration from talus or exposed bedrock fractures ("rock"), while the remaining nineteen developed in soil and/or vegetated land cover. Figure 11 shows pictures of each of these types of channel heads, with a complete collection of pictures for all channel heads found in Appendix B. Soil piping was also prevalent, and in several instances flow would emerge from the subsurface, proceed as channelized flow downslope, and then disappear to the subsurface only to again emerge downslope along a single flow path. Of the surveyed points, 82.9% were characterized as channelized flow (CF), 14.5% as flow without channelization (F), and 2.6% as channels with no observed flow (C). For observed channel heads, we noted 21 to be a product of convergent subsurface flow, 8 of convergent overland flow, 1 that was inactive and too overgrown to be characterized, and none with unmistakable signs of mass wasting.

Table 3: Data for observed channel heads at Loch Vale.

Point ID	Feature Type	Channel Head Formation Process	Elevation (m)	Aspect	α_s	tan β	TWI
Aa01	CF	cof	3107.8	S	7312.49	11.01	6.50
Ab03	CF	csf	3110.9	E	9.55	2.12	1.50
Ac03	CF	csf	3109.5	S	2.41	20.10	-2.12
Ad05	CF	csf	3117.8	S	120.96	17.99	1.91
Ae06	CF	cof	3122.4	S	9918.42	20.00	6.21
Ah09	CF	cof	3149.5	S	1.00	8.53	-2.14
Ak06	CF	csf	3154.3	S	1.39	20.26	-2.68
Aka02	CF	csf	3153.3	N	4.41	15.55	-1.26
Al16	CF	csf	3164.7	N	1.69	4.23	-0.92
Am03	CF	csf	3161.5	S	1.57	9.23	-1.77
Ama06	CF	csf	3163.3	N	823.17	11.18	4.30
An14	CF	csf	3164.5	E	6.36	50.00	-2.06
Ao07	CF	csf	3160.0	E	35531.50	5.00	8.87
Ap17	CF	cof	3180.9	E	5.69	4.13	0.32
Apa08	CF	cof	3165.2	N	47.80	15.01	1.16
Apb08	C	cof	3173.2	E	18.26	16.28	0.11
Apc05	CF	csf	3175.9	N	3.27	16.97	-1.65
Apca03	CF	csf	3175.0	N	787.95	14.33	4.01
Aq16	CF	csf	3182.4	W	2613.36	15.81	5.11
Aqa06	C	unknown	3179.8	W	24.48	13.43	0.60
Ba03	CF	csf	3174.2	E	69.56	28.99	0.88
Bb05	CF	csf	3205.2	S	93049.30	8.55	9.29
Bc08	CF	cof	3226.5	S	909.41	51.54	2.87
Bca01	CF	csf	3203.6	S	4.88	22.00	-1.51
Bd03	CF	cof	3245.8	S	24.39	56.08	-0.83
Be08	CF	csf	3201.1	E	4633.32	0.00	22.95
Bf02	CF	csf	3201.4	N	64.47	0.00	18.67
Bh06	CF	csf	3219.8	E	51.21	40.01	0.25
Bi07	CF	csf	3256.1	N	106.21	19.09	1.72
Bia01	CF	csf	3249.1	E	1.00	29.08	-3.37

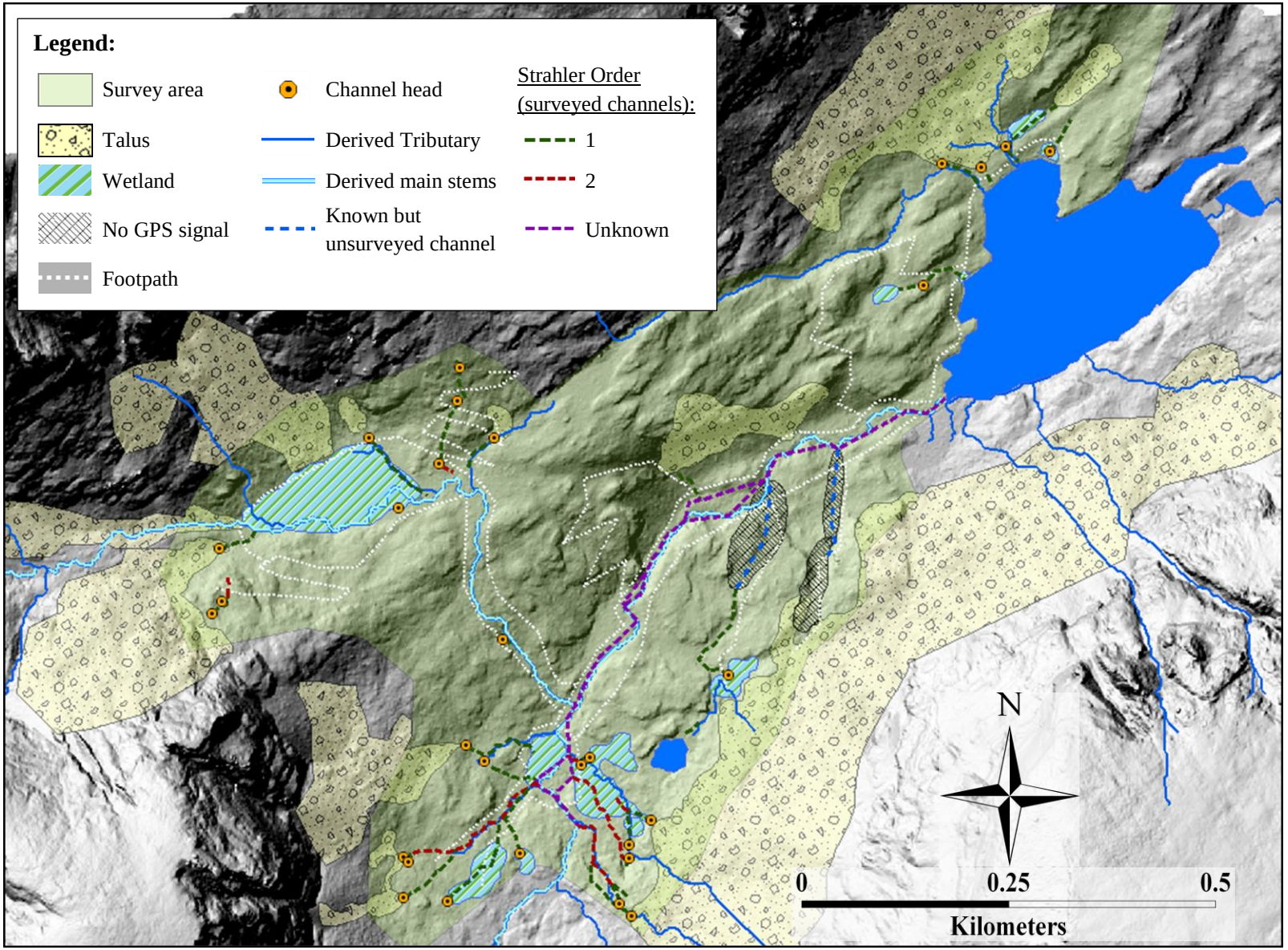

Figure 9: Field survey results of the Loch Vale stream network. Derived channels are from the 1m DEM with D8 and an applied T_α of 40,485m^2. Polygon features are hand-drawn approximations based on field observation.

a)

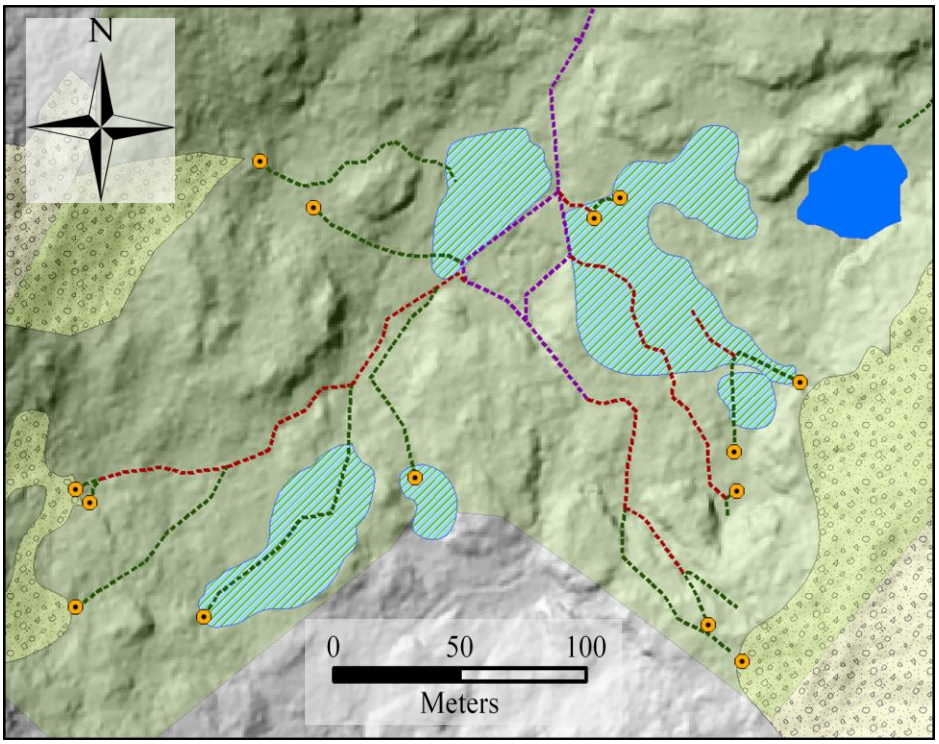

b)

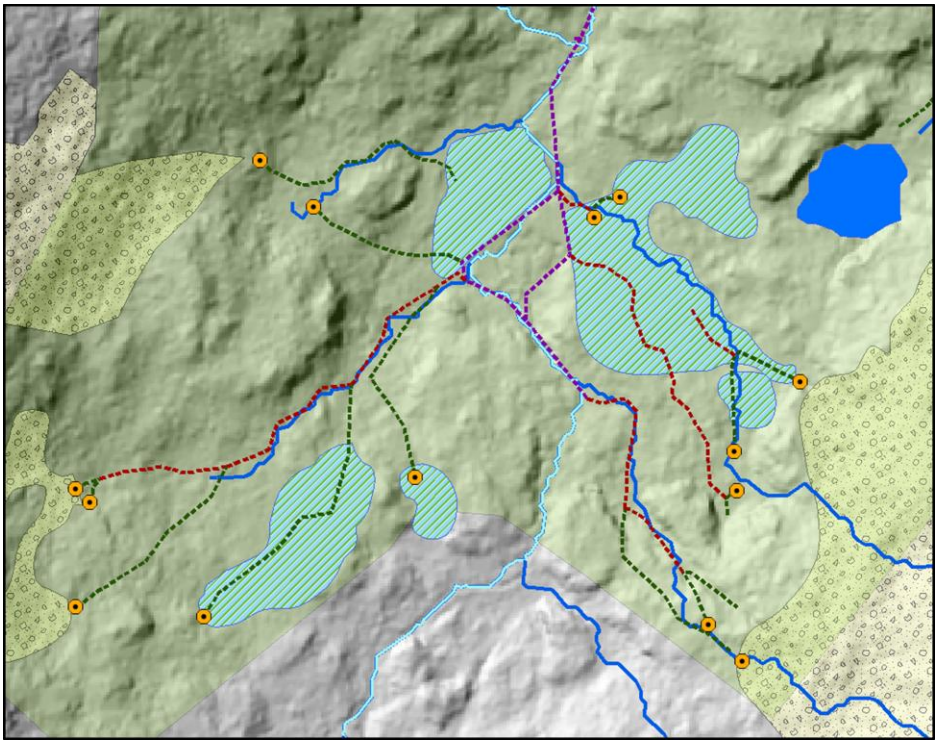

Figure 10: Expanded view of field survey results for a densely channelized portion of survey area, with a) surveyed channels only; and b) surveyed channels overlain on to sample derived channel network. A legend with symbol explanations is found in Figure 9.

a) Point ID: Ad05

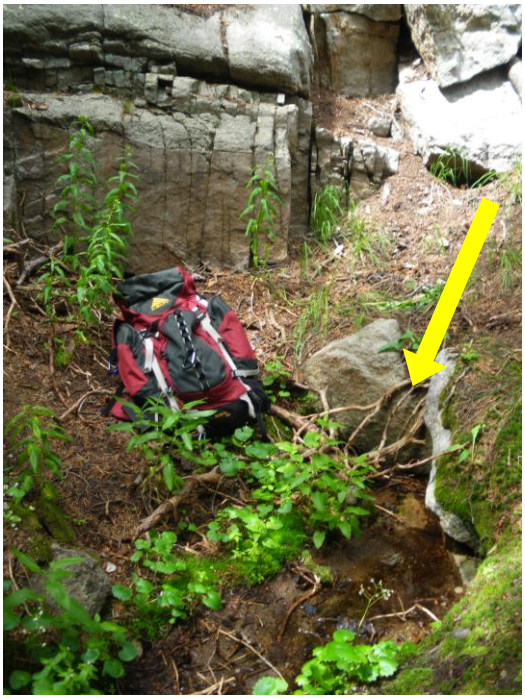

b) Point ID: Ba03

c) Point ID: Ao07

d) Point ID: Aqa96

Figure 11: Photographs showing examples of observed channel initiation, a) at the point of exfiltration from talus, b) at fractures in exposed bedrock, c) over soil and vegetated land cover, and d) at an old overgrown channel head with no active flow (channel banks denoted by red dotted line; flow begins ~2m downslope).

Relationship to surface variables

Here we investigate which, if any, observable environmental and topographic variables relate to the location of surveyed channel heads at Loch Vale. We first investigate the relationship between channel heads and previously discussed geomorphic process domains by plotting channel heads with our slope-area plot (Figure 12). Results show points appearing in every process domain region without any apparent trends, relationship to regions, or obvious contributing area threshold. We then categorize channel head points according to formation process, aspect, and upslope land cover, but again see a lack of natural groupings according to these surface variables (Figure 13). Quantifying extent of land cover types upslope of our channel heads may provide additional information on factors influencing observed contributing areas. We attempted to delineate upslope contributing areas above each channel head point with our 1m raster. However, the divergent nature of the D∞ flow partitioning complicates this procedure and was not compatible with this process in either ArcGIS or RiverTools, thus requiring the use of the D8 flow direction raster to delineate upslope areas. As a consequence,

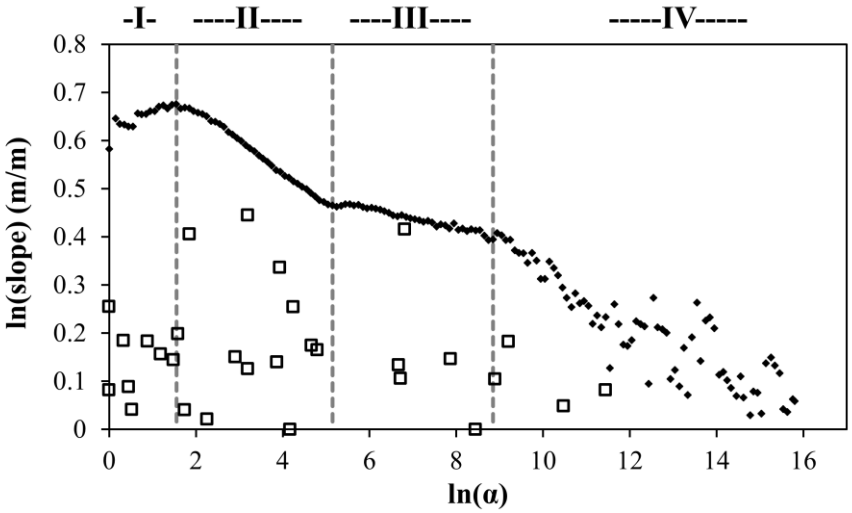

Figure 12: Catchment slope-area plot including points for observed channel heads (squares).

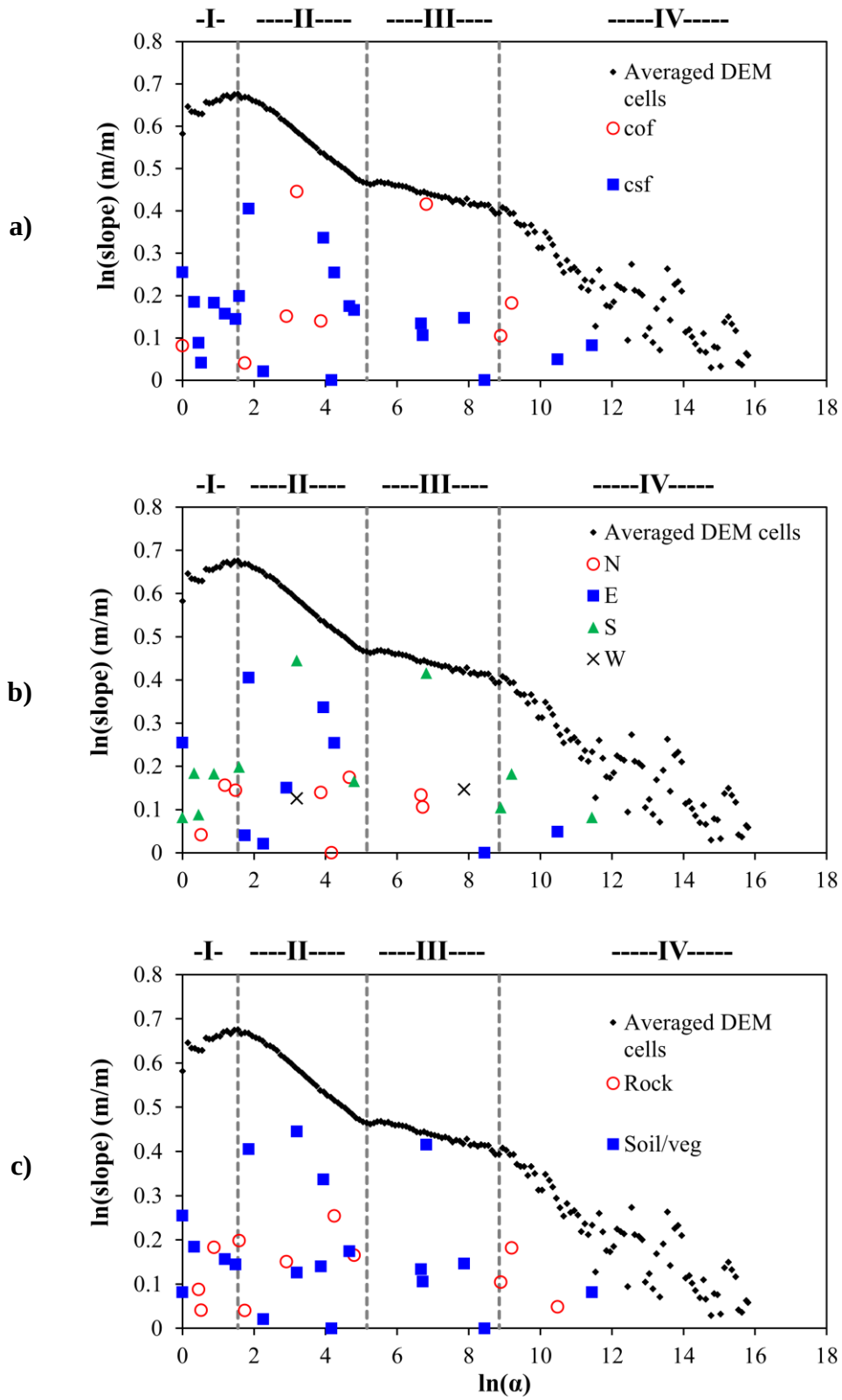

Figure 13: Slope-area plot with observed channel head points categorized by a) formation process, b) aspect, and c) observed upslope land cover.

our results produced individual contributing areas of only one pixel for many channel heads, with an insufficient number large enough to be useful in digital interpretation of land cover.

Next, we explored the statistical nature of our extracted variables for evidence of relationships with observed channel head locations. Table 4 displays mean $\ln(\alpha_s)$ and TWI calculated for our sample of 30 channel heads according to environmental variables of elevation, aspect, slope, formation process, and upslope land cover type. Figure 14 summarizes the distributions of $\ln(\alpha_s)$ and TWI according to these variables with box and whisker plots. There again is no readily apparent variation in mean values of either $\ln(\alpha_s)$ or TWI according to these variables. Here we see wide spread in TWI values relative to the means, with outliers at 22.95 and 18.67.

Table 4: Mean $\ln(\alpha_s)$ and TWI for surveyed channel heads categorized by environmental variables. Values were extracted from the 1m D∞ raster.

Variable		Mean $\ln(\alpha_s)$	Mean TWI
Elevation (m)	**High (> 3208)**	3.72	0.13
	Mid (3158-3208)	4.55	4.02
	Low (< 3158)	3.48	0.99
Aspect	**North**	3.66	3.25
	East	3.98	3.27
	South	4.33	1.43
	West	5.53	2.85
Slope (%)	**Steep (> 56.9)**	3.95	0.06
	Moderate (18.7 – 56.9)	2.99	-0.13
	Shallow (< 18.7)	4.58	4.08
Formation process	**cof**	4.58	1.77
	csf	4.00	2.96
Upslope land cover	**Rock**	4.54	3.30
	Soil/veg	3.89	2.14

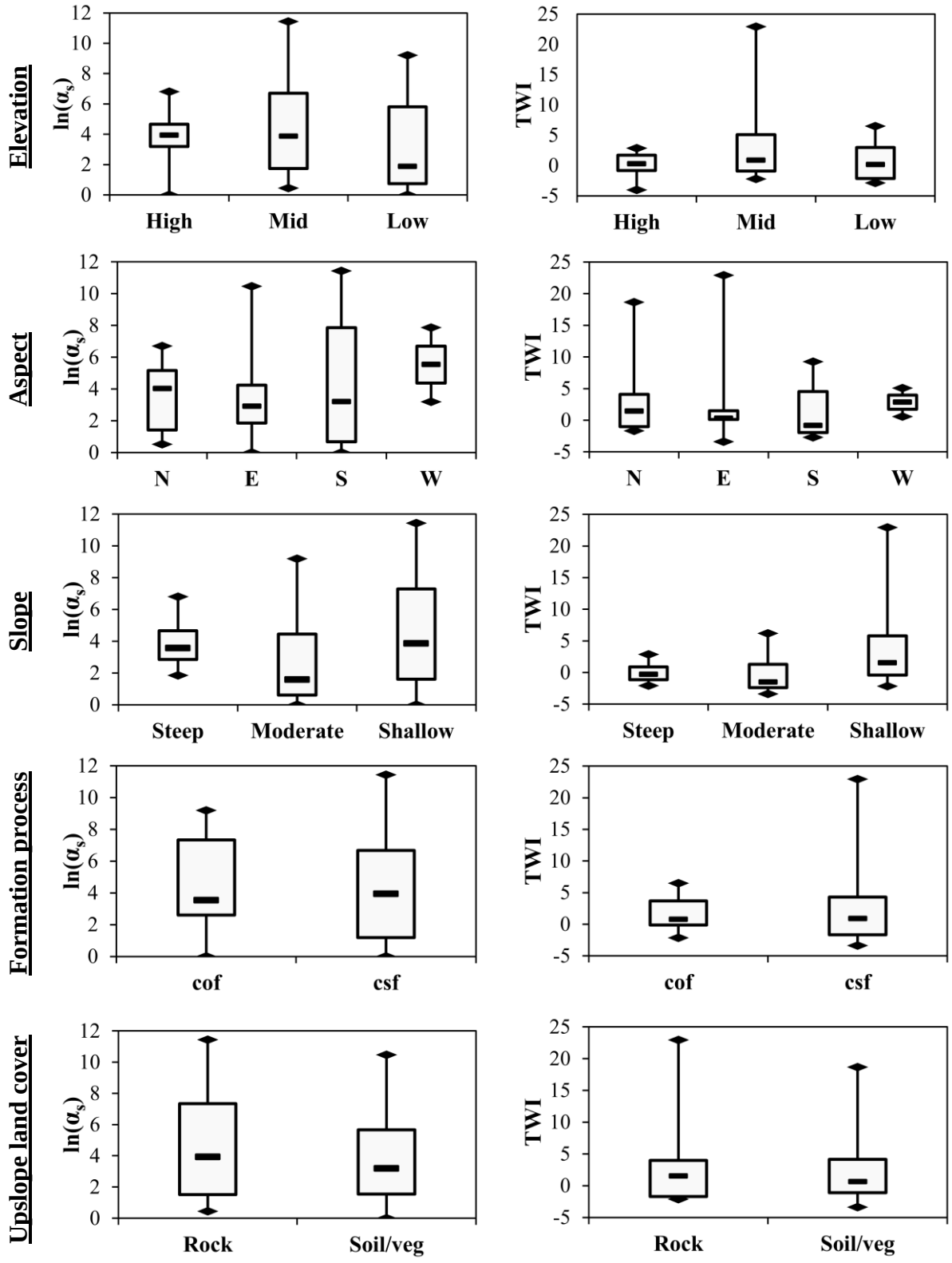

Figure 14: Box and whisker plots of $\ln(\alpha_s)$ and TWI at observed channel heads, categorized by environmental variables.

With no readily apparent relationships thus far, single-factor ANOVA was used to test for statistically significant difference in our group means. This test is relatively robust and useful for comparing means of two or more groups with unequal sample sizes, but relies on the assumptions of normality, homogeneity of variance and independence among all groups (Bewick et al., 2004). We applied a natural logarithmic transformation on all data prior to analysis, which is a basic method for improving adherence to these assumptions and the reliability of end results (Curtiss, 1943; Keene, 1995). Using the single-factor ANOVA tool in Microsoft Excel's data analysis package, if our calculated F-value (F) exceeds a reference critical F-value (F_{crit}) chosen based on number of groups (u), sample size within each group (n) and significance level p = 0.05, there is a significant difference between the means. Given a difference, in order to identify which specific groups vary between each other the Scheffe test is employed where if a calculated test statistic (TS) for two comparison groups exceeds a critical value (CV), their means are shown to be significantly different. Here,

$$CV = df_{bg} * F_{crit} \tag{6}$$

where df_{bg} = between groups degrees of freedom, given by

$$df_{bg} = u - 1 \tag{7}$$

TS is then calculated by

$$TS = (\bar{x}_1 - \bar{x}_2)^2 * \left[ms\left(\frac{1}{n_1} + \frac{1}{n_2}\right)\right]^{-1} \tag{8}$$

where ms = within group mean squares ("variance"), x_1= mean for variable of interest of first group, x_2 = mean for variable of interest of second group, n_1 = sample size of first group, and n_2 = sample size of second group. Within group variance is calculated by

$$ms = \frac{\Sigma(x^2) - \left[\left(\frac{(\Sigma x_1)^2}{n_1}\right) + \left(\frac{(\Sigma x_2)^2}{n_2}\right) + \left(\frac{(\Sigma x_3)^2}{n_3}\right)\right]}{df_{wg}} \quad (9)$$

where df_{wg} is within groups degrees of freedom, given by

$$df_{wg} = \sum_{i=1}^{u} (n_i - 1) \quad (10)$$

We repeated this analysis for all pairs of means for each variable. Results of ANOVA are reported in Table 5, which show no variable with a calculated F larger than F_{crit}. Thus, with 95% confidence we found no statistically significant differences between group means as a result of any surface variable tested. Therefore, a Scheffe test is not needed here.

Table 5: ANOVA results for ln(α_s) and TWI at observed channel heads according to various surface variables as extracted from the 1m D∞ raster. F_{crit} values are based on significance level of p = 0.05. Log-transformed values of α_s are used to address the assumptions of equal sample variance required for ANOVA.

Variable	**Source of Variation**	**ln(α_s)**				**TWI**			
		df	*F*	F_{crit}	p-value	*df*	*F*	F_{crit}	p-value
Elevation	Between groups	2	0.308	3.35	0.737	2	1.20	3.10	0.316
	Within groups	27				27			
	Total	29				29			
Aspect	Between groups	3	0.174	2.98	0.913	3	0.191	2.98	0.901
	Within groups	26				26			
	Total	29				29			
Slope	Between groups	2	0.578	3.35	0.568	2	1.74	3.35	0.195
	Within groups	27				27			
	Total	29				29			
Formation process	Between groups	1	0.165	4.21	0.688	1	0.212	4.21	0.649
	Within groups	27				27			
	Total	28				28			
Upslope land cover type	Between groups	1	0.259	4.20	0.615	1	0.253	4.20	0.619
	Within groups	28				28			
	Total	29				29			

Relationship to DEM resolution

The second objective for this portion of the analysis is to examine how the choice of DEM resolution used to extract our attributes for surveyed channel heads influences the values themselves. Table 6 shows summary statistics for $\ln(\alpha_s)$ and TWI as extracted from our 1, 10, and 30m rasters for surveyed channel heads. Results show an increase in $\ln(\alpha_s)$ with each subsequent increase in grid cell size. Log-transformed values are presented here for consistency and for use in ANOVA. Un-transformed mean α_s values are 5205.0, 2635.8, and 5713.1m for the 1, 10, and 30m rasters, respectively. Maximum $\ln(\alpha_s)$ is considerably higher for the 1 and 30m raster as compared to the 10m raster, while minimum is simply the $\ln(\alpha_s)$ of 1 pixel. Mean TWI values increase as cell size increases, and maximum TWI is also higher for the 1 and 30m. Box and whisker plots for $\ln(\alpha_s)$ and TWI are presented in Figure 15.

Table 6: Summary statistics of D∞ $\ln(\alpha_s)$ and TWI for surveyed channel heads at Loch Vale.

	$\ln(\alpha_s)$ (m)			**TWI**		
	Mean	Max.	Min.	Mean	Max.	Min.
1m	4.13	11.44	0	2.56	22.95	-3.37
10m	6.57	9.70	2.30	4.04	8.90	-1.50
30m	6.61	11.53	3.40	5.13	22.36	-0.69

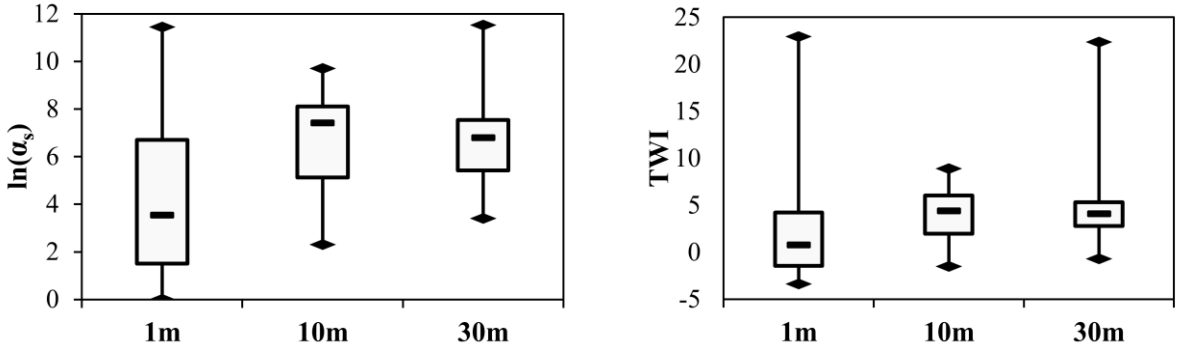

Figure 15: Box and whisker plots of $\ln(\alpha_s)$ and TWI at observed channel heads as extracted from 1, 10, and 30m rasters.

Table 7: ANOVA results of $\ln(\alpha_s)$ and TWI at observed channel heads for different DEM resolutions. F_{crit} values are based on significance level of p = 0.05.

	$\ln(\alpha_s)$				**TWI**			
ANOVA	*df*	*F*	F_{crit}	p-value	*df*	*F*	F_{crit}	p-value
Between groups	2	9.62	3.10	0.0002	2	2.15	3.10	0.122
Within groups	87				87			
Total	89				89			
Scheffe Test	1m – 10m	1m – 30m	10m – 30m		1m – 10m	1m – 30m	10m – 30m	
	6.20	6.20	6.20		6.20	6.20	6.20	
	14.19	14.67	0.0040		1.42	4.27	0.76	

ANOVA shows that our calculated *F* exceeds F_{crit} indicating a significant difference between means for $\ln(\alpha_s)$ as a result of varying grid cell size (Table 7). No difference is found for TWI. Given our results for $\ln(\alpha_s)$, a Scheffe test with the same significance level of p = 0.05 shows that a difference exists specifically between the 1 and 10m rasters as well as the 1 and 30m rasters, but not the 10 and 30m.

4.3 Discussion

Relationship to surface variables

A fundamental assumption in DEM-based channel network derivation is that channel initiation can be predicted by surface topography. Results of our field survey for the actual channel network at Loch Vale suggest otherwise. No predictable relationship was observed between channel head locations and geomorphic process domains extracted from our DEMs. Nor did we find any statistically significant difference in mean contributing area and TWI thresholds for observed channel heads as a result of elevation, aspect, or slope. Results were similar when comparing variation in formation process and upslope land cover type, with slope-area analysis and ANOVA showing no differences in channel head locations according to these variables. Our findings for Loch Vale are consistent with those of similarly complex terrain, with Jaeger et al. [2007] and Orlandini et al. [2011] both concluding that surface threshold parameters were poorly correlated with channel head locations as a result of subsurface controls. However, surface parameters have been shown to be dominant influences in channel network development in some environments similar to Loch Vale. Henkle et al. [2011] did find Front Range channel heads to be mainly associated with region III of their slope-area analysis and that surface variables of local slope, contributing area, basin length, annual precipitation and elevation accounted for just over half the variation in channel head location, with the other half attributed to unmeasured subsurface controls. In contrast, evidence for Loch Vale suggests that important influences on channel initiation are not captured by surface topography or other readily observable characteristics. Additionally, we observed a complexity and irregularity in surface water features in the field that one would not expect given the assumption of topographic and surface controls

on channel network development. It is therefore likely that subsurface processes including bedrock topography, piping through talus and porous soil, and fractured bedrock have a significant influence on stream channel formation at Loch Vale.

Relationship to DEM resolution

Accepting the conclusion that observed channel formation is a primarily function of subsurface processes, we nevertheless examine further the nature of derived contributing area and TWI, as it is common practice to characterize basins by a single topographic threshold. Even when field data are available, using a single averaged value extracted from rasters to surveyed points can produce wide ranging results dependent on the resolution of the topographic data. We previously showed an increase in contributing area with grid cell size, and thus it would be expected this results in higher contributing areas extracted to observed channel heads with coarser resolution DEMs. By doing this with our 1, 10, and 30m rasters, we show that mean $\ln(\alpha_s)$ and TWI increase with grid cell size. ANOVA confirms a significant difference in mean $\ln(\alpha_s)$ associated with grid cell size at Loch Vale, specifically between our 1 and 10m as well as our 1 and 30m rasters. In a coarse raster, large grid cells drain more upslope area, so a single channel head point falling within this cell can thereby overestimate flow accumulation applied to that specific channel. This risk is balanced by one associated with fine resolution data and the error inherent in lower accuracy surveying methods. When using fine resolution DEMs to extract topographic variables to surveyed points, GPS positional errors of only a few meters could result in channel head points being placed over grid cell locations on a raster that do not match their real world location. This can lead to large differences in flow accumulation values between adjacent cells and inaccuracies in thresholds associated with a single channel head, especially

when based on single-direction flow partitioning or in very rugged landscapes. The same concerns may arise due to the positional errors of the original elevation data. The likelihood of this effecting our results is minimal, as the horizontal errors for our original 1m DEM is estimated to be less than or equal to 1.04 cm. It is important to consider both the resolution of topographic data and errors associated with field data collection when attempting to characterize channel formation by threshold contributing area, as DEM resolution can considerably influence the nature of any derivative channel networks. Given our sub-meter GPS accuracy as well as the short hillslope lengths and fine scale of hydrologic processes at Loch Vale, we will apply mean α_s and TWI values extracted from our 1m D∞ raster as "observed" values in our subsequent network derivation analysis.

5. Channel Network Derivation

5.1 Methods

The third phase of our study uses derivative rasters from previous steps with three approaches for identifying a channel network in a GIS. First, we analyze NHD flow lines as a test network. Additional test networks are derived in ArcMap by applying both flow accumulation and TWI channel initiation thresholds (Table 8) to rasters of each resolution using both D8 and D∞ flow partitioning algorithms. To accomplish this, all raster cells with values below the given threshold were set to null in the raster calculator tool, with the remaining being considered channelized and assigned a value of 1. From a gridded representation of channelized versus unchannelized cells, we can convert our channel rasters to line and point features for

Table 8: Test flow accumulation and TWI thresholds for channel network derivation.

Symbol	Threshold Value	Source
$T\alpha_1$	$468m^2$	Predicted contributing area threshold identified through analysis of slope-area relationship for the 1m D∞ raster (Figure 8c), per method discussed Ijjasz-Vasquez and Bras [1995]
$T\alpha_2$	$1{,}480m^2$	Predicted contributing area threshold identified through two-phase linear regression on slope-area relationship for the 1m D∞ raster (Figure 8b)
$T\alpha_3$	$5{,}205m^2$	Mean flow accumulation for the field surveyed channel heads in Loch Vale, as extracted from the 1m D∞ raster
$T\alpha_4$	$40{,}485m^2$	Mean contributing area extracted from 1m D8 raster to channel initiation points on the NHD flow line product
$T\alpha_5$	$129{,}372m^2$	Mean contributing area extracted from a 10m D8 flow accumulation raster in Henkle et al. [2010] for Front Range locations within the same elevation range as Loch Vale
T_{twi1}	2.56	Mean TWI for the field surveyed channel heads in Loch Vale, as extracted from the 1m D∞ raster
T_{twi2}	4.04	Mean TWI for the field surveyed channel heads in Loch Vale, as extracted from the 10m D∞ raster
T_{twi3}	5.18	Mean TWI for the field surveyed channel heads in Loch Vale, as extracted from the 30m D∞ raster

spatial analysis. To ensure a valid comparison to our surveyed network, all test networks were clipped to the extent of the surveyed area and portions overlapping areas of known lakes were removed.

These derivation methods produced a set of 48 test channel networks, plus the existing NHD network, that can be compared for accuracy to the observed data. We employ several tools to characterize accuracy, the first being simple visual inspection for a qualitative assessment based on the surveyed network and our general field knowledge of Loch Vale. Given the limitations in modeling channel networks based solely on topography, a simple visual interpretation of our resulting test networks is a useful evaluation tool. This process contains inherent subjectivity, but with the aid of our surveyed map we can interpret results visually using qualitative criteria. The most obvious is general number and density of channels. At first glance it is easy to assess whether or not a derived network over or under-predicts channel density. Related to this is the appearance of "feathering" which manifests as an overabundance of parallel channels branching off from reaches onto planar hillslopes. Indeed, one proposed criteria for identifying a contributing area threshold is that which is just large enough to avoid significant feathering (Montgomery and Foufoula-Georgiou, 1993). In contrast, it is important to consider how oversimplification of a network neglects lower order channels. A second important criterion is how well the headward extent of channelization matches that of our known channels. Finally, we apply a general assessment of the network's ability to accurately place real channels. An additional criterion might be the representation of disjointedness and flow divergence; however these features are often irregular and hard to predict based on current resolutions of topographic data. When assessing validity of a derived network through visual interpretation, one should strike a reasonable balance between channel density, headward extent and general positional

accuracy of channels. Based on this we evaluate the quality of our derived networks relative to each other and categorize each as either "above average", "average", or "below average". An above average rating is assigned to networks with aforementioned characteristics similar to the observed channel network, a below average rating to those networks having very few of these characteristics in common with the observed network, and an average rating to networks that fall somewhere between above and below average.

Drainage density is also calculated quantitatively for each network. Drainage density is a common scalable mathematical characterization of a channel network, given by:

$$D_d = \frac{L_T}{A} \tag{11}$$

where D_d is drainage density in length^{-1}, L_T is total channel length within the basin and A is basin area. For this analysis we restrict basin area to include only the extent of the field survey, which allows for valid comparison between derived and observed networks. Total channel length is computed by first converting our stream channel raster to polylines connecting the cell centers of each channelized pixel. Total channel length is then simply the sum of each individual channel segment.

Next, we calculate the horizontal Euclidean distance of surveyed points to the nearest channelized point in each test network to produce a distribution of positional errors relative to our reference channel points. To assess performance we calculate root mean squared error (RMSE) for each test network. RMSE is used instead of mean absolute error because it increases the contribution of larger errors to the metric by squaring each error, and when dealing with small headwater channels in heavily dissected terrain these larger errors greatly reduce the utility of a channel derivation method.

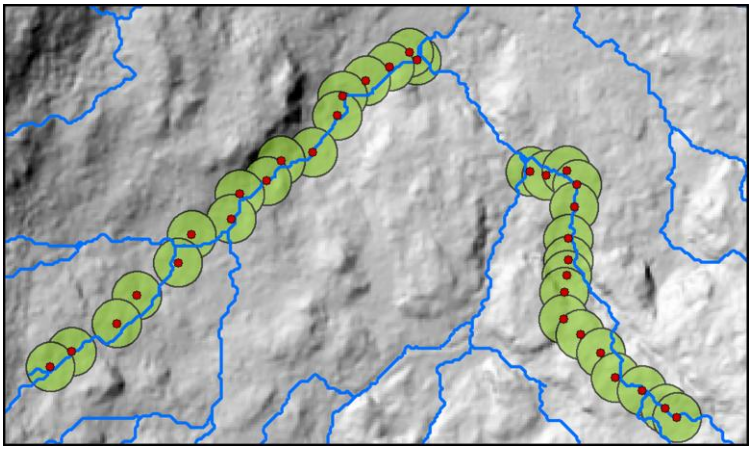

Figure 16: Schematic representation of feature accuracy assessment with buffer size such that 95% of survey points (red points) are less than or equal to this distance from derived network channels (blue lines).

A method for assessing positional accuracy of test features against a more accurate reference feature is outlined in Goodchild and Hunter [1997]. This involves defining a buffer size around the reference line that contains a given percentage (e.g., 95%) of the total length of the test feature. In our study the sampling frequency was not dense enough to produce a continuous representation of a linear reference network, so we alter the analysis by calculating the horizontal Euclidean distance from our surveyed points to the nearest derived channelized point for each network. Then, starting at 0.0m we increase our buffer size in 0.5m increments to determine the size needed such that 95% of surveyed points lie within this distance from the derived channel network (Figure 16). This analysis is only suitable for testing positional accuracy of predicted reaches that actually exist in our surveyed network (i.e., true positives), so we selected a sample of six test reaches, consisting of 70 points, which were both predicted by a test networks using $T\alpha_3$ and T_{twi2}, and were confirmed to exist by survey data. These include the surveyed reaches Be, Ah, Ap, Aq, upper A (Icy Brook; points 20-10), and lower A (points 09-01). All else equal, setting different topographic thresholds for a given DEM resolution and flow

direction algorithm results in differences of headward extent of channelization but not in the locations of channels. Thus, here we are not assessing performance of our thresholds but rather we address how DEM resolution and flow partitioning influence the positional accuracy of successfully predicted channel reaches.

Finally, the ability of each method and DEM to accurately represent channel initiation points is examined using two performance indices described in Orlandini, et al. [2011]. By defining a radial buffer around each test channel initiation point, performance is quantified by summing the number of correctly predicted channel heads (true positives, or *TP*), and dividing by the sum of *TP* and the number of channel heads predicted that do not actually exist (false positives, or *FP*). Given by Equation 12, this index (r) characterizes the reliability of each result, that is, how well it avoids generating false positives. Reliability scores range from 0 to 1, with values closer to 1 performing better.

$$r = \frac{\sum(TP)}{\sum(TP) + \sum(FP)} \tag{12}$$

Each method is also examined for its sensitivity (s) by Equation 13, which characterizes its ability to avoid missing channel heads.

$$s = \frac{\sum(TP)}{\sum(TP) + \sum(FN)} \tag{13}$$

where *FN* is false negatives, or channel heads that exist in the field but are not predicted. Again, values range from 0 to 1, with higher values indicating better performance. Both scores are used in conjunction to assess performance of test networks, as good derivation methods should avoid both predicting non-existent channel heads and missing real ones. In this analysis we defined our

radial buffer to be 30m, equal to the edge length of our largest grid cell size. Derived channel heads were identified manually in GIS from channelized points overlain onto a hillshade raster. Channel head points were selected at the farthest upslope points of channelization within the surveyed area. In a few cases, following flow lines upslope led to clustered groups of channelized pixels; for these cases, we used our best estimate of the precise location of the furthest upslope channel initiation. This method contains some subjectivity in identifying channel heads, however is used because an accurate flow network cannot be resolved for the D∞ cell data format with either of our GIS platforms. Once our channel head points were identified, we calculated the nearest horizontal Euclidean distance between our derived channel heads and the surveyed channel heads. Distances less than or equal to the radial buffer are *TP* while those greater than the radial buffer are *FP*. Lastly, distances from our surveyed heads to the nearest derived channel heads were extracted, and those exceeding our radial buffer are *FN*.

5.2 Results

Visual interpretation

Depending on the channel derivation method used, we see large differences in resulting channel networks. Table 9 presents the results of a visual assessment for our derived networks based on the previously defined evaluation criteria. Figure 17 shows several examples of our results, with a complete collection of test networks presented in Appendix C. The lowest two flow accumulation thresholds produced channel networks with densities far greater than observed, and were rated as below average. $T\alpha_1$ is smaller than the area of a single 30m grid cell, resulting in the entire watershed being defined as channelized for the 30m resolution DEMs. $T\alpha_3$

Table 9: Qualitative network ratings based on visual assessment as compared to the known channel network at Loch Vale. A "+" symbolizes above average networks, "—" symbolizes average networks, and those marked with "**X**" were below average.

Flow algorithm	**DEM**	**Tα_1**	**Tα_2**	**Tα_3**	**Tα_4**	**Tα_5**	**T$_{twi1}$**	**T$_{twi2}$**	**T$_{twi3}$**	**NHD**
D8	1m	**X**	**X**	—	+	—	**X**	**X**	**X**	**X**
	10m	**X**	**X**	—	+	—	—	+	+	
	30m	**X**	**X**	**X**	—	—	**X**	—	—	
D∞	1m	**X**	**X**	—	+	—	**X**	**X**	**X**	
	10m	**X**	**X**	**X**	+	—	**X**	—	—	
	30m	**X**	**X**	**X**	—	—	**X**	—	—	

offers a slight improvement, with D8 at 1 and 10m resolution and D∞ at 1m resolution rated as average; however the number of channels is still higher than observed, and channels mostly initiate far up what are actually walls of bedrock cliffs. Additionally, we see some degree of unnatural parallel feathering. The Tα_3 D8 30m and D∞ 10 and 30m networks are highly over-channelized and rated as below average. Tα_4 provides perhaps the best representation of the network, capturing many lower order channels and reasonable headward extents. The total number of channels is also on par with the known density. Here the 1 and 10m networks for both flow algorithms were rated as above average. The 30m networks for Tα_4 are average with some false positives and higher headward extents. Finally, for Tα_5 there is a drop-off in quality due to underrepresentation of channels, but it still produces a reasonable representation of the network with some lower order reaches accurately displayed, so we rated all Tα_5 networks as average. We saw a similar trend in the quality of our T$_{twi}$ derived networks as threshold values increase. The smallest TWI threshold greatly over-predicts channelization and is rated below average, with the exception of the D8 10m raster which has slightly lower density but still some feathering. Both T$_{twi2}$ 1m networks provide over-channelized results; however the T$_{twi2}$ D8 10m

is an above average representation of the network. Some headward extents are unnaturally high but are generally agreeable to the observed network. The remaining three T_{twi2} networks are acceptable but slightly over-channelized, most notably an artificial branching from Andrew's Creek in the center of the D∞ images. This same unnatural feature appears in the T_{twi3} D∞ 10m image, which we assign an average rating along with both T_{twi3} 30m networks. Here the 1m rasters are again far too dense and rated as below average. The T_{twi3} D8 10m raster gives us an above average representation of the network, on par with the T_{twi2}, and likely provides the best representation after those in $T\alpha_4$. The NHD network represents the two main drainages satisfactorily but greatly under-predicts channelization, missing all but two lower order channels.

We also see examples of flow divergence in D∞ networks that are in agreement with the known network (Figure 18a); however there are also several instances where these features are missed (Figure 18b). This inconstancy limits the D∞'s advantages in steep terrain such as Loch Vale, where physiographic features that lead to divergence are almost impossible to capture with even 1m resolution.

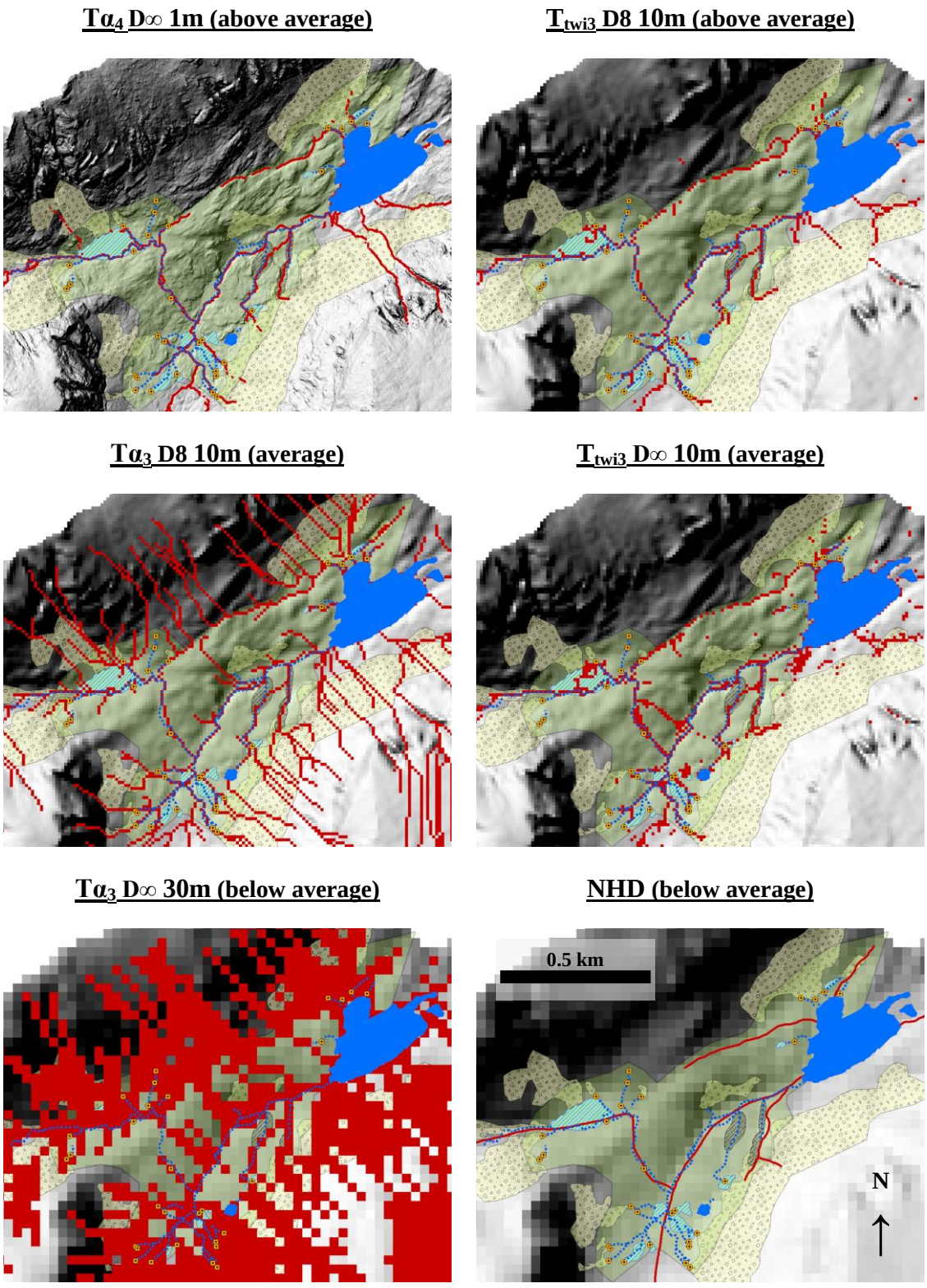

Figure 17: Examples of derived networks showing above average, average, and below average visual representations.

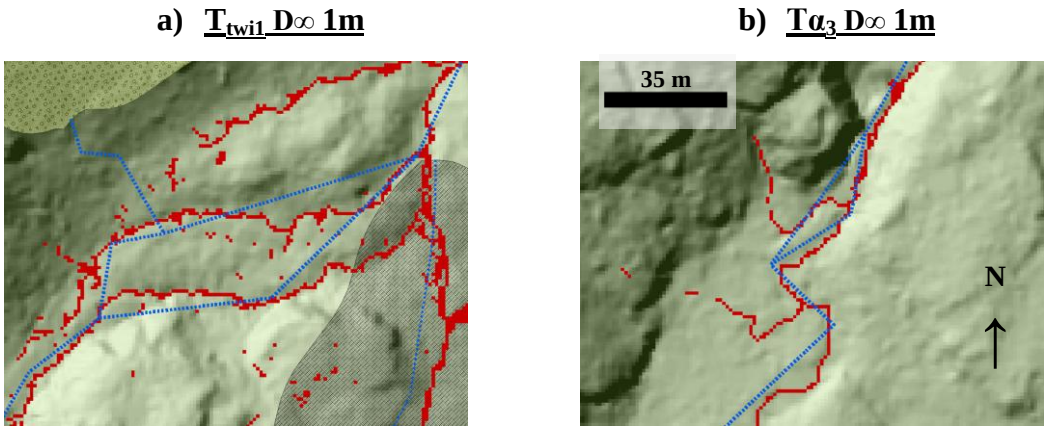

Figure 18: Examples of D∞ (a) capturing and (b) missing observed channel divergence.

Drainage density

When dividing the total surveyed channel length of 4,277m by the surveyed area of 537,800m^2 we get an observed drainage density of 0.0080m^{-1}. Figure 19 shows calculated drainage density for our derived networks. Drainage densities will be inversely proportional to threshold values, as is clearly evident for all of the derived networks. As a measure of total channel length, all $T\alpha_4$ and $T\alpha_5$ networks; the T_{twi2} D8 10 and 30m; T_{twi2} D∞ 30m; T_{twi3} D8 10 and 30m; and T_{twi3} D∞ 10 and 30m networks provide reasonable approximations relative to the surveyed network. The NHD drainage density under represents channel length with a value of 0.0047, and would be even lower were it not for a long reach of surface channel in the northern portion of the survey area that was not observed in the field. This highlights the limitations of drainage density as a performance measure, since it does not take into account positional accuracy or successful representation of any particular channel.

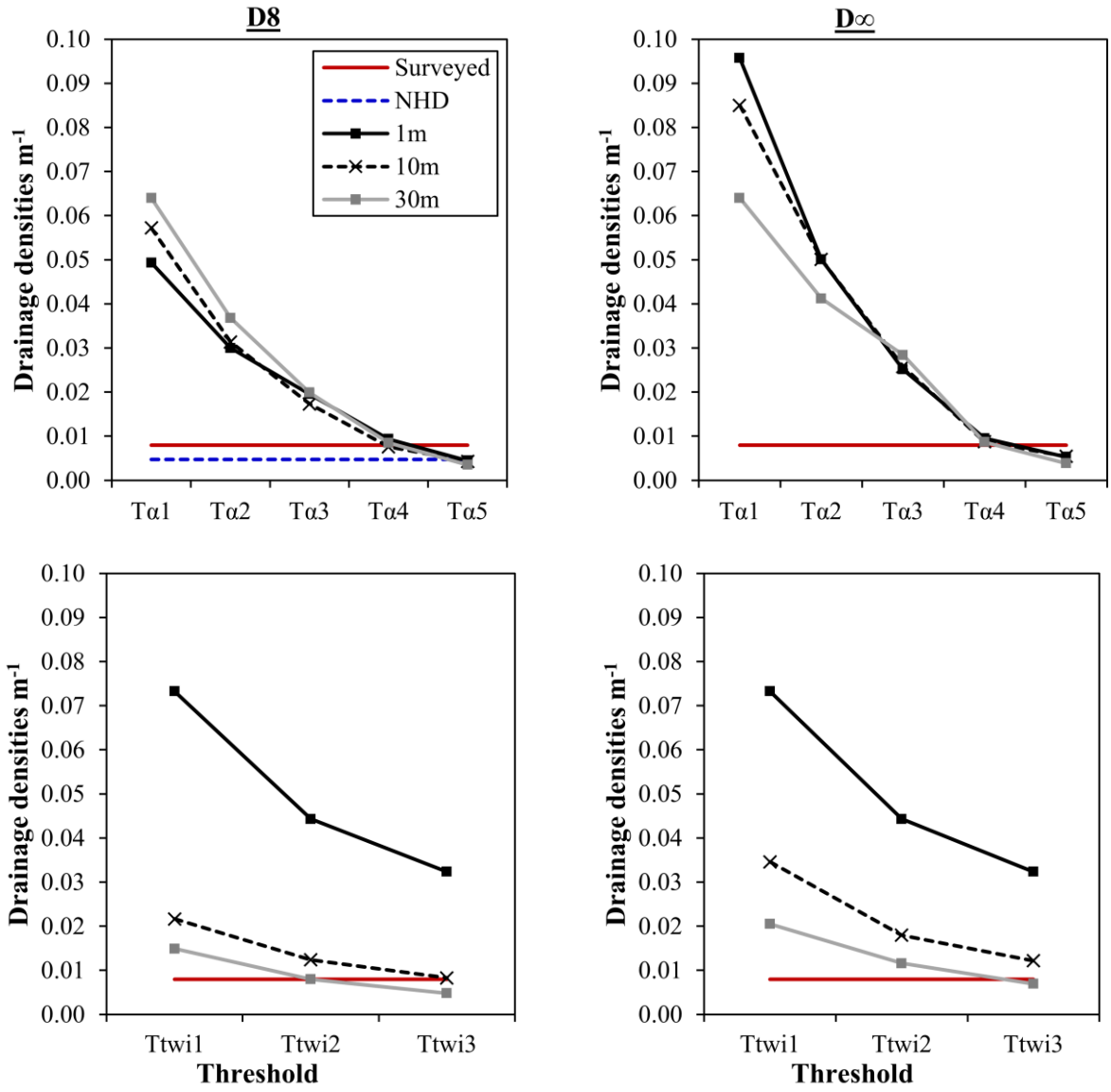

Figure 19: Drainage densities for derived and field-surveyed channel networks, as calculated with a survey area of 537,800m^2.

Positional error

Table 10 displays RMSE between surveyed channel points and the nearest derived channel points. Error increases with grid cell size due to the inherent increase in uncertainty with a loss of resolution. We also see a positive relationship with RMSE and threshold value. In a majority of derived networks, for a given cell size and threshold value there is lower positional

error for D∞ when compared to D8, with the exceptions of $T\alpha_1$ 30m, $T\alpha_4$ 30m, $T\alpha_5$ 10 and 30m, T_{twi2} 10m and T_{twi3} 1m. TWI RMSE tends to be lower when compared to flow accumulation thresholds producing relatively similar drainage densities.

Table 10: RMSE in meters between surveyed channelized points and derived networks.

Flow algorithm	DEM	$T\alpha_1$	$T\alpha_2$	$T\alpha_3$	$T\alpha_4$	$T\alpha_5$	T_{twi1}	T_{twi2}	T_{twi3}
D8	1m	3.7	8.3	13.8	31.7	62.2	2.3	5.4	7.2
	10m	5.4	8.3	11.7	36.0	58.5	9.1	12.9	26.8
	30m	12.2	13.7	17.5	30.8	62.5	22.1	30.7	44.2
D∞	1m	3.2	6.3	9.7	30.5	62.0	1.7	3.4	7.2
	10m	4.7	6.7	9.6	32.0	59.5	7.5	15.4	24.5
	30m	12.2	13.1	15.0	33.8	70.2	19.8	26.5	31.9

Table 11: Results of the feature accuracy assessment showing the buffer widths (m) needed for each test network such that 95% of survey points are less than or equal to this distance from derived network channels.

DEM	$T\alpha_3$		T_{twi2}		NHD
	D8	D∞	D8	D∞	
1m	10.5	8.5	5.0	2.5	
10m	8.0	7.0	8.0	7.0	n/a
30m	26.0	20.0	27.5	22.0	

Feature accuracy assessment

Results for the feature accuracy assessment are presented in Table 11. For the 1m networks, T_{twi2} D∞ has the shortest buffer width, which is interpreted as having 95% confidence that the positional error between our survey points and derived channels is ±2.5m. T_{twi2} performs the better for all 1m networks, with D∞ also outperforming D8 for all networks. In contrast, $T\alpha_3$ has lower error than T_{twi2} with a 30m resolution. At a 10m resolution, $T\alpha_3$ and T_{twi2} perform equally well. The NHD network does not contain enough lower order reaches to be included in this analysis.

Channel head prediction index

None of the derived networks perform very well in placement of channel heads based on channel head prediction index scores, with no values at or near 1 for reliability and only two for sensitivity (Figure 20). The $T\alpha_5$ 1 and 10m networks as well as the NHD network produced scores of 0.00 for both indices. Results do however allow us to examine the relative reliability and sensitivity of each network. We omitted channel head prediction scores for the extremely over-channelized networks, which displayed hundreds of channel head points and would have produced unreasonable index scores. T_{twi2} D8 30m is the most reliable predictor of channel heads, with T_{twi3} D8 10m; $T\alpha_5$ D∞ 30m and D8 10m; $T\alpha_4$ D8 10 and 30m and $T\alpha_4$ D∞ 30m also scoring relatively high. That is, these networks do the best at not producing channel heads that do not actually exist. Networks that do the poorest job of this include the aforementioned networks scoring zero as well as $T\alpha_1$ D8 10m and D∞ 10m; $T\alpha_2$ D∞ 10m,$T\alpha_3$ D8 30m, and T_{twi1} D∞ 30m. The network that was the most sensitive, i.e. did not miss existing channel heads, is T_{twi3} D8 1m. Also scoring well are $T\alpha_1$ D8 1m and D∞ 1m; $T\alpha_2$ D∞ 1m, and T_{twi2} D∞ 10m. In addition to

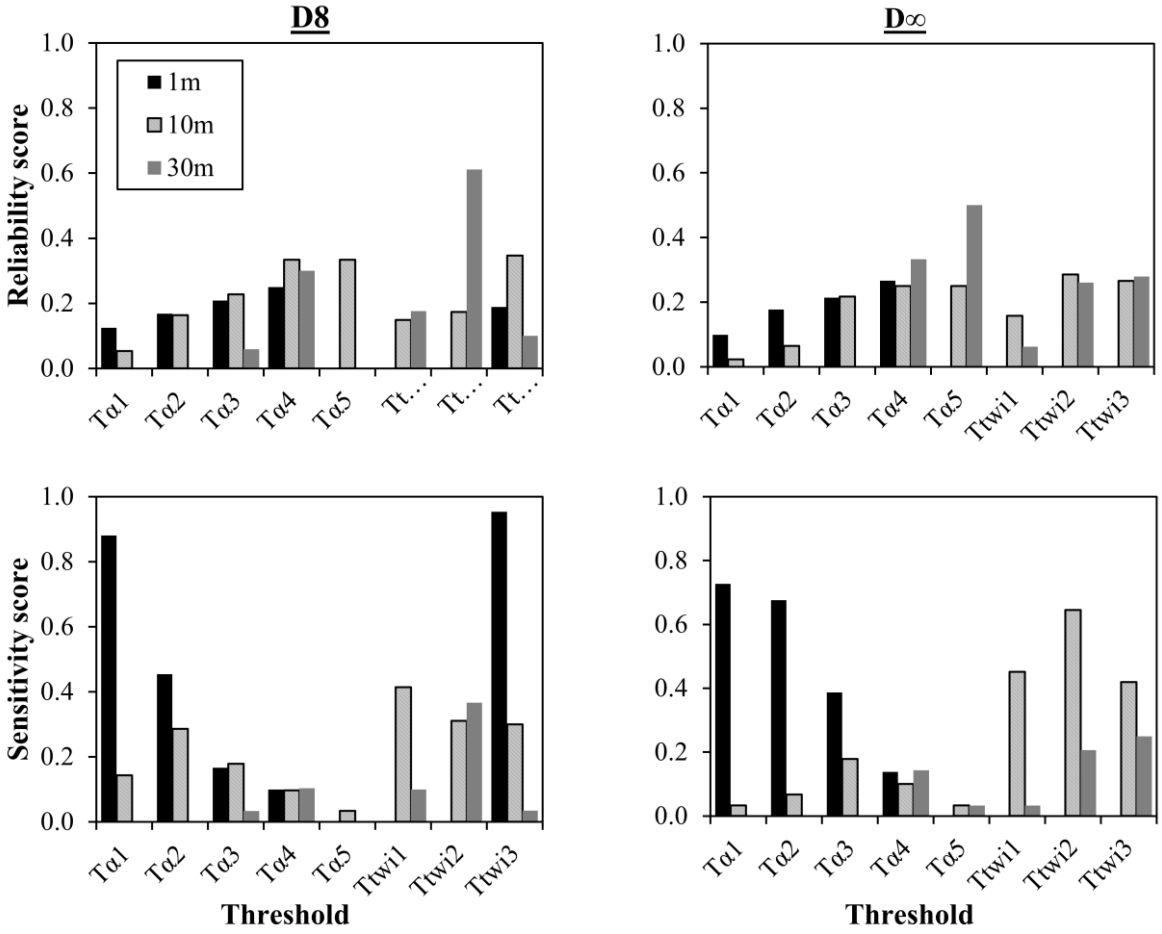

Figure 20: Reliability and sensitivity channel head prediction index scores for derived networks. Although not shown here, the NHD network produced a score of 0.00 for both reliability and sensitivity. Networks not scored due to an unreasonably high number of channel heads are $T\alpha_1$ D8 30m, $T\alpha_1$ D∞ 30m, $T\alpha_2$ D8 30m, $T\alpha_2$ D∞ 30m, T_{twi1} D8 1m, T_{twi1} D∞ 1m, T_{twi2} D8 1m, T_{twi2} D∞ 1m,

those scoring 0.00, $T\alpha_1$ D∞ 10m, $T\alpha_3$ D8 30m, $T\alpha_5$ D8 10m and D∞ 10 and 30m, and T_{twi3} D8 30m performed very poorly. It is interesting to note that several of the more reliable networks are relatively insensitive, while more sensitive networks are relatively unreliable. This may be because reliable networks are less dense and therefore will perform poorly for sensitivity, and vice versa.

5.3 Discussion

Visual inspection

Performance metrics and statistical characterizations can provide rigorous and transferable evaluation criteria for hydrologists, but when studying an area there is often no substitute for on-the-ground knowledge of the actual catchment. Applying this qualitative understanding to our derived networks yields perhaps the most valuable results when evaluating network performance. Utilizing our basic criteria for visual inspection, we determined that the most useful channel networks are derived from both D8 and D∞ algorithms using $T\alpha_4$ at 1 and 10m resolutions; as well as T_{twi2} D8 10m and T_{twi3} D8 10m. These networks strike the best balance of low order channel representation and general number of channels with reasonable headward extent of channelization. Lower thresholds for both flow accumulation and TWI typically resulted in over channelized networks and initiation points too far up hillslopes. In some places these channels began halfway up talus fields or what are essentially bedrock cliffs. This reinforces our notion that geological information proves very important to the channel network at Loch Vale. The NHD network was found to be inconsistent with what was observed in the field and represented only higher order channels that could likely be observed from aerial imagery while missing almost all of our surveyed channels.

When considering DEM resolution, a 10m cell size provides the greatest number of networks rated as either "average" or "above average". Although it is possible to derive useful networks given an appropriate threshold at a 1m resolution, it generally fared poorly with the thresholds we tested, with only six networks rated as "average" or "above average". Given the additional computing power necessary to work with 1m resolution data, using 10m flow

accumulation and TWI rasters can provide acceptable channel network results. Performance according to flow direction algorithm did not show any obvious advantage for D∞ versus D8. This observation was in agreement with McMaster [2002] who saw no benefits for network accuracy in steep terrain as a result of using D∞ versus D8. Both flow accumulation and TWI are able to produce acceptable channel networks given appropriate thresholds and DEM resolution. TWI is able to represent many localized areas of ground saturation known to be pervasive in the field during the snowmelt runoff season. This also allows TWI to capture saturation in larger wetlands, which may provide additional utility in wetland hydrology applications. However, the degree of complexity and irregularity makes quantifying the accuracy of this characteristic extremely difficult. The same is true for D∞ and its ability to represent channel discontinuity and divergence. Further investigation into benefits of TWI and D∞ for channel network derivation in complex glaciated terrain is warranted.

Finally, we see that the flow accumulation and TWI thresholds we derived from DEM slope-area relationships provide the worst channel network representation overall because they over-predict channelization. This supports the earlier finding that locations of observed channel initiation were unrelated to these topographic variables.

Drainage density

Channel initiation thresholds that are dependent on both contributing area and slope produce networks with higher drainage density in steeper landscapes, which is generally seen in nature for a given climate and lithology (Montgomery and Foufoula-Georgiou, 1993; Kirby et al., 2002). Thus, we might expect that Loch Vale has a relatively high drainage density due to the steep nature of its topography. Typical values of drainage density range from 2 km^{-1} to 100km^{-1}

(Dingman, 2002). Converting from meters to kilometers, our surveyed drainage density is $8km^{-1}$. This is within the expected range albeit on the very low end. We found that most of our drainage densities derived using DEM-based contributing area thresholds were higher than what was observed, while the NHD network is almost half of observed. Our most accurate results are for drainage density are $T\alpha_4$, $T\alpha_5$, T_{twi2} and T_{twi3}.

Drainage density has some value as an initial metric for judging the quality of derived networks, but it only allows us to compare the total amount of channel length and not the spatially explicit accuracy. Less sophisticated hydrologic models may only require total channel length as an input parameter, but drainage density alone is less useful for many hydrologic applications. Despite showing that TWI can do well to capture the total length of channelization, its spatial discontinuity will raise additional considerations when attempting to model flow towards a single outlet.

Positional error

We find RMSE relative to the surveyed network to increase with threshold value. This is due to the fact that lower thresholds produce denser networks and inherently shorter distances from our surveyed points, despite the possibility it is not modeling the same channel. With a few exceptions, derived networks generally have a lower RMSE for D∞ when compared to D8. The driving factors behind this are not readily apparent, as the networks where this is not the case include a range of thresholds and cell sizes with similar drainage densities.

Like drainage density, RMSE results should be used with caution, as they are limited to only the positional accuracy of derived networks near our surveyed network, so erroneous upslope channelization or channels in areas with no surveyed flow lines will not be factored into

this performance measure. Also, simply having a denser channel network and finer resolution DEM leads to lower RMSE. Both of these limitations represent an issue common when attempting to compare continuous features with discrete points because of the inability to explicitly match a point from one as a point from the other. The linear feature accuracy test presented in Goodchild and Hunter [1997] attempted to address this, yet still relies on continuous representation for both the test and reference features and involves limiting analysis extent to features that exist in both modeled representations and the real world.

Feature accuracy assessment

To address the limitations of interpreting positional error, we apply a modified version of the linear feature accuracy test from Goodchild and Hunter [1997]. For a given resolution and threshold type, results show that D∞ outperforms D8. This advantage may not outweigh the limited compatibility of the D∞ algorithm with turn-key GIS stream derivation platforms commonly available. At fine resolution TWI has smaller 95% confidence buffer size, but at coarse resolution flow accumulation offers narrower confidence bands.

Channel head prediction index

Consistent with conclusions in our observed channel network analysis, all of our networks perform poorly when predicting channel initiation. Simply deriving less dense networks can reduce appearance of channel heads that do not exist (more reliable); however calibration in this manner will sacrifice the ability to correctly depict existing channel heads (sensitivity). Overall, the best networks for predicting channel initiation should simultaneously

be reliable and sensitive. A simple interpretation might be the highest average index score, but users must be aware of the tradeoffs if sacrificing one for the other.

Because of the complexity in channel initiation processes, channel head prediction continues to be an active area of research. For watersheds where derivation methods allow for accurate channel head prediction, further studies might attempt to compare index scores against a large sample of grid cell sizes to identify predictable relationships between grid cell size and performance. Also, our results suggest the need for more comprehensive quantitative metrics to evaluate derived channel networks against observed data. Those used here have limitations and must be interpreted carefully, and often in isolation. For example, channel head reliability and sensitivity can be misunderstood in isolation, as often networks performing well in one metric score poorly in another. There is no one quantifiable method for effectively assessing *overall* network accuracy.

6. Conclusions

The purpose of this study was to investigate the influence of digitally derived topographic variables on channel network formation. To accomplish this, our objectives were to (1) test how differences in gridded DEM resolution affect spatially distributed topographic parameters important to channel network derivation, (2) map the actual channel network at Loch Vale and examine the influence of surface variables on channel initiation, and (3) evaluate performance of common methods for deriving channel networks from gridded topographic data by comparing to the mapped network at Loch Vale.

For initial DEM analysis of Loch Vale, increasing grid cell size leads to a loss of information and visual detail for slope, specific contributing area, and topographic wetness index. This also causes increased mean specific contributing area and topographic wetness index with a shift in their cumulative frequency distributions toward higher values; most notably from the 1m DEM to coarser resolutions. D∞ flow direction algorithm has same effect, although to a lesser extent. When using a spatially static topographic threshold, coarser DEMs will model more channelization and likely lead to flashier simulated hydrographs with higher peak flows. These results show that the 1m DEM contains the most topographic information and suggests that it is the most appropriate resolution when deriving hydrologically important parameters from topography at Loch Vale. A slope-area scatterplot analysis revealed expected geomorphic signatures; however they corresponded to unreasonably small hillslope lengths and predicted contributing area thresholds which are not shown to be valid for the Loch Vale channel network. This is a potentially significant finding that warrants re-examining the relationship between

slope-area landscape characterization, geomorphic process scale, DEM resolution and the observed channel network form in steep headwater catchments.

A field survey revealed a complex and discontinuous channel network that one would not expect given an assumption of topographic control on channelization. When analyzing readily observable surface variables, we found no systematic relationship to locations of channel initiation. This leads us to conclude that subsurface processes, such as soil piping, bedrock topography, macropore flow and bedrock fractures have a significant influence on channel formation at Loch Vale.

Finally, our topographically derived channel networks generally perform poorly when compared to the observed network. This supports the conclusion that thresholds based on topography are largely inadequate for Loch Vale. Spatially variable thresholds may improve results, however given the dominance of subsurface controls results would not be physically related to the nature of channelization and would primarily rely on calibration based on known channel network data. We also find that the NHD network greatly oversimplifies channelization and has little value for detailed mapping for high-elevation headwaters. Despite the inability to explain channelization via topography, we can make some useful conclusions for improving performance of DEM derived channel networks from topographic thresholds. At Loch Vale, the 10m DEM performs the best overall while the 1m DEM is also useful given an appropriate threshold value, which will differ from the thresholds that are most effective for coarser DEMs. The 30m DEM performed poorly, thus the use of DEMs coarser than 10m for channel network derivation should be avoided. When evaluating the accuracy of modeled channel networks, results should be validated against field surveyed data. We found that the most useful

performance assessment tool is qualitative assessment based on field knowledge, suggesting the need for more comprehensive quantitative performance metrics.

The intent of this study was not to develop a new methodology for deriving accurate channel networks for a glaciated high-elevation catchment, but rather to test how well some fundamental and often unacknowledged assumptions in channel network derivation hold in such an environment. We found that assumptions of topographic control on channel initiation are not valid at Loch Vale. These assumptions are fundamental to the derivation methods tested here and so often used in a variety of environmental applications, so it is important that users understand their limitations when applying them in landscapes like Loch Vale where surface topography does not control locations of channel initiation.

References

Anderson M., and Kneale, P. (1982), The influence of low-angled topography on hillslope soil-water convergence and stream discharge, *Journal of Hydrology, 57*, 65–80.

Benavides-Solorio, J. (2003), Post-fire runoff and erosion at the plot and hillslope scale, Colorado Front Range. Ph.D. Dissertation, Colorado State University, Fort Collins, CO.

Beven, K and Kirby, M. (1979), A physically based, variable contributing area model of basin hydrology. *Hydrological Sciences*, *24(*1), 43 – 69.

Bewick, V. et al. (2004). Statistics Review 9: One-way analysis of variance. *Critical Care*, *8*(2). 130-136.

Brardinoni, F., and Hassan, M. (2006), Glacial erosion, evolution of river long profiles, and the organization of process domains in mountain drainage basins of coastal British Columbia, *Journal of Geophysical Research*, *111*, DOI 10.1029/2005JF000358.

Chirico, G. et al. (2005), On the definition of the flow width for calculating specific catchment area patterns from gridded elevation data. *Hydrological Processes*, *19*(13), 2539-2556.

Clow, D. et al. (2003), Ground water occurrence and contributions to streamflow in an alpine catchment, Colorado Front Range. *Ground Water*, *41*(7), 937-950.

Coffman, D. et al. (1972), New topologic relationships as an indicator of drainage network evolution. *Water Resources Research*, *8*(6), 1497-1505.

Curtiss, J. (1943), On transformations used in the analysis of variance. *The annals of mathematical statistics*, *14*(2), 107-122.

Deng, Y. et al. (2007), DEM resolution dependencies of terrain attributes across a landscape. *International Journal of Geographical Information Science*, *21*(2), 187-213.

Dietrich, W. et al. (1992), Erosion thresholds and land surface morphology. *Journal of Geology*, *20*, 675-679.

Dietrich, W. et al. (1993), Analysis of erosion thresholds, channel networks, and landscape morphology using a digital terrain model. *Journal of Geology*, *101*, 259-278.

Dingman, S. (2002), *Physical Hydrology*, second edition, 646 pp., Waveland Press, Inc., Long Grove, IL.

Evans, J., et al. (2006). Introduction to Discrete Return LiDAR. http://www.cnrhome.uidaho.edu/remotesensing, University of Idaho Remote Sensing and Research Lab, Moscow, ID.

Frankenberger, J. et al. (1999), A GIS-based variable source area hydrology model. *Hydrological Processes*, *13*(6), 805-822.

Galant, J. and Hutchinson, F. (2011), A differential equation for specific catchment area. *Water Resources Research, 47,* DOI 10.1029/2009WR008540.

Garcia-Corona et al. (2004), Effect of heating on some soil physical properties related to its hydrological behavior in two-north-western Spanish soils, *International Journal of Wildland Fire*, *13*, 195-199.

Gilbert, G. (1877), *Geology of the Henry Mountains*. 160pp., U.S. Geographical and Geological Survey, Washington, D.C.

Goodchild, M. and Hunter, G. (1997), A simple positional accuracy measure for linear features. *Geographical Information Science, 11*(3), 299-306.

Grayson, R. and Western, A. (2001). Terrain and the distribution of soil moisture. *Hydrological Processes*, *15*(13), 2689-2690.

Hancock, G. and Evans, K. (2006). Channel head location and characteristics using digital elevation models. *Earth Surface Processes and Landforms, 31*(7), 809-824.

Henkle, J. et al. (2011), Locations of channel heads in the semiarid Colorado Front Range, USA. *Geomorphology*, *129*(4-5), 309-319.

Henkle, J. (2010), Channel initiation in the semiarid Colorado Front Range. M.S. Thesis, Colorado State University, Fort Collins, CO.

Horton, R. (1945), Erosional development of streams and their drainage basins; hydrological approach to quantitative morphology.*Geological Society of America Bulletin*, *56*(3), 275.

Ijjasz-Vasquez, E. and Bras, R. (1995), Scaling regimes of local slope versus contributing area in digital elevation models. *Geomorphology, 12*(4), 299-311.

Iverson, L. et al. (1997), A GIS-derived integrated moisture index to predict forest composition and productivity of Ohio forests (U.S.A.). *Landscape Ecology*, *12*, 331-348.

Jaeger, K. et al. (2007), Channel and perennial flow initiation in headwater streams: management implications of variability in source area size. *Environmental Management*, *40*, 775-786.

Kampf, SK, BB Mirus. (2012), Subsurface and surface flow leading to channel initiation, in J Shroder Jr., E Wohl (eds.), *Treatise in Geomorphology*, Elsevier (in press).

Keene, O. (1995), The log transformation is special. *Statistics in Medicine, 14*, 811-819.

Kirby, M., et al. (2002), The influence of land use, soils and topography on the delivery of hillslope runoff to channels in SE Spain. *Earth Surface Processes and Landforms*, *27*, 1459-1473.

Le Coz, M., et al. (2009), Assessment of Digital Elevation Model (DEM) aggregation methods for hydrological modeling: Lake Chad basin, Africa. *Computers and Geosciences*, *35*, 1661-1670.

Lehner, B., et al. (2006). HydroSHEDS technical documentation, version 1.0. http://hydrosheds.cr.usgs.gov, Conservation Science Program of World Wildlife Fund, Washington, DC.

Lin, H. et al. (2006), Soil moisture patterns in a forested catchment: A hydropedological perspective. *Geoderma*, *131*, 345-368.

Lyon, S. et al. (2004), Using a topographic index to distribute variable source area runoff predicted with the SCS curve-number equation. *Hydrological Processes*, *18* (15), 2757-2771.

McMaster K. (2002), Effects of digital elevation model resolution on derived stream network positions. *Water Resources Research*, *38*(4), DOI 10.1029/2000WR000150.

Montgomery, D. and Dietrich, W. (1989), Source areas, drainage density, and channel initiation. *Water Resources Research*, *25*(8), 1907-1918.

Montgomery, D. and Dietrich, W. (1994), Landscape dissection and drainage area-slope thresholds. *Process Models and Theoretical Geomorphology*, pp. 221-246, John Wiley, New York.

Montgomery, D. and Foufoula-Georgiou, E. (1993), Channel network source representation using digital elevation models. *Water Resources Research*, *29*(12), 3925–3934.

National Atmospheric Deposition Program. (2012). NADP/NTN Wet Deposition Data- Loch Vale CO98, October 1983 – August 2011, http://nadp.sws.uiuc.edu/, NADP Program Office, Champaign, IL.

O'Callaghan, J. and Mark, D. (1984), The extraction of drainage networks from digital elevation data. *Computer Vision, Graphics, and Image Processing*, *28*, 323-344.

Orlandini, S. and Moretti, G. (2009), Determination of surface flow paths from gridded elevation data. *Water Resources Research*, *45*, doi:10.1029/2008WR007099.

Orlandini, S., et al. (2011), On the prediction of channel heads in a complex alpine terrain using gridded elevation data. *Water Resources Research*, *47*(2), 1-12.

Passalacqua, P., et al. (2010), Testing space - scale methodologies for automatic geomorphic feature extraction from lidar in a complex mountainous landscape. *Water Resources Research, 46*, 1-17.

Quinn, P., et al. (1991), The prediction of hillslope flow paths for distributed hydrologic modeling using digital terrain models. *Hydrological Processes, 5*, 59-79.

Scheidegger, A. (1966), Effect of map scale on stream orders. *Bulletin of the International Association of Scientific Hydrology, 11*, 56-61.

Sorenson, R. et al. (2005), On the calculation of the topographic wetness index: evaluation of different methods based on field observations. *Hydrology and Earth Systems Sciences Discussions, 2*, 1807-1834.

Tarboton, D. (1989), The analysis of river basins and channel networks using digital terrain data. Ph.D. Dissertation, Massachusetts Institute of Technology, Cambridge, MA.

Tarboton, D. et al. (1991), On the extraction of channel networks from digital elevation data. *Hydrological Processes, 13*(1), 81-100.

Tarboton, D. (1997), A new method for the determination of flow directions and upslope areas in grid digital elevation models. *Water Resources Research, 33*(2), 309-319.

Temme, A. et al. (2005), Algorithm for dealing with depressions in dynamic landscape evolution models. *Computers & Geosciences, 32*, 452-461.

Vides-Solorio, J. (2003), Post-fire runoff and erosion at the plot and hillslope scale, Colorado Front Range. Ph.D. Dissertation, Colorado State University, Fort Collins, CO.

Weekes, A. (2009). Process domains as a unifying concept to characterize geohydrological linkages in glaciated mountain headwaters. Ph.D. Dissertation, University of Washington, Seattle, WA.

Western, A. et al. (1999), Observed spatial organization of soil moisture and its relation to terrain indices. *Water Resources Research, 35*(3), 797-810.

Willgoose, R. (1989), A physically based channel network and catchment evolution model. Ph.D. Dissertation, Massachusetts Institute of Technology, Cambridge, MA.

Wolock, D. and McCabe, G. (1995), Comparison of single and multiple flow direction algorithms for computing topographic parameters in TOPMODEL. *Water Resources Research, 31*(5), 1315-1324.

Wolock D. and McCabe, G. (2000), Differences in topographic characteristics computed from 100- and 1000-m resolution digital elevation model data. *Hydrological Processes, 14*, 987–1002.

Woods, R. and Sivapalan, M. (1997). A connection between topographically driven runoff generation and channel network structure. *Water Resources Research, 33*(12), 2939-2950.

Wu, S. et al. (2008), A study on DEM-derived primary topographic attributes for hydrologic applications: Sensitivity to elevation data resolution. *Applied Geography, 28*, 210-223.

Zhang W., and Montgomery D. (1994), Digital elevation model grid size, landscape representation, and hydrologic simulations. *Water Resources Research, 30*(4), 1019–1028.

Appendices

Appendix A: Raw field data of surveyed channel points

Legend

Feature type:
- CF = channel with flow
- C = channel with no flow
- F = flow with no channel

Channel Head Formation Process:
- csf = convergent subsurface flow
- cof = convergent overland flow
- L = Landsliding

Field Notes:
- * = denotes a channel head

Point ID	Feature Type	Channel Head Formation Process	Northing (UTM)	Easting (UTM Zone 13)	Field Notes
Ab01	F		4460283.633	444000.113	
Ab02	F		4460265.496	443976.224	
Ab03	CF	csf	4460268.793	443953.040	* exfiltrates from rock below meadow
Ab04	F		4460229.327	443860.959	saturated meadow from pt 03-05
Ab05	F		4460216.980	443799.572	fans to top of meadow
Ab06	F		4460187.346	443785.460	exfiltrates from talus
Ae01	F		4460145.296	443742.310	wide saturated marshy area with visible flow path
Ae02	F		4460161.604	443695.157	
Ae03	F		4460139.314	443691.420	
Ae04	CF		4460123.465	443670.683	
Ae05	CF		4460077.553	443644.232	
Ae06	CF	cof	4460053.888	443640.064	* ~10m below meadow
Ae07	F		4460058.798	443631.149	
Ae08	F		4460038.743	443616.317	flows from bottom of saturated marshy meadow
Aa01	CF	cof	4460020.959	443634.923	* fans into wide saturated marshy area
Aa02	F		4459978.991	443590.285	
Aa03	F		4459952.110	443574.638	
Aa04	F		4459921.979	443562.302	
Aa05	F		4459901.455	443549.707	
Ac01	CF		4459867.483	443552.860	fans into 3 channels at Loch
Ac02	CF		4459823.252	443519.107	
Ac03	CF	csf	4459816.583	443532.054	*, exfiltrates from talus
Ad01	CF		4459818.847	443539.837	3 small tributaries from talus
Ad02	CF		4459807.961	443540.039	

Ad03	CF		4460576.162	444124.160	
Ad04	CF		4460581.734	444127.756	
Ad05	CF	csf	4460590.231	444134.320	*, exfiltrates from talus
Ag01	F		4460606.247	444143.352	
Ag02	F		4460614.427	444148.163	
Ag03	F		4460564.003	444086.842	
Ag04	F		4460571.250	444076.068	exfiltrates from talus
An01	F		4460582.006	444072.819	fans into wide saturated marsh
An02	CF		4460589.190	444078.236	
An03	CF		4460622.829	444119.120	
An04	CF		4460630.541	444133.180	
An05	CF		4460537.604	444055.187	
An06	CF		4460548.049	444049.042	poor reception (17 pts)
An07	CF		4460557.011	444043.010	poor reception (12 pts)
An08	CF		4460534.113	444040.369	poor reception (13 pts)
An09	CF		4460548.826	444031.579	small trib
An10	F		4460554.790	444018.777	
An11	F		4460559.334	444003.334	
An12	CF		4460561.822	443996.449	poor reception (51 pts)
An13	F		4460423.921	444022.929	
An14	CF	csf	4460432.077	444012.513	* emerges from talus field
Ao01	CF		4460438.125	444005.114	
Ao02	CF		4460435.370	443988.394	
Ao03	CF		4460428.535	443984.816	
Ao04	CF		4460417.978	443975.065	poor reception (16 pts)
Ao05	F		4460416.579	443961.019	no reception
Ao06	F		4460413.376	443944.588	poor reception (17 pts)
Ao07	CF	csf	4460224.298	443871.034	* poor reception (54 pts)
Ap01	CF		4460118.728	443862.516	joins with Icy (divergent segment)
Ap02	CF		4460164.447	443710.549	joins Icy above marsh
Ap03	CF		4460187.163	443697.373	under snow (width not determined)
Ap04	CF		4460188.475	443686.077	small trib
Ap05	CF		4460198.277	443682.983	
Ap06	CF		4460056.553	443750.667	
Ap07	CF		4460015.584	443745.916	trib here
Ap08	CF		4460005.724	443736.561	under snow
Ap09	CF		4459991.028	443724.408	
Ap10	CF		4459986.702	443715.034	poor reception (20 pts)
Ap11	CF		4459974.570	443706.503	short trib from upper marsh
Ap12	CF		4459959.792	443720.598	
Ap13	CF		4459962.500	443731.917	
Ap14	CF		4459956.179	443744.028	
Ap15	CF		4459900.240	443707.262	
Ap16	CF		4459894.548	443702.151	
Ap17	CF	cof	4459886.704	443690.998	*
Apa08	CF	cof	4460024.248	443620.100	* extends from bottom of a marsh
Apa07	CF		4459860.549	443553.044	
Apa06	CF		4459855.287	443557.234	

Apa05	CF		4459854.899	443562.855	
Apa04	CF		4459852.634	443566.365	
Apa03	CF		4459857.137	443570.780	
Apa02	CF		4459858.166	443578.322	
Apa01	CF		4459852.622	443565.979	joins with Ap just above fishing meadow
Apb01	CF		4459850.002	443568.091	joins with Ah
Apb03	CF		4459834.545	443557.679	generally marshy and treeless area
Apb02	CF		4459831.491	443562.456	
Apb04	CF		4459830.075	443572.154	
Apb05	CF		4459824.173	443580.896	
Apb06	CF		4459819.664	443583.625	
Apb07	C		4459811.673	443583.087	
Apb08	C	cof	4459798.537	443587.680	*, also took garmin point
Apc01	CF		4459796.105	443595.201	poor reception (29 pts)
Apc02	CF		4459782.590	443600.062	
Apc03	CF		4459778.048	443599.051	poor reception (28 pts)
Apc04	CF		4459773.234	443604.682	
Apc05	CF	csf	4459766.765	443608.252	*emerges from under large fallen tree below talus; next to Icy transect
Apca01	CF		4459758.619	443613.408	
Apca02	CF		4459751.384	443613.633	
Apca03	CF	csf	4459742.385	443614.531	*, poor reception (29 pts)
Aq01	CF		4459739.380	443625.827	
Aq02	CF		4459736.451	443620.965	
Aq03	CF		4459729.207	443621.781	
Aq04	CF		4459795.719	443626.745	
Aq05	CF		4459790.008	443638.365	
Aq06	CF		4459783.434	443651.374	
Aq07	CF		4459813.424	443606.504	Flat, generally saturated area around flowpath
Aq08	CF		4459801.263	443614.281	channel reincised by short plung from exposed rock
Aq09	F		4459795.745	443622.336	Flow over exposed rock
Aq10	CF		4459794.057	443624.702	
Aq11	CF		4459788.963	443623.034	
Aq12	CF		4459755.159	443624.730	~1.5m cascade
Aq13	CF		4459864.565	443511.521	
Aq14	CF		4459869.794	443508.998	channel splits (flow divergence into Aq and Aqa
Aq15	CF		4459872.317	443503.901	
Aq16	CF	csf	4459873.376	443498.044	*, small weir gage, emerges from talus
Aqa01	CF		4459874.792	443494.145	emerges from talus and joins Aq
Aqa02	M		4459878.627	443490.445	observed flow through talus via opening
Aqa03	F		4459880.770	443486.442	becomes very rocky and fans, infiltrates, Aqaa joins, evidence of past sheetwash
Aqa04	CF		4459879.425	443482.447	
Aqa05	CF		4459872.895	443475.155	flow begins ~2.5 meters below channel head
Aqa06	C	unknown	4459872.291	443467.346	*, old overgrown channel bed

Aqaa03	C		4459864.820	443460.794	
Aqaa02	C		4459862.781	443449.221	
Aqaa01	C		4459868.502	443436.775	entire channel bounded by exposed bedrock, overgrown grasses
Al01	CF		4459872.945	443432.482	
Al02	F		4459831.908	443513.892	generally saturated area without a distinct channelized flowline
Al03	F		4459835.076	443507.673	
Al04	CF		4459834.180	443494.135	still in marsh
Al05	CF		4459835.609	443486.970	
Al06	CF		4459838.910	443477.225	
Al07	CF		4459847.383	443461.081	
Al08	CF		4459854.200	443454.140	
Al09	CF		4459824.281	443515.767	
Al10	CF		4459827.613	443512.419	
Al11	CF		4459821.593	443503.898	
Al12	CF		4459815.562	443493.869	
Al13	CF		4459809.025	443483.782	
Al14	CF		4459800.498	443481.435	
Al15	CF		4459784.685	443470.971	
Al16	CF	csf	4459781.066	443457.175	*, emerges from rocky soil
Ala01	F		4459772.381	443451.174	eroded rocky bed but no definable banks
Ala02	F		4459766.702	443439.435	exfiltrating from crack in large bedrock outcrop
Am01	CF		4459756.113	443435.848	joins Ama
Am02	CF		4459749.251	443418.773	
Am03	CF	csf	4459737.205	443412.871	*, emerges from talus/rocky soil
Ama06	CF	csf	4459723.093	443395.071	*, emerges from boulder at edge of meadow, USGS mark (pic 418)
Ama03	CF		4459711.115	443386.541	
Ama05	CF		4459698.948	443367.092	
Ama04	CF		4459692.519	443357.940	joins with Am
Ama02	CF		4459814.864	443499.728	enters marshy area
Ama01	CF		4459808.532	443492.983	loses consolidated flow in marsh after this point
Ah01	CF		4459798.223	443485.661	could not acquire satellite signal the rest of the channel
Ah02	CF		4459785.404	443477.063	disappears underground, re-emerges later
Ah03	CF		4459776.139	443483.457	
Ah04	CF		4459765.382	443490.678	
Ah05	CF		4459752.215	443493.604	disappears underground and re-emerges ~5m later
Ah06	CF		4459744.795	443495.564	
Ah07	CF		4459782.448	443469.535	rechannelizes under brush
Ah08	F		4459775.679	443468.989	fans into marshy area
Ah09	CF	cof	4459754.301	443468.339	*, forms from draining marsh
Af02	CF		4459730.829	443461.336	
Af01	CF		4459728.746	443449.083	point of confluence with Icy
B01	CF		4459717.149	443440.456	~3m above confluence with Icy

Bh01	M		4459698.426	443415.643	enters Andrew's Creek through subsurface
Bh02	CF		4459688.408	443409.772	
Bh03	M		4459746.503	443400.743	meanders through talus
Bh04	CF		4459749.257	443392.170	
Bh05	CF		4459746.987	443376.333	emerges from subsurface
Bh06	CF	csf	4459742.348	443361.426	*, initiates from talus (briefly), then disappears to subsurface
Ba01	CF		4459740.067	443357.928	confluence with Andrews Creek
Ba02	CF		4459744.272	443367.384	
Ba03	CF	csf	4459740.757	443365.239	*, emerges after large boulder
Bc01	CF		4459734.662	443363.583	
Bc02	CF		4459776.494	443564.577	
Bc03	CF		4459774.847	443571.522	
Bc04	CF		4459776.712	443580.251	
Bc05	CF		4459770.798	443584.803	
Bc06	CF		4459761.277	443583.538	point of exfiltration
Bc07	F		4459747.541	443581.055	point of infiltration (underground for Bc07-Bc06)
Bc08	CF	cof	4459738.321	443581.034	* head forms after cascades from rock
Bca01	CF	csf	4459731.768	443580.285	*, 1m long trib
Bd01	F		4459724.613	443579.284	point of infiltration (disjointed segment)
Bd02	CF		4459712.938	443579.066	
Bd03	CF	cof	4459706.335	443586.189	*
Bd04	F		4459698.424	443595.065	point of exfiltration (no-channelized flow)
Bb05	CF	csf	4459687.783	443601.331	*, exfiltrates from talus
Bb04	CF		4459682.254	443612.854	infiltrates into talus
Bb03	CF		4459674.470	443622.852	exfiltrates from talus
Bb02	CF		4459670.615	443627.752	
Bb01	CF		4459731.968	443582.398	enters into backwater ponded area
Ai01	CF		4459728.384	443587.685	
Ai02	CF		4459706.292	443603.571	braided channels between pt 2 and 3
Ai03	CF	cof	4459698.491	443608.410	drains from embryo pond, disappears under large boulder
Bg01	n/a		4459685.888	443613.497	water emerges and puddles, no further flow downslope
Bi01	CF		4459685.144	443614.204	reinfiltrates
Bi02	CF		4459706.196	443606.746	
Bi03	CP		4459698.053	443618.380	emerges as ponded area (~7x5m with banks)
Bi04	CF		4459691.997	443625.515	re-emerges, ponded, immediately reinfiltrates
Bi05	CF		4459921.962	443558.699	infiltrates underground
Bi06	CF		4459989.642	443485.581	
Bi07	CF	csf	4459994.966	443481.069	*,emerges from boulder and rocky soil
Bia01	CF	csf	4459997.705	443475.691	* emerges from soil and reinfiltrates ~2m downslope
Bj01	CP		4460199.500	443432.461	general size of ponded area
Bj02	CP		4460207.736	443434.158	general size of ponded area

Bj03	CP		4460219.566	443439.270	general size of ponded area
A24	CF		4460230.468	443459.206	point of divergence
A22	CF		4460236.490	443465.098	divergent segment of Icy
A21	CF		4460195.438	443416.068	divergent segment of Icy below A22
A20	CF		4460196.796	443412.651	single stem of icy below Ak
A23	CF		4460202.824	443401.879	divergent segment of Icy
A19	CF		4460225.817	443400.743	
A18	CF		4460232.647	443400.794	point of confluence with Andrew's
A17	CF		4460244.988	443405.167	
A16	CF		4460262.610	443410.889	point of short divergence during high flows
A15	CF		4460281.080	443421.195	
A14	CF		4460205.937	443399.949	point of flow divergence in high flows
A13	CF		4460283.445	443430.513	same segment as point 7 divergence
A12	CF		4460304.314	443421.982	point opposite 8 on main stem
A11	CF		4460320.049	443424.838	just above a divergence before steep section
A10	CF		4460328.170	443418.996	
A09	CF		4460168.436	443384.496	point of divergent flow
A08	CF		4460177.851	443369.331	same segment as point 12 divergence
A07	CF		4460188.081	443356.400	point opposite 13 on main stem
A06	CF		4460196.181	443350.654	point on main stem where 13's segment rejoins
A05	CF		4460202.751	443340.377	
A04	CF		4460214.684	443336.117	
A03	CF		4460221.077	443327.938	point of confluence after short divergence
A02	CF		4460236.231	443317.309	
A01	CF		4460154.304	443350.760	flows into the Loch
Ak01	CF		4460153.555	443351.610	
Ak02	CF		4460090.744	443274.101	
Ak03	CF		4460126.302	443181.988	
Ak04	CF		4460122.721	443178.561	
Ak05	CF		4460117.635	443176.561	
Ak06	CF	csf	4460114.659	443170.983	*emerges from subsurface after Ak
Aka01	CF		4460112.499	443159.990	about a 2.5m tributary, joins Ak here
Aka02	CF	csf	4460106.357	443139.627	*, emerges from soil
Bf01	CF		4460073.924	443146.601	confluence with marshy area
Bf02	CF	csf	4460061.596	443149.208	*, emerges from subsurface about 3m above confluence
Be01	CF		4460047.391	443147.411	Confluence with Andrews Creek
Be02	CF		4460039.032	443146.162	
Be03	CF		4460036.101	443138.238	
Be04	CF		4460032.550	443134.978	
Be05	CF		4460028.341	443129.855	
Be06	CF		4460043.151	443142.515	
Be07	CF		4460046.491	443153.335	USGS stream gage
Be08	CF	csf	4460045.469	443147.389	* emerges 10m downslope from talus
Aj01	CP		4460049.737	443142.264	ponded (with banks) surface water

Appendix B: Photographs of observed channel heads

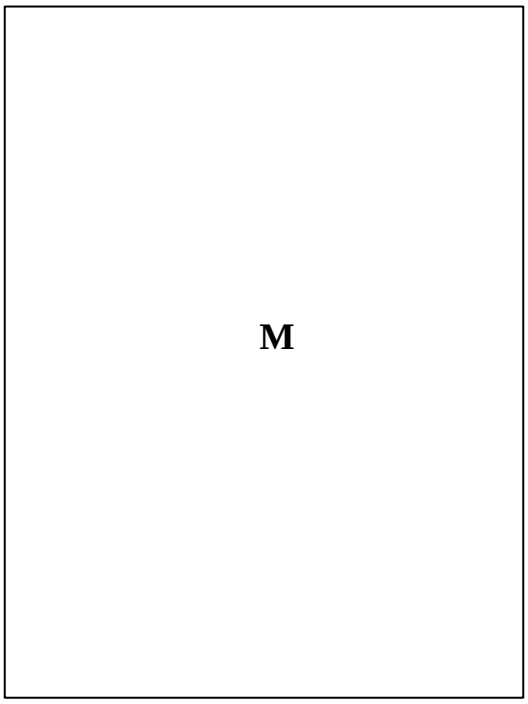

Point ID: Aa01

Point ID: Ab03

Point ID: Ac03

Point ID: Ad05

Point ID: Ae06

Point ID: Ah09

Point ID: Ak06

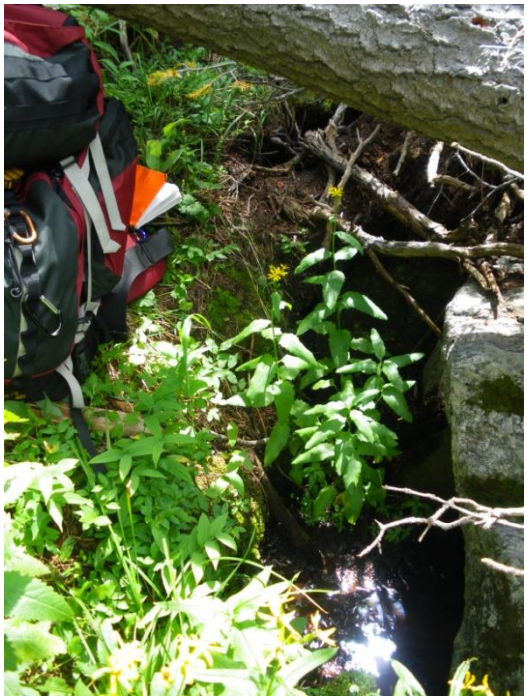

Point ID: Aka02

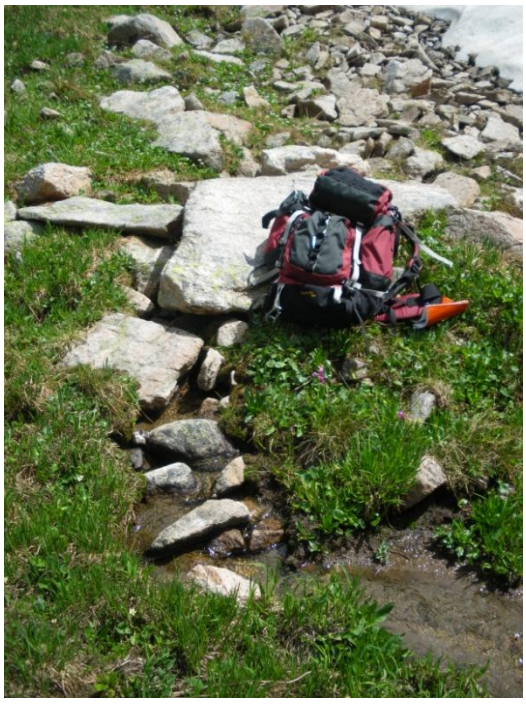

Point ID: Al16

Point ID: Am03

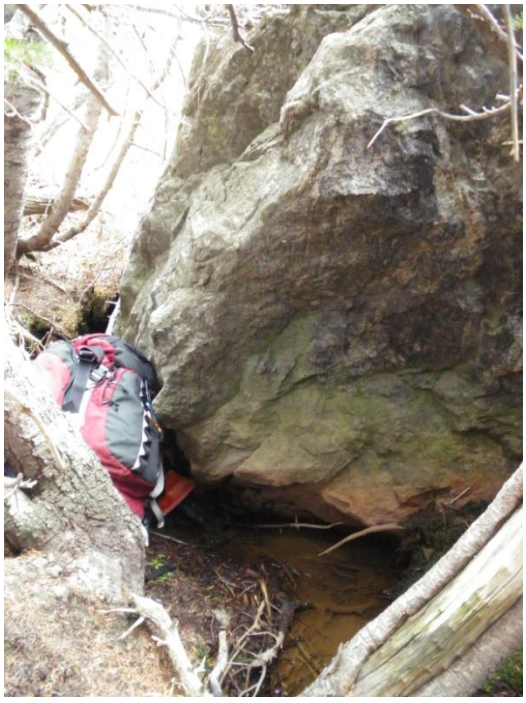

Point ID: Ama06

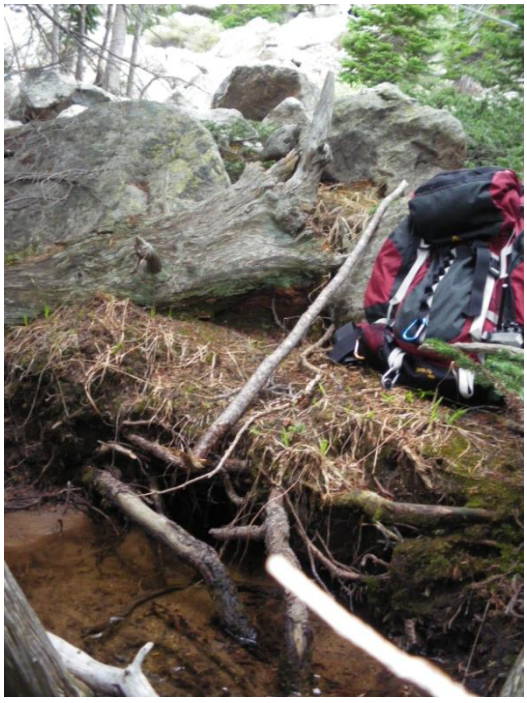

Point ID: An14

Point ID: Ao07

Point ID: Ap17

Point ID: Apa08

Point ID: Apb08

Point ID: Apc05

Point ID: Apca03

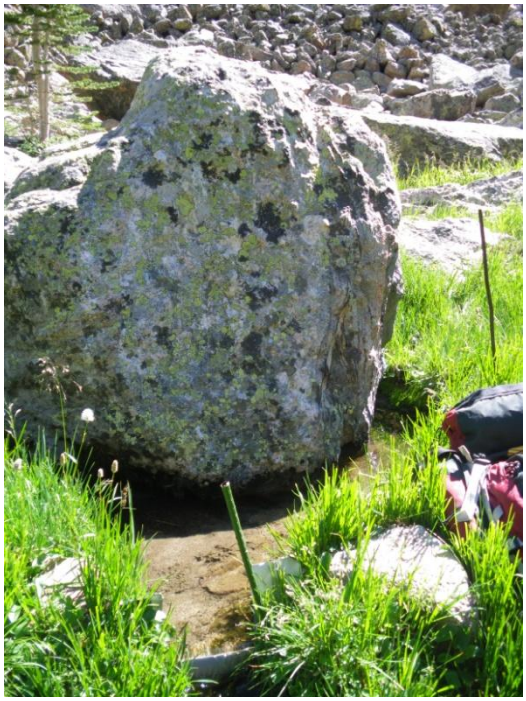

Point ID: Aq16

Point ID: Aqa06

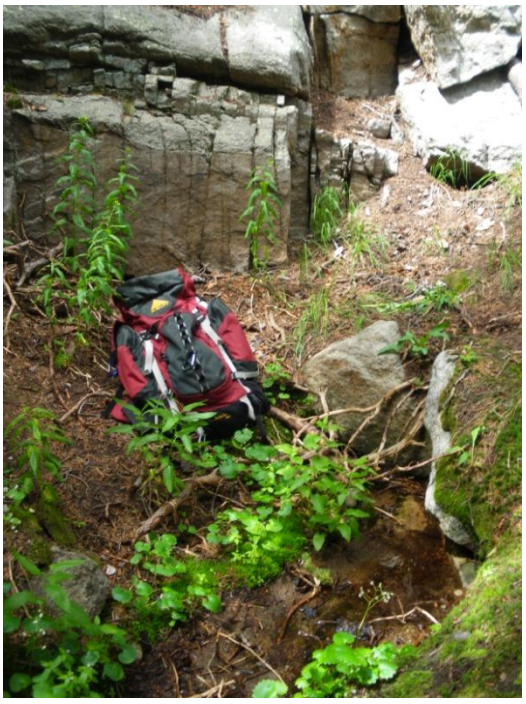

Point ID: Ba03

Point ID: Bb05

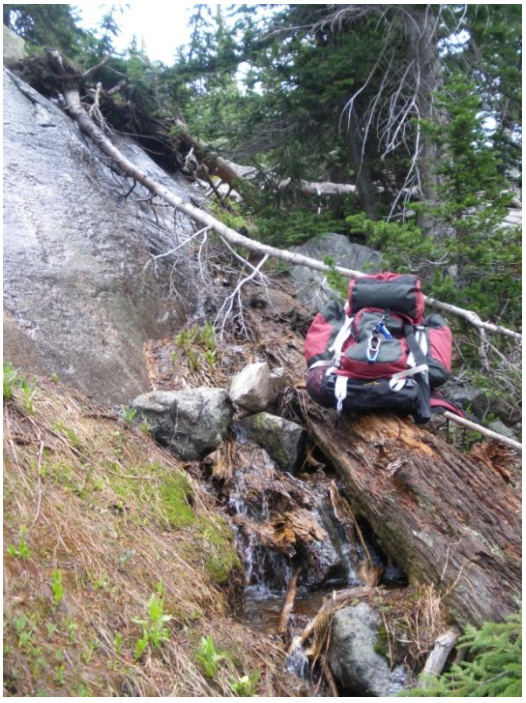

Point ID: Bc08

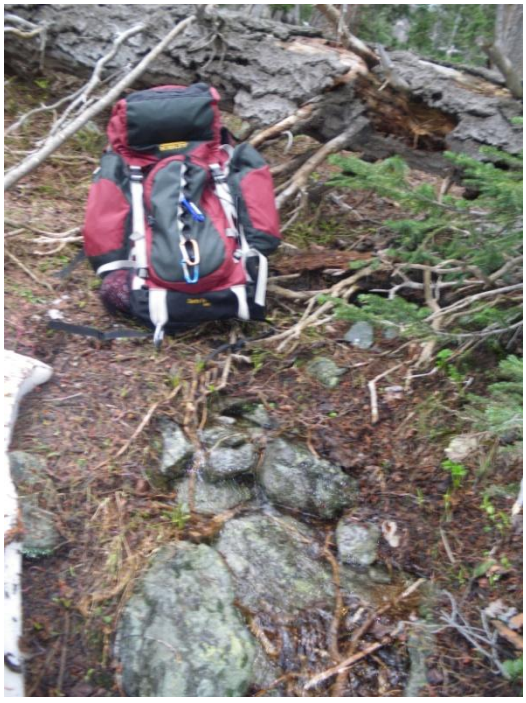

Point ID: Bca01

Point ID: Bd03

Point ID: Be08

Point ID: Bf02

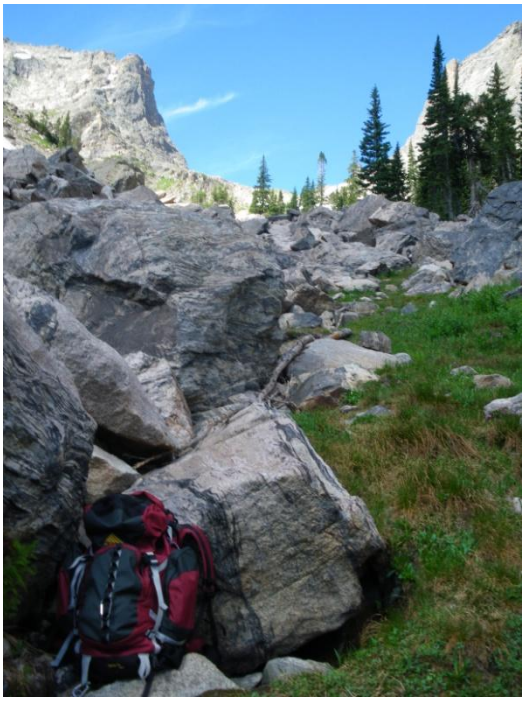

Point ID: Bh06

Point ID: Bi07

Point ID: Bia01

Appendix C: Derived channel networks

$T\alpha_1$: 468m^2

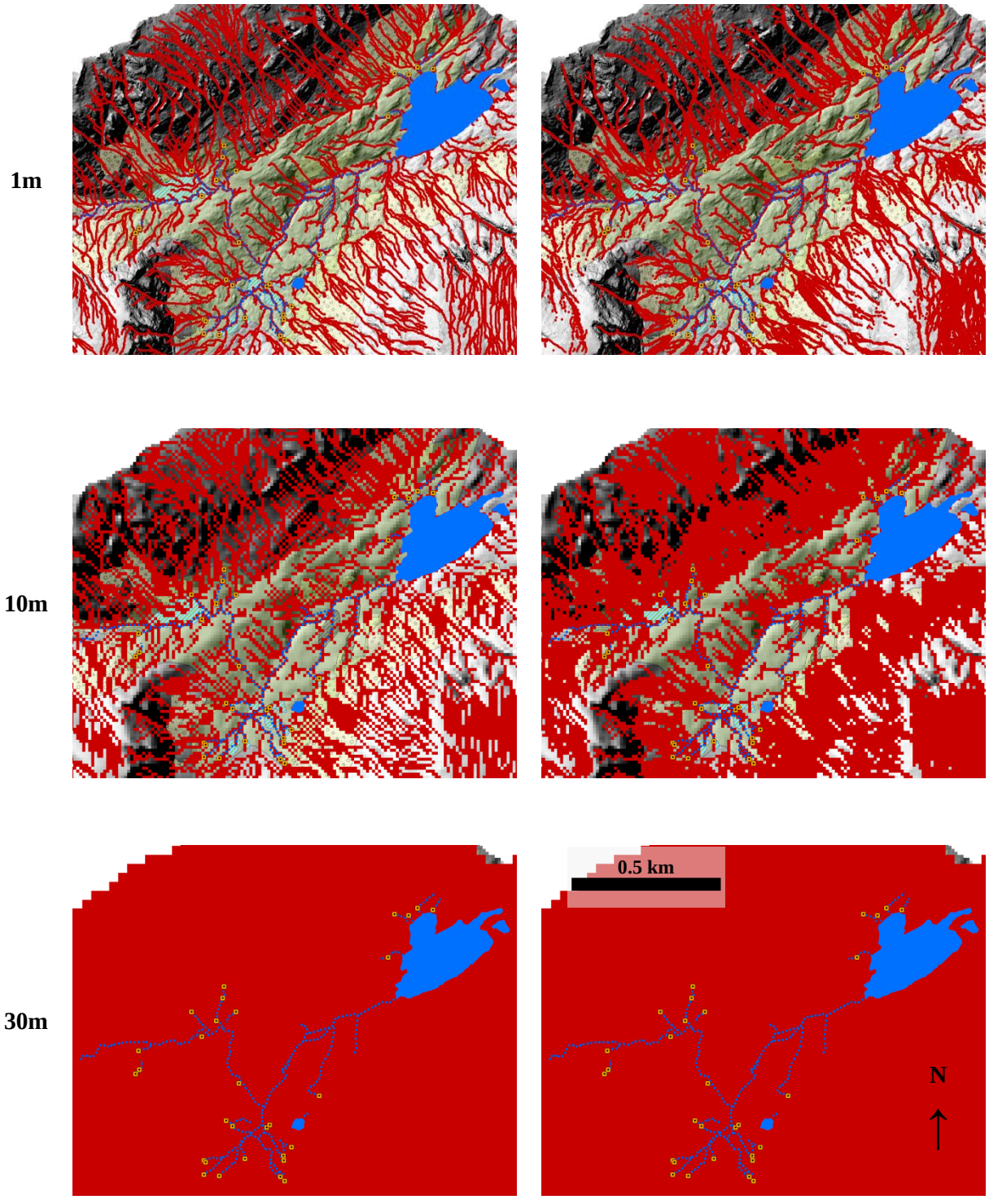

$T\alpha_2$: 1,480.3m^2

D8 **D∞**

1m

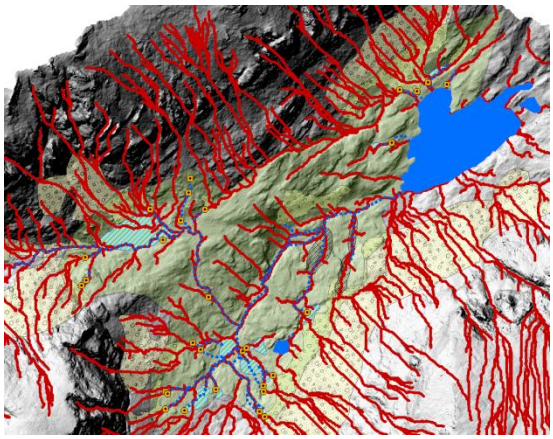

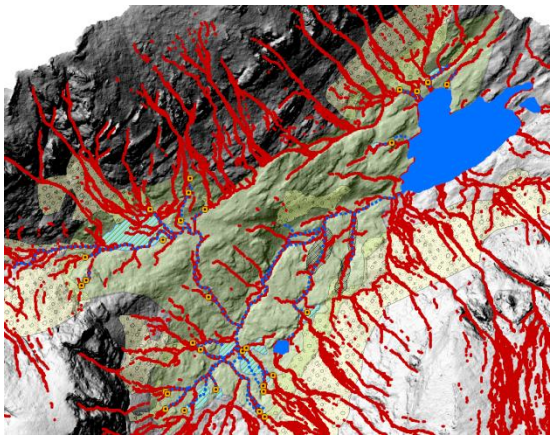

10m

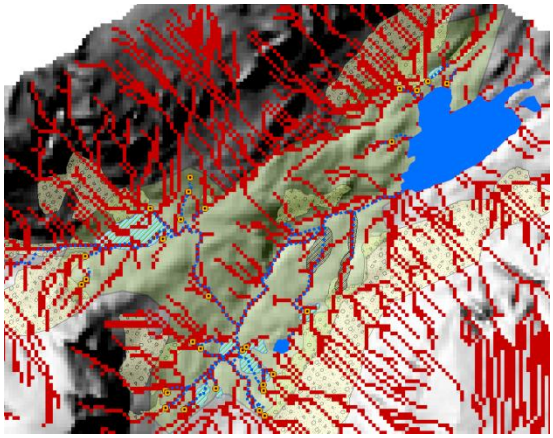

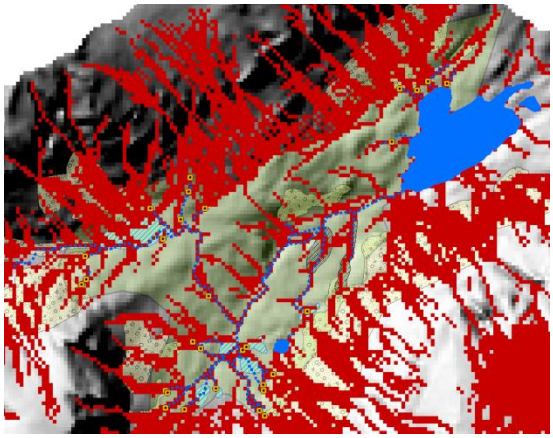

30m

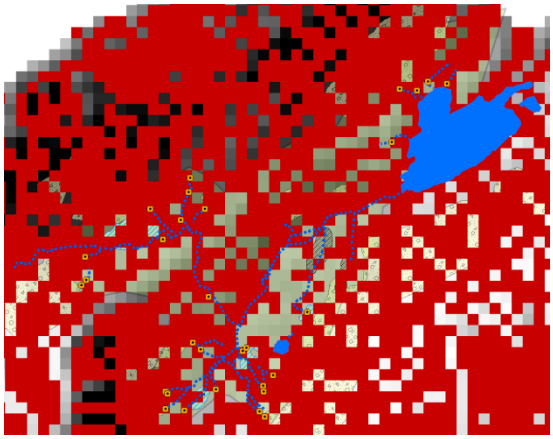

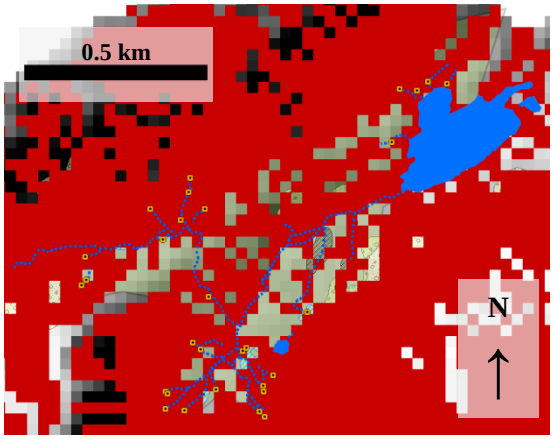

$T\alpha_3$: 5,205m^2

	D8	**D∞**
1m	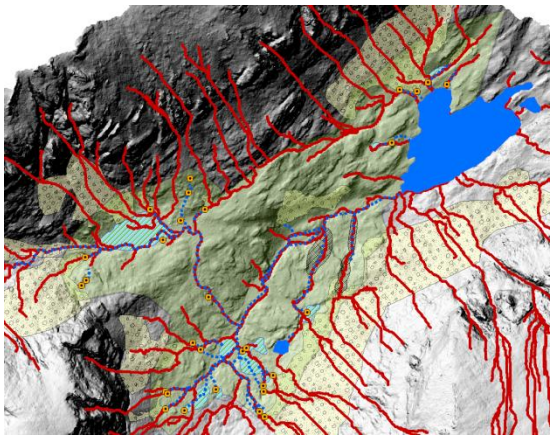	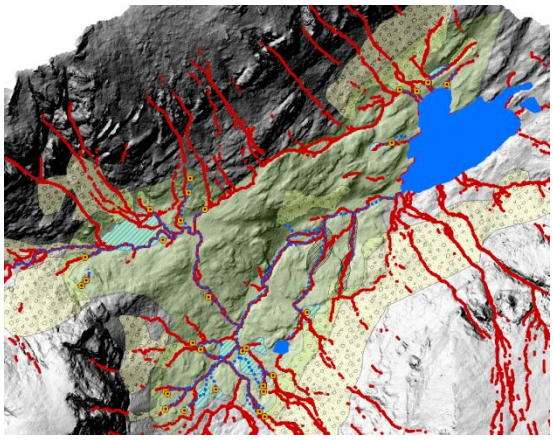
10m	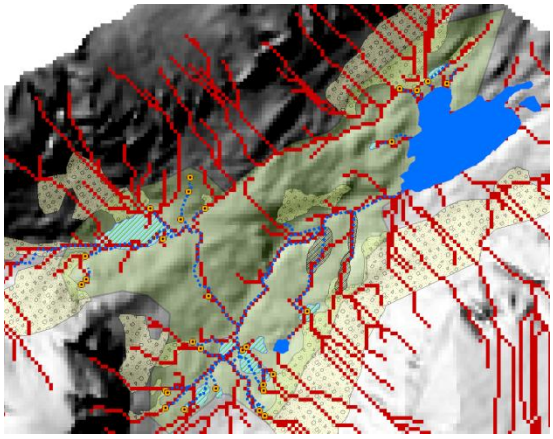	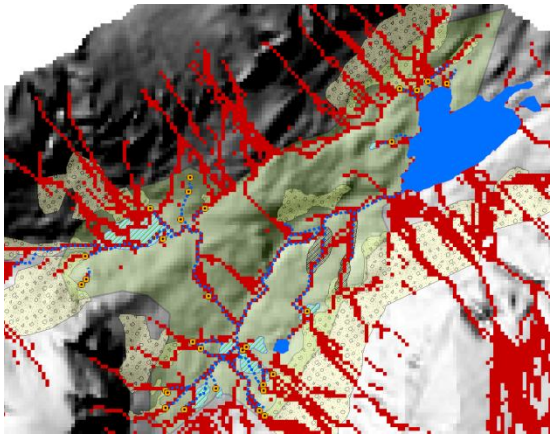
30m	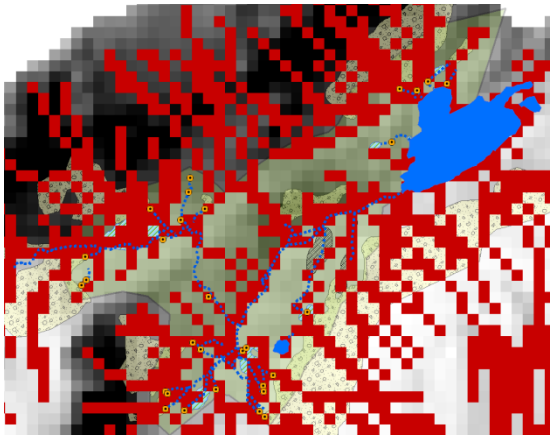	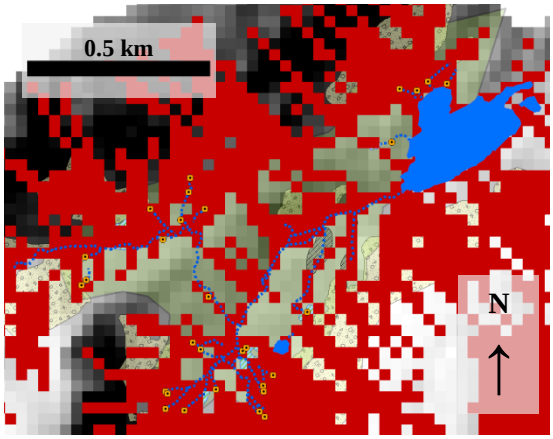

$T\alpha_4$: 40,485m^2

D8 **D∞**

1m

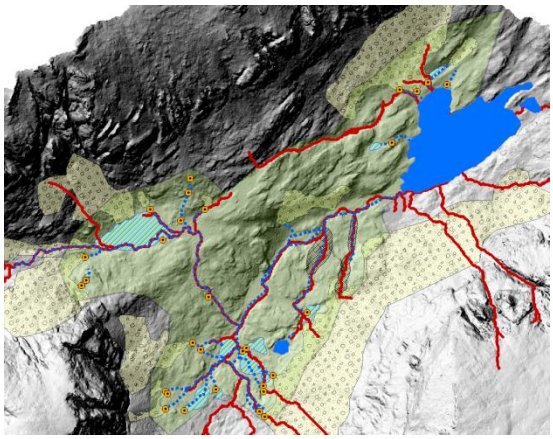

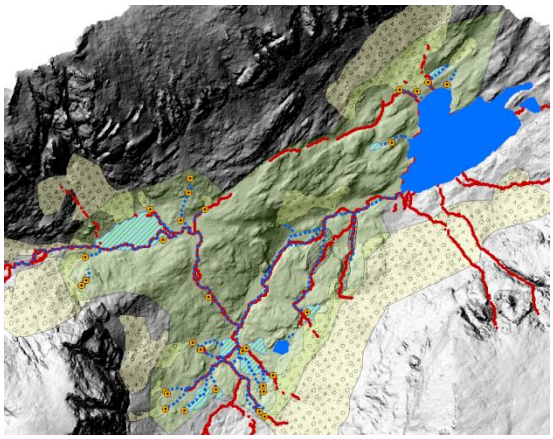

10m

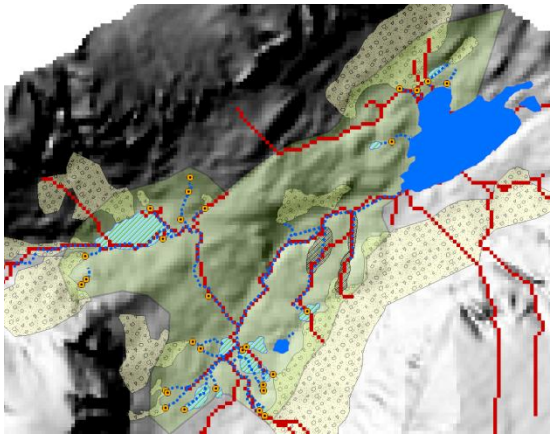

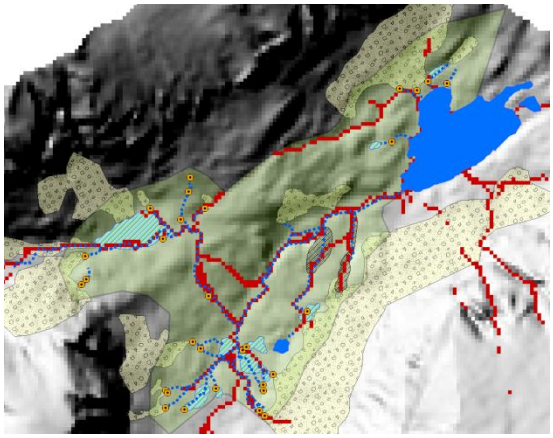

30m

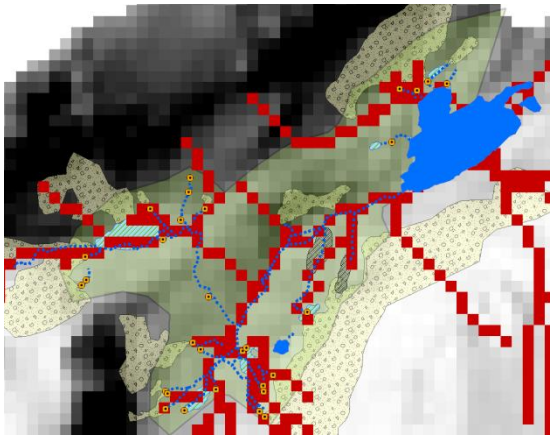

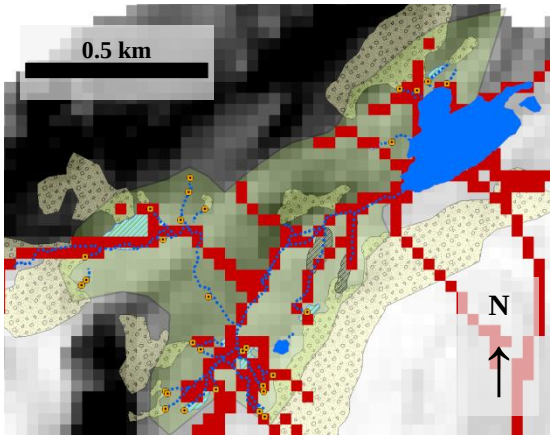

$T\alpha_5$: 129,372m^2

D8 **D∞**

1m

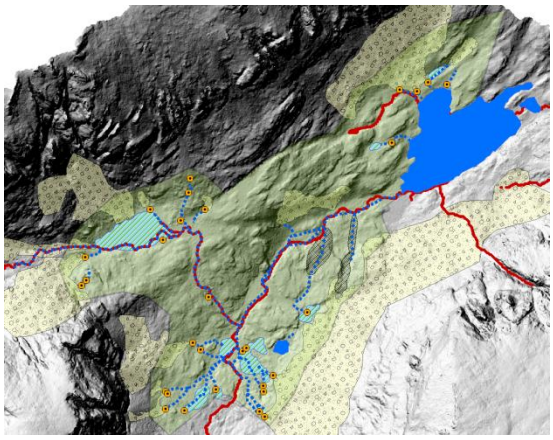

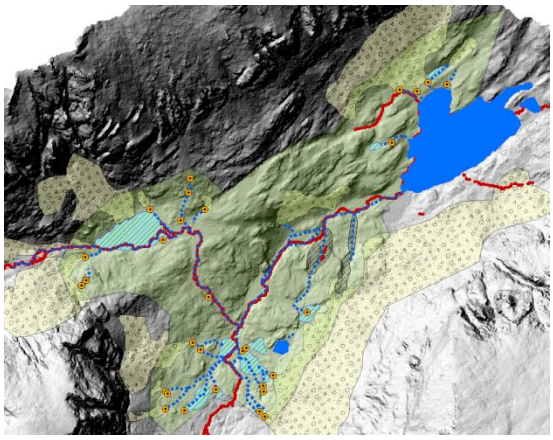

10m

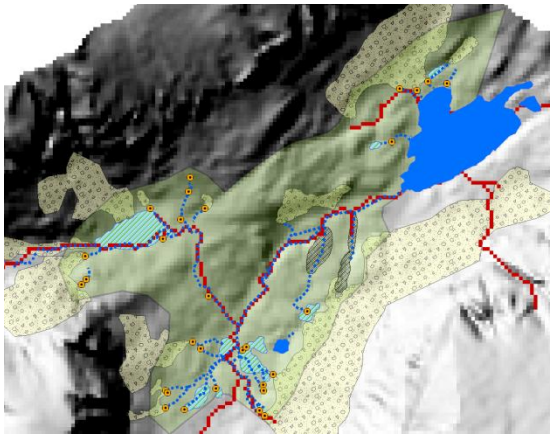

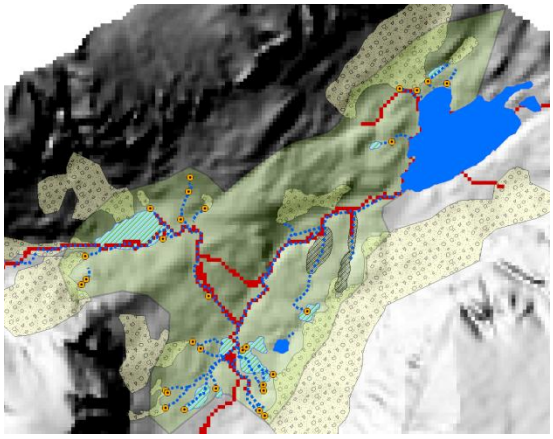

30m

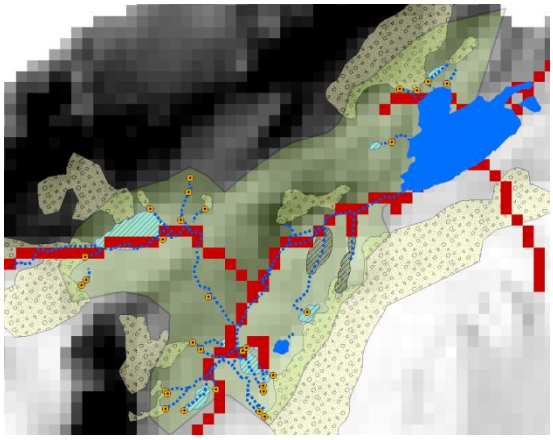

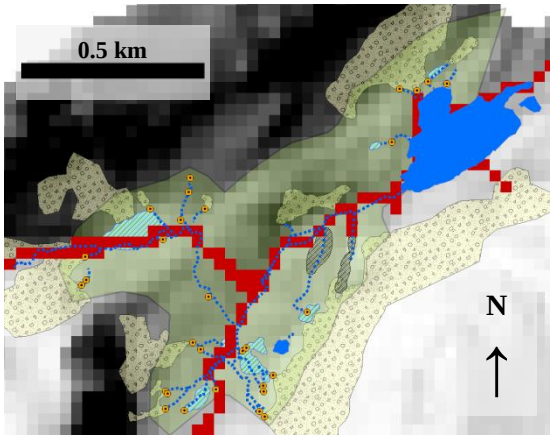

$Ttwi_1$: 2.56

	D8	**D∞**
1m	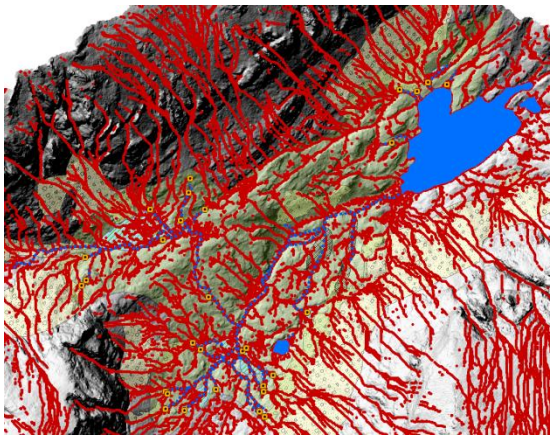	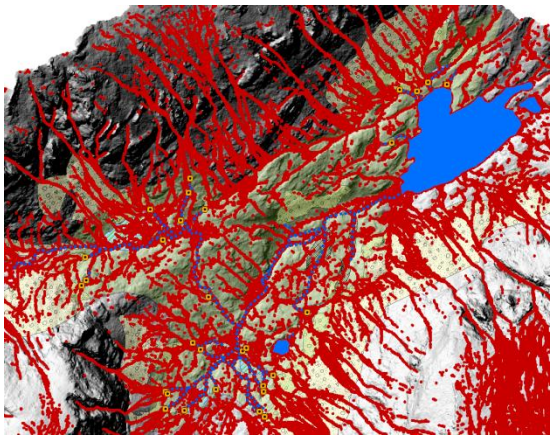
10m	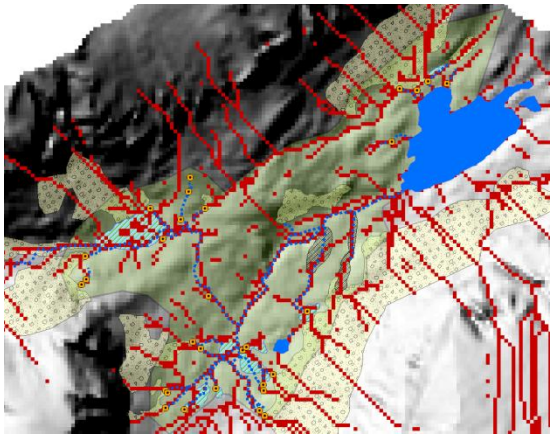	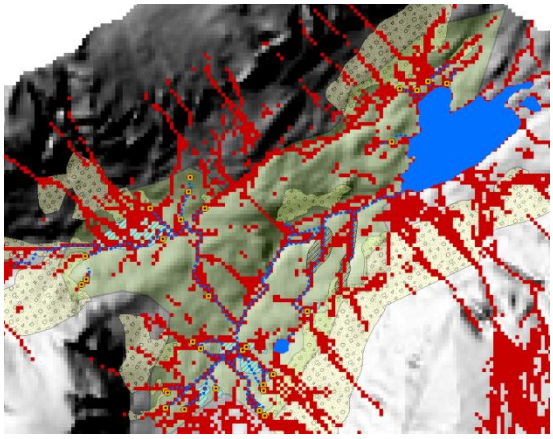
30m	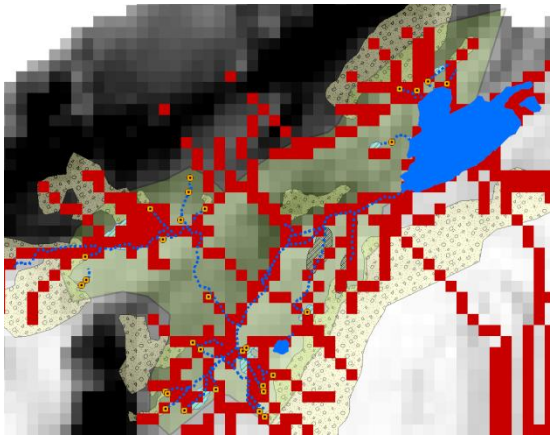	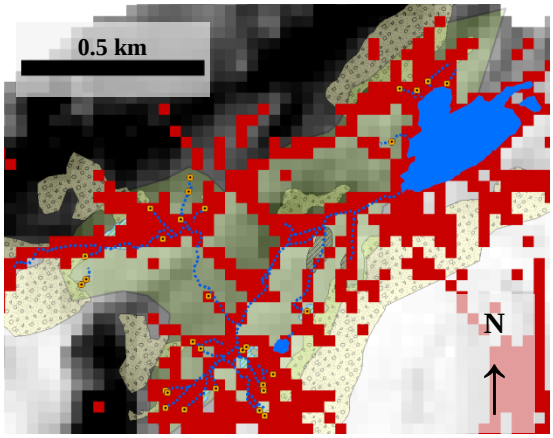

Ttwi$_2$: 4.04

D8 **D∞**

1m

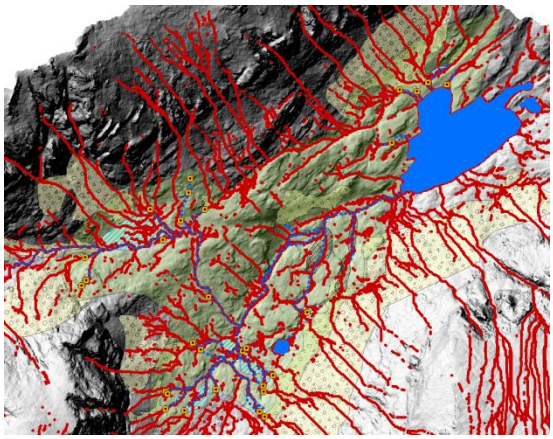

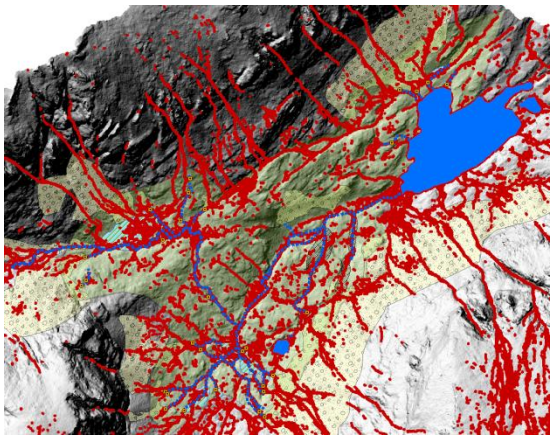

10m

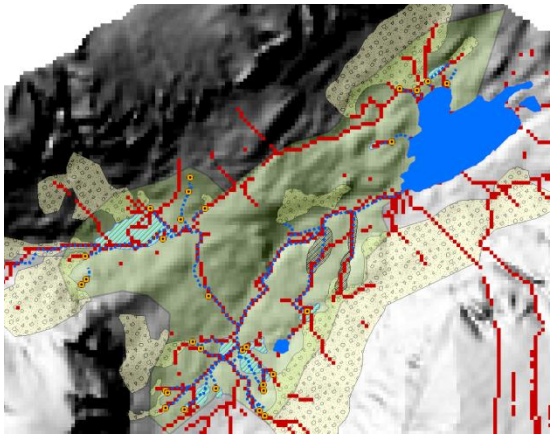

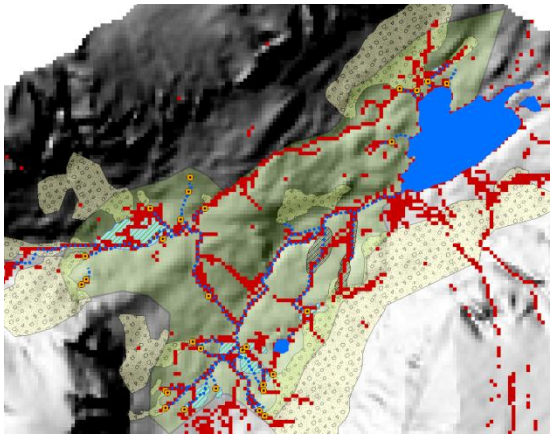

30m

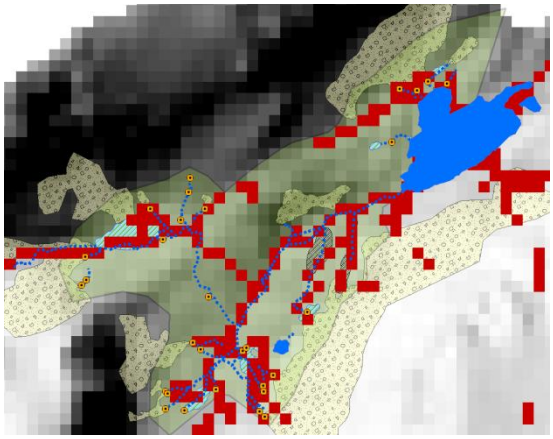

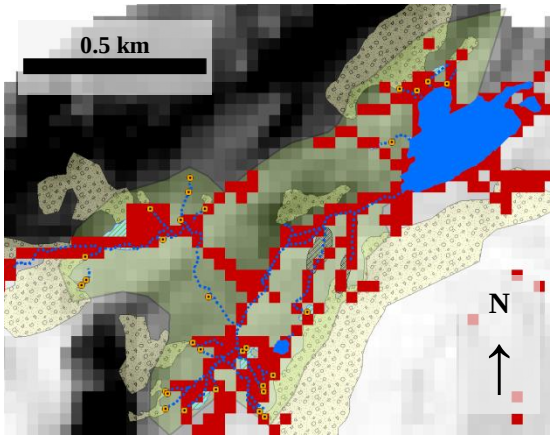

$Ttwi_3$: 5.18

	D8	**D∞**
1m	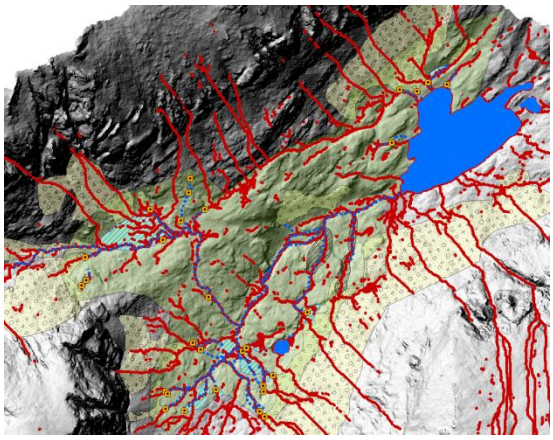	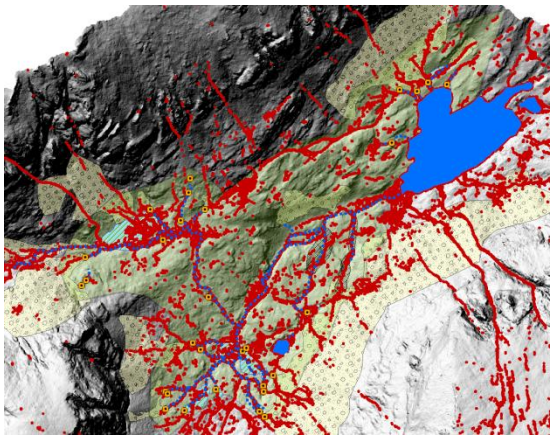
10m	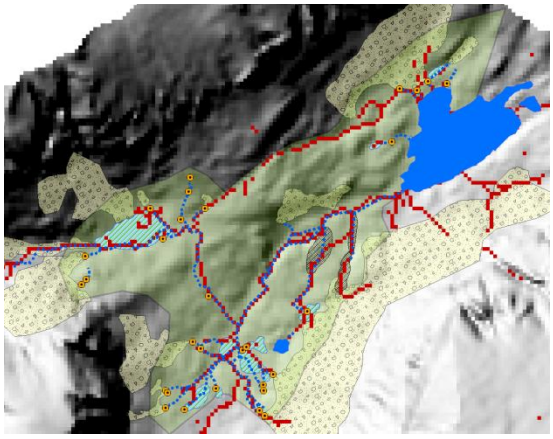	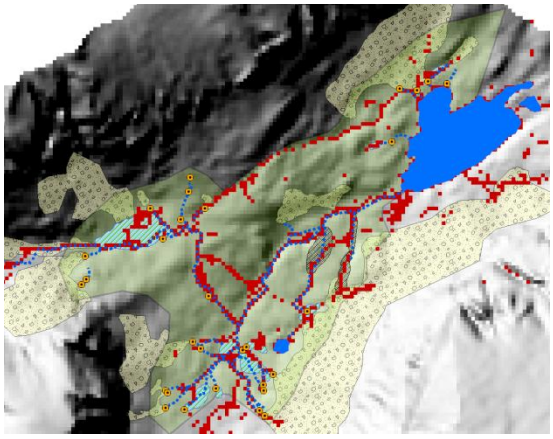
30m	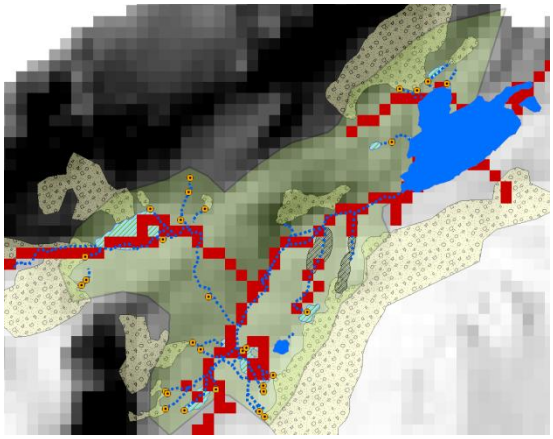	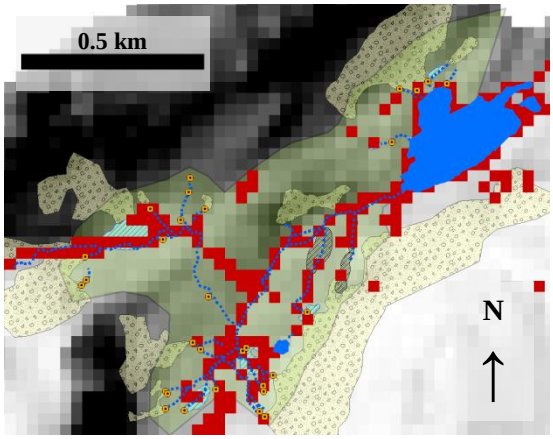

NHD

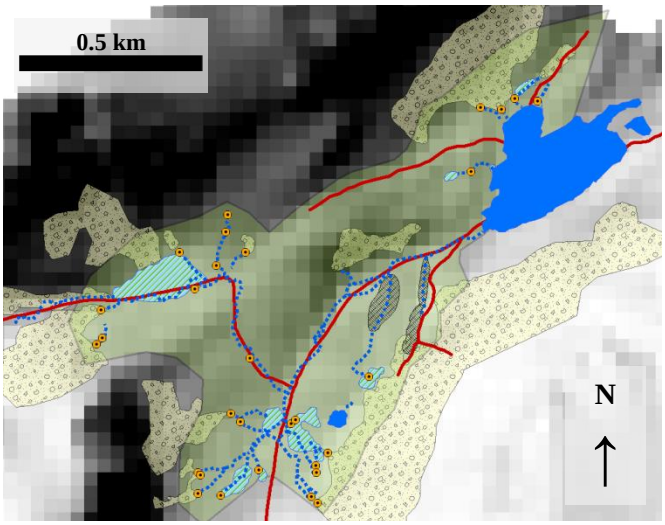

Appendix D: ArcGIS data architecture

File geodatabase schematic

LochVale_ThesisData.GDB

-Field Map

Surveyed area, glaciers, lakes, talus, wetlands

Survey channel points, survey channel heads, feature accuracy test sample reach points

NHD Flowlines, surveyed flowlines, no signal flowline, survey footpath

-One_Meter, Ten_Meter, Thirty_Meter

Catchments (All of Loch Vale)

Outlets, $\ln(\alpha_s)$, $\ln(\tan \beta)$, TWI, derived channel network points, derived channel heads

derived channel network lines, derived channel heads

-Rasters: Hillshades, aspect, flow direction, flow accumulation (# of cells), α_s, $\ln(\alpha_s)$, slope (rise/run), tan β (percent), $\ln(\tan \beta)$, TWI, derived channel networks

-Near Tables: Feature accuracy tests, surveyed heads to derived heads, derived heads to surveyed heads, surveyed channel network points to derived channel network points

Object naming conventions

Object Description	Object Type	Naming Convention
Catchment outlet	Point	Outlet_[DEM resolution]
Catchment area	Polygon	Catchment_[DEM resolution]
DEM	Raster	DEM_[DEM resolution]
Sink filled DEM	Raster	DEM_[DEM resolution]_fil
Hillshade	Raster	hillsha_[DEM resolution]
Slope (rise/run)	Raster	[Flow direction algorithm]_[DEM resolution]_slp
Slope (percent)	Raster	[Flow direction algorithm]_[DEM resolution]_slppct
Natural log of slope (percent)	Raster	[Flow direction algorithm]_[DEM resolution]_lslppct
Flow direction	Raster	[Flow direction algorithm]_[DEM resolution]_fdr
Flow accumulation (# of cells)	Raster	[Flow direction algorithm]_[DEM resolution]_fac
Specific contributing area	Raster	[Flow direction algorithm]_[DEM resolution]_sca
Natural log of specific contributing area	Raster	[Flow direction algorithm]_[DEM resolution]_lnsca
Topographic wetness index	Raster	[Flow direction algorithm]_[DEM resolution]_twi
1m D∞ tan β for extraction to slope area plot	Points	ln_slope_1m
1m D∞ α_s for extraction to slope area plot	Points	ln_sca_1m
Derived channel network	Raster	[Threshold]_[Flow direction algorithm]_[DEM resolution]
Derived channel network	Points	[Threshold]_[Flow direction algorithm]_[DEM resolution]_pt
Derived channel network	Polylines	[Threshold]_[Flow direction algorithm]_[DEM resolution]_line
Derived channel network clipped to survey area with lake extent erased	Polylines	[Threshold]_[Flow direction algorithm]_[DEM resolution]_line_clip
Derived channel network heads	Points	[Threshold]_[Flow direction algorithm]_[DEM resolution]_heads
NHD flowlines clipped to Loch Vale	Polylines	NHD_Flowlines_LV
NHD flowlines clipped to survey area	Polylines	NHD_Flowlines_LV_clip
Surveyed area	Polygon	SurveyArea
Survey footpath	Polyline	Survey_Path
Areas with no GPS signal	Polygon	No_Signal
Known flowlines not surveyed	Polylines	NoSig_Flowline_Clip

Surveyed channel network (all points collected)	Points	Survey_ChannelPts_ALL
Surveyed channel network for analysis	Points	Survey_ChannelPts_ref
Surveyed channel network for analysis	Polylines	Survey_flowline
Surveyed channel heads	Points	Survey_ChannelHeads
Surveyed reaches for feature accuracy test	Points	AccuracyTest_reaches
Distances from surveyed channel points to derived channel points (for distribution of errors analysis)	Near Table	[Threshold]_[Flow direction algorithm]_[DEM resolution]_dist
Distances from surveyed sample reaches points to derived channel points (feature accuracy test)	Near Table	AccuracyTest_[Threshold]_[Flow direction algorithm]_[DEM resolution]
Distances from surveyed channel heads points to derived channel heads (channel head prediction index)	Near Table	SurveyHeads_indx_[Threshold]_[Flow direction algorithm]_[DEM resolution]
Distances from derived channel heads to surveyed channel heads (channel head prediction index)	Near Table	[Threshold]_[Flow direction algorithm]_[DEM resolution]_heads_indx

GIS processing flow chart

DEM Analysis:

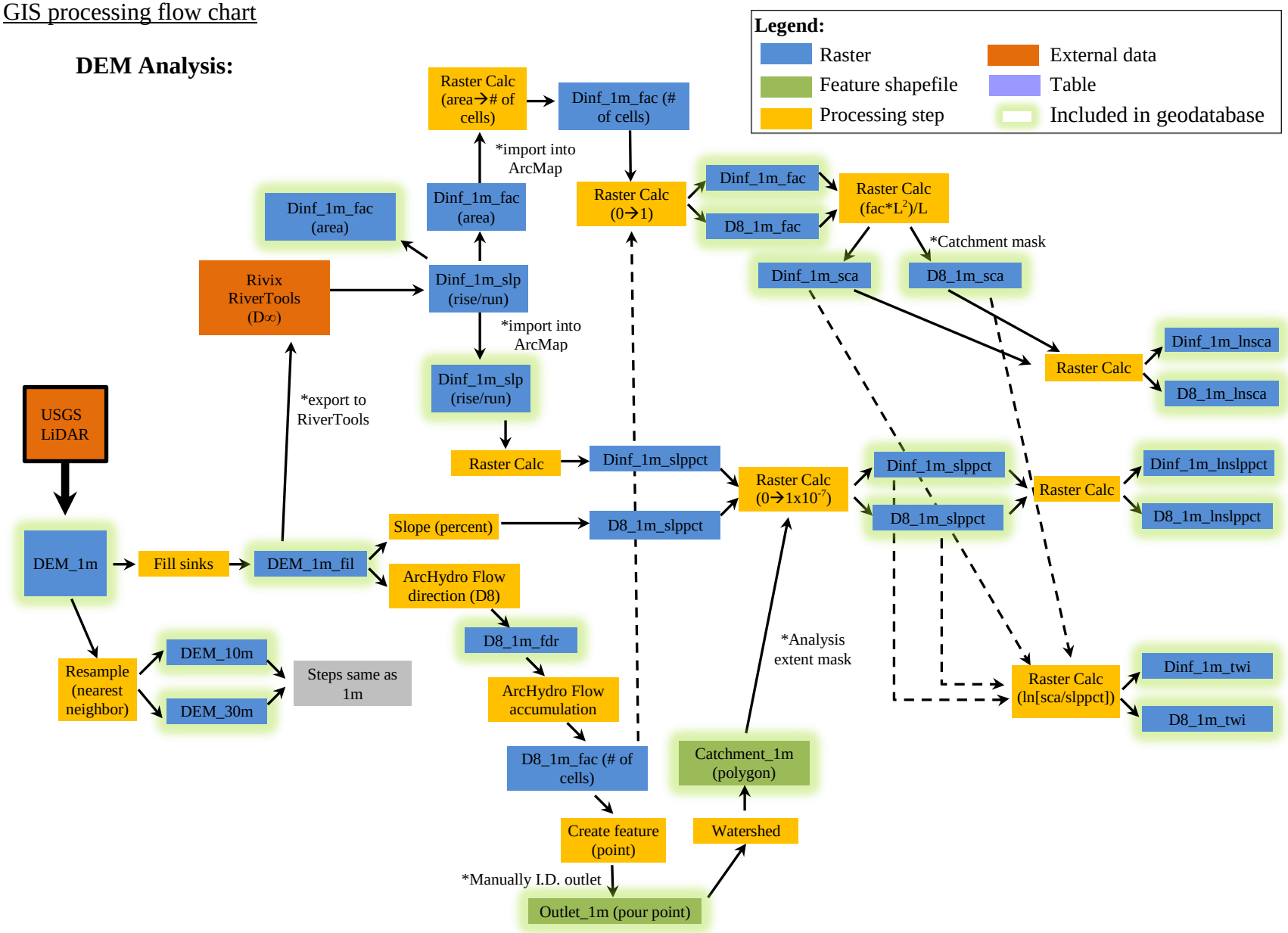

Observed network analysis:

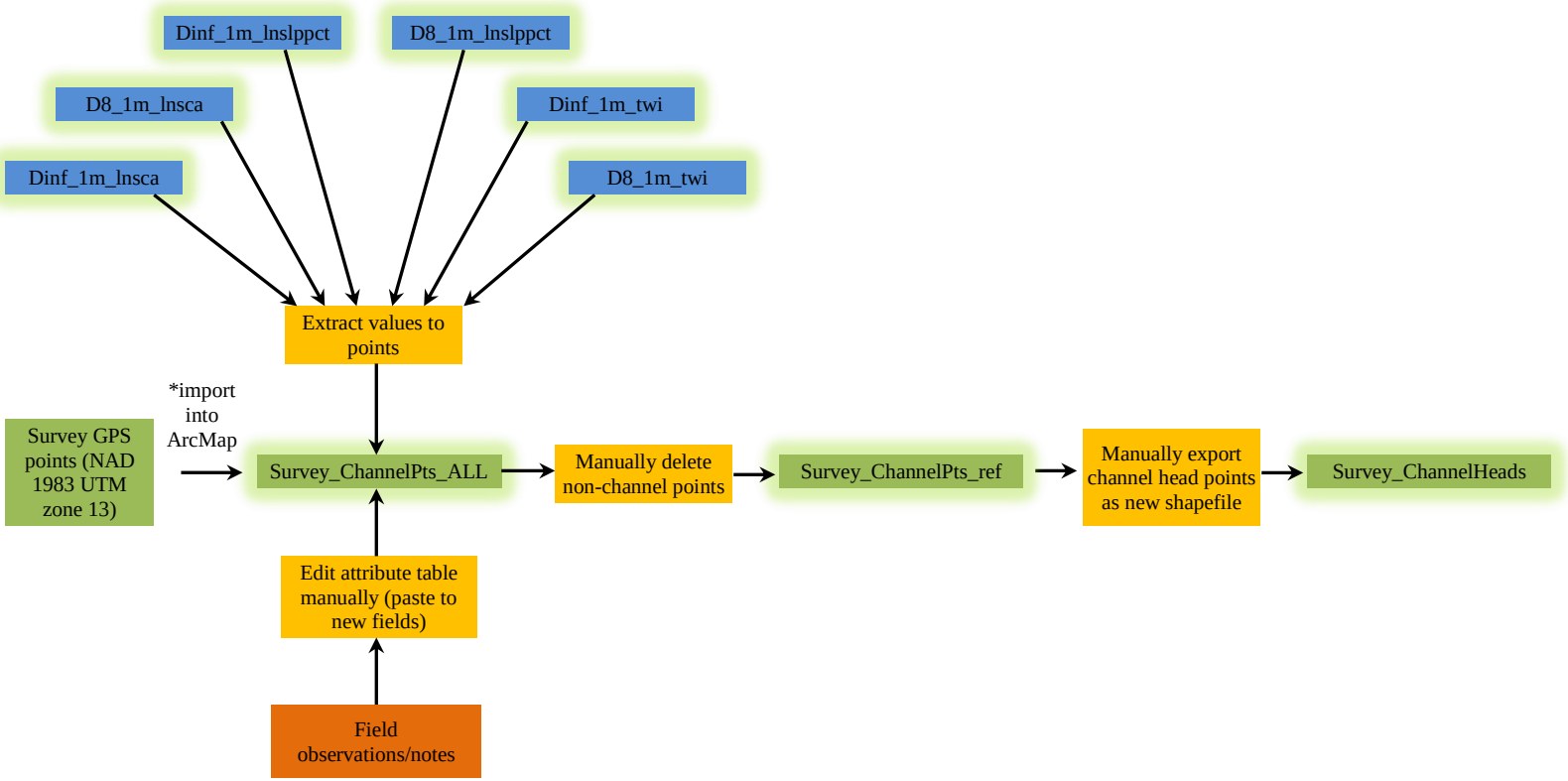

Channel Network Derivation:

Channel network derivation

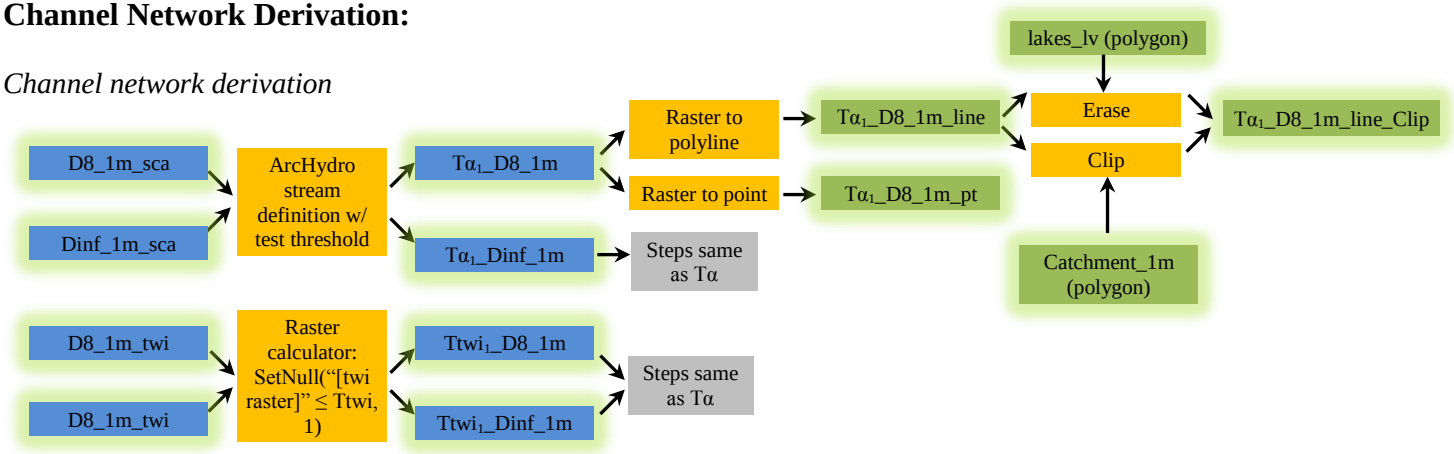

Positional error

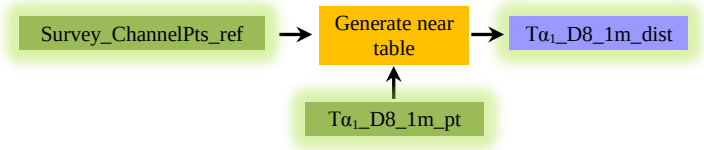

Feature accuracy assessment

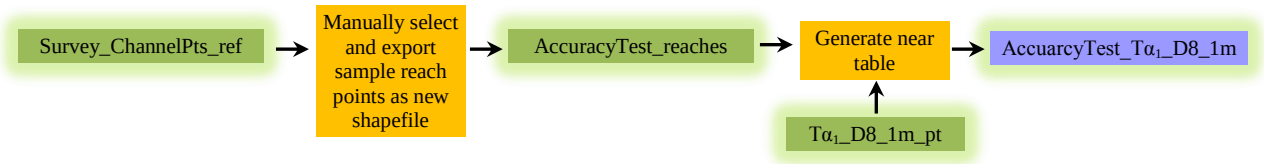

Channel head prediction index